UNIVERSITY OF CUKUROVA
INSTITUTE OF NATURAL AND APPLIED SCIENCES

PhD THESIS

Filiz KARAÖMERLİOĞLU

OPTICAL PROPERTIES OF MULTILAYER ANTIREFLECTION COATING SYSTEMS ON A FERROELECTRIC BASE

DEPARTMENT OF PHYSICS

ADANA, 2008

INSTITUTE OF NATURAL AND APPLIED SCIENCES

UNIVERSITY OF CUKUROVA

OPTICAL PROPERTIES OF MULTILAYER ANTIREFLECTION COATING SYSTEMS ON A FERROELECTRIC BASE

By Filiz KARAÖMERLİOĞLU

A THESIS OF DOCTOR OF PHILOSOPHY

DEPARTMENT OF PHYSICS

We certify that the thesis titled above was reviewed and approved for the award of degree of the Doctor of Philosophy by the board of jury on 31/01/2008.

Signature Prof. Dr. Emirullah MEHMETOV Advisor	Signature Prof. Dr. Süleyman GÜNGÖR Member

Signature Prof. Dr. Bahtiyar SALAMOV Member	Signature Prof. Dr. Metin ÖZDEMİR Member	Signature Assoc. Prof. Dr. Turgut İKİZ Member

This PhD Thesis is performed in Department of **PHYSICS** of Institute of Natural and Applied Sciences of Cukurova University.
Registration Number:

Prof. Dr. Aziz ERTUNÇ
Director
The Institute of Natural and Applied Science

This study was financially supported by Research Found of Cukurova University.

Project Number: **FEF2004D7**

ÇUKUROVA ÜNİVERSİTESİ

FEN BİLİMLERİ ENSTİTÜSÜ

FERROELEKTRİK TEMELLİ ÇOKKATMANLI YANSITMASIZ SİSTEMLERİN OPTİK ÖZELLİKLERİ

Filiz KARAÖMERLİOĞLU

DOKTORA TEZİ

FİZİK ANABİLİM DALI

Bu tez 31/01/2008 tarihinde aşağıdaki jüri üyeleri tarafından oy birliği / oy çokluğu ile kabul edilmiştir.

İmza Prof. Dr. Emirullah MEHMETOV Danışman	İmza Prof. Dr. Süleyman GÜNGÖR Üye

İmza Prof. Dr. Bahtiyar SALAMOV Üye	İmza Prof. Dr. Metin ÖZDEMİR Üye	İmza Doç. Dr. Turgut İKİZ Üye

Bu tez Enstitümüz **FİZİK** Anabilim Dalında hazırlanmıştır.
Kod No:

Prof. Dr. Aziz ERTUNÇ
Enstitü Müdürü

Bu Çalışma Ç. Ü. Bilimsel Araştırma Projeleri Birimi Tarafından Desteklenmiştir.

Proje No: **FEF2004D7**

ABSTRACT
PhD THESIS

OPTICAL PROPERTIES OF MULTILAYER ANTIREFLECTION COATING SYSTEMS ON A FERROELECTRIC BASE

Filiz KARAÖMERLİOĞLU

DEPARTMENT OF PHYSICS
INSTUTE OF NATURAL AND APPLIED SCIENCES
UNIVERSITY OF CUKUROVA

Advisor: Prof. Dr. Emirullah MEHMETOV
Year: 2008, Pages: 137
Jury: Prof. Dr. Emirullah MEHMETOV
Prof. Dr. Süleyman GÜNGÖR
Prof. Dr. Bahtiyar SALAMOV
Prof. Dr. Metin ÖZDEMİR
Assoc. Prof. Dr. Turgut İKİZ

Antireflection coatings have had the greatest impact on optics. Characteristics of the ferroelectric based multilayered antireflection coating systems are investigated. Multilayer antireflection coatings consisting of insulator thin films have been modeled in the region between 400 nm and 800 nm visible bands of electromagnetic spectrum to reduce reflectance from ferroelectric based substrate. In this type of antireflection coating we can regulate the optical properties of system by external electric or thermal field. In order to design and simulate the normal incidence wideband visible multilayer AR coatings we have developed a Fortran software program based upon Fresnell equations. It is used different types of layers which are two-different materials like ZnSe and ZrO_2 for even-folded multilayer (two-, four-, six-, eight-, ten-, and twelve-layer) antireflection coatings, and ZnSe, ZrO_2, and Ag_2AsS_3 for odd folded (three-, six-, nine-, and twelve-layer). It is used ferroelectric material, $LiNbO_3$ as the substrate. The optical thicknesses of each layer are equal to a quarter-wave thick at a certain wavelength.

Key Words: Multilayer, Antireflection Coating, Ferroelectric

ÖZ
DOKTORA TEZİ

FERROELEKTRİK TEMELLİ ÇOK KATMANLI YANSITMASIZ SİSTEMLERİN OPTİK ÖZELLİKLERİ

Filiz KARAÖMERLİOĞLU

ÇUKUROVA ÜNİVERSİTESİ
FEN BİLİMLERİ ENSTİTÜSÜ
FİZİK ANABİLİM DALI

Danışman: Prof. Dr. Emirullah MEHMETOV
Yıl: 2008, Sayfa: 137
Jüri: Prof. Dr. Emirullah MEHMETOV
Prof. Dr. Süleyman GÜNGÖR
Prof. Dr. Bahtiyar SALAMOV
Prof. Dr. Metin ÖZDEMİR
Doç. Dr. Turgut İKİZ

Yansıtmasız kaplamaların optikte muazzam etkileri vardır. Ferroelektrik tabanlı yansıtmasız kaplamalı çok katmanlı sistemlerin özellikleri incelendi. Yansıtmayı azaltmak amacıyla ferroelektrik alt tabana sahip yalıtkan ince filmlerden oluşan çok katmanlı yansıtmasız kaplamalar elektromanyetik spektrumun görünür bölgesinin 400 nm ile 800 nm arasındaki alanda tasarlandı. Bu tür yansıtmasız kaplamalarda sistemin optik özellilerini dış elektrik alan ile veya ısı ile kontrol edebiliriz. Çok katmalı yansıtmasız kaplamaları görünür bölge içinde dik gelme durumunda simülasyonunu yapabilmek için Fresnell denklemleri temelinde bir Fortran yazılım programı geliştirdik. Çift-katlı çok katmalı (iki, dört, altı, sekiz, on ve on iki katmanlı) yansıtmasız kaplamalar için ZnSe ve ZrO_2 malzemeleri, tek-katlı (üç, altı, dokuz ve on iki katmanlı) olanlar için ise ZnSe, ZrO_2, ve Ag_2AsS_3 malzemeleri kullanıldı. Alt taban olarak da ferroelektrik malzeme olan $LiNbO_3$ kullanıldı. Her bir tabakanın optik kalınlığı çeyrek-dalga kalınlığına eşittir.

Anahtar Kelimeler: Çok Katman, Yansıtmasız Kaplama, Ferroelektrik

ACKNOWLEDGEMENTS

I would like to express my gratitude to my advisor Prof. Dr. Emirullah MEHMETOV for all of his supports, guidance, suggestions, patience and encouragement on initiating, improving and completing this study.

I would also like to express my appreciation to Prof. Dr. Metin ÖZDEMİR for his kind cooperation, suggestions, and supports.

I would like to thank to Prof. Dr. Bahtiyar SALAMOV providing support to find articles, and for kind cooperation.

I would like to thank to Prof. Dr. Süleyman GÜNGÖR, and Assoc. Prof. Dr. Turgut İKİZ for their kind cooperation, and supports; and to Prof. Dr. Yüksel UFUKTEPE head of the Department of Physics for his supports.

I would like to thank to our group members, Assist. Prof. Dr. Faruk KARADAĞ, Assist. Prof. Dr. Süleyman ÇABUK for their kind cooperation, and supports.

I would like to thank to Academic Research Projects Unit of Cukurova University providing support to this work.

I would also like to thank to my parents İmran-İsmail Hakkı KARAÖMERLİOĞLU and my sisters Neşe and Deniz for their help, moral support, encouragement and patience.

CONTENTS **PAGE**

LIST OF FIGURES **PAGE**

LIST OF TABLES **PAGE**

LIST OF SYMBOLS

E	The Electric vector in Electromagnetic Field
H	The Magnetic vector in Electromagnetic Field
D	The Electric Displacement Vector
P	The Polarization
T_c	Curie Temperature
T_0	Transition Temperature
ε	The Permittivity of a Medium
ε_0	The Permittivity of Free Space, $8.85.10^{-12}$
η	Susceptibility
C	Curie Constant
V	The Applied Voltage
d	The Film Thickness
P_s	The Spontaneous Polarization
T	The Temperatures
I	Instantaneous Current
t_s	The Switching Time
X	The External Stress
p_0	A Reversible Microscopic Dipole
q	A Charge
η_0	The Refractive Index of Incident Medium
η_1	The Refractive Index of First Layer
η_2	The Refractive Index of Second Layer
η_3	The Refractive Index of Third Layer
η_4	The Refractive Index of Fourth Layer
η_s	The Refractive Index of Substrate
δ	The Phase Factor
λ	The Wavelength of The Light
θ_0	The Angle of Incidence in the Incident Medium

θ_1	The Angle of Oblique Incidence
N	The Complex Refractive Index, $N = n - ik$
n	The Real Part of The Refractive Index
Y	The Optical Admittance of a Surface or Multilayer
ρ	The Amplitude Reflection Coefficient
R	The Reflectance
T	The Transmittance
A	The Absorbtance
q	A Number of layers
M	A Product Matrix
B	A Normalized Electric Field Amplitude
C	A Normalized Magnetic Field Amplitude
$\mathscr{Y}$	The Admittance of Free Space
ϕ	The Phase Shift on Reflection
I	The Intensity of The Wave
λ_0	The Reference Wavelength
δ_r	The Phase Thickness of The r^{th} Layer
θ_r	The Incidence Angle of The r^{th} Layer
n_r	The Optical Admittance of The r^{th} Layer
η_p	The Optical Admittance for p-Polarization
η_s	The Optical Admittance for s-Polarization
$n(T)$	The Refractive Index Depend on Temperature on Ferroelectric Phase
$n(P)$	The Refractive Index Depend on Spontaneous Polarization on Ferroelectric Phase
$n(0)$	The Refractive Index on Non-Polar Phase
ΔP	The Polarization Difference on Ferroelectric Phase
$\lambda_0/4$	A Quarter-Wave Optical Thickness
H	Represents A Quarter-Wave of High Index
M	Represents A Quarter-Wave of Intermediate Index
L	Represents A Quarter-Wave of Low Index

a	Air
s	Substrate
n_H	The High Refractive Index
n_M	The Intermediate Refractive Index
n_L	The Low Refractive Index
n_s	The Refractive Index of Substrate
n_a	The Refractive Index of Air

1.INTRODUCTION

Antireflection coatings have had the greatest impact on optics; they still exceed all the other types of coatings. In some applications antireflection coatings are required for the reduction of surface reflections. In other not only reflection is reduced but also transmittance is increased considerably. As it is a known fact that radiations incident upon the surface of an optical material is separated into reflected, transmitted, absorbed and scattered fractions. The fraction of available energy that is distributed among these is determined by the refraction indices. Antireflection coatings can range from a single layer having virtually zero reflectance at just one wavelength, to a multilayer system of many layers having virtually zero reflectance over a wide spectral range (Asghar et al., 2003a).

Antireflection coatings are essential components of optical systems. A lot of books and many hundreds of papers and patents have been devoted to this coating. Multilayer optical coatings are successfully employed in various fields, such as optical and scientific instrumentation manufacturing, astronomy, spectroscopy, medicine, optical and electro-optical systems in telecommunications, consumer products etc. Because of military needs it is improved optical instruments ranging from binoculars to periscopes and bombsights in World War II. The growth in defense and aircraft industry is continued and also in the continuing growth in general optics, the enormous expansion of the chemical industry and its need for infrared and visible analytical tools, the need for narrowband contrast enhancing filters in astronomy, and then, very significantly, the laser. AR coatings have been widely used in many applications including glass lenses, eyeglasses, mirrors, solar cells, IR diodes, multipurpose broad and narrow band-pass filters, architectural and automotive glass and displays such as cathode ray tubes, as well as plasma, liquid crystal and flat panel displays. A great number of laboratories and experts are involved in designing and manufacturing modern optical coatings.

Nowadays, optical coatings are essential features of virtually all optical systems. A rapid development of optical systems and their applications in industry is necessary to study the lower reflection of the multilayer antireflection coatings in the

visible spectral region. It is significant to study multilayer antireflection coatings due to the wide use of this type of coatings in engineering practice. Multilayer antireflection coatings based on ferroelectric has not been studied till now and this subject is still current. Hence it is believed that the results of this study have practical importance owing to the military applications.

The goal of this thesis is to achieve a broader band visible antireflection coating design with multilayer structure that is, using multilayer antireflection coating to get zero reflectance at wavelength gap. The reflectance must be low enough so that even incident weak signals can be realized. There are two ways in order to reduce reflection further: making the optical characteristics of layers more sensitive using external effects; or using more than two materials. When this type of systems is developed, reflection is expressed with per thousands. If more than two different materials are used, it may not be preferable from the point of technology. Therefore, when we choose coating materials or substrate which is a sensitive material with temperature and/or external electrical field like ferroelectric materials, we can change refractive index of that material at $\lambda/4$ degree with small voltage-temperature difference which we applied to it just then. So, the same material shows like a material having two-different refractive index. Hence we accordingly change the film thicknesses simultaneously. Since the optical thicknesses of the layers, $n_j d_j$ are designated as fractions of $\lambda/4$, with λ_0 being a certain basic wavelength.

In this thesis, we theoretically investigated characteristics of ferroelectric based multilayer antireflection coatings which are consisted of insulator thin films in the visible spectral region. Through our analytical calculations, the major discussion is depended on the calculated reflectance with the optical matrix theory. The reflectance curves in the 400-800 nm visible region of electromagnetic spectrum for 2, 4, 6, 8, 10 and 12 layers, and for 3, 6, 9, and 12 layers have been simulated and plotted in Fortran program based upon Fresnell equations. The reflectance is nearly zero, but even if it is not a low reflectance, the important thing is that bandwidth is broad in the visible region of reflectance. In order to design visible multilayer antireflection coatings with the normal incidence wideband we used different types of layers which are two-different materials like zinc selenide (ZnSe) and zirconia

(ZrO_2) for even folded multilayer antireflection coatings, and ZnSe, ZrO_2, and proustite (Ag_2AsS_3) for odd folded, and the ferroelectric substrate, lithium niobate ($LiNbO_3$). Precise and accurate knowledge of the optical properties of $LiNbO_3$ based multilayer structure in the UV and visible regions is important because of the increasing application of the structure in optical and electro-optical devices, including planar optical waveguides and electro-optic and acousto-optic modulators. The reasons which we prefer these materials are that they are available and easily obtained, their price is reasonable and they don't react with each other while they are sensitive enough to external effects such as temperature and external electric field.

2. REVIEW OF LITERATURE

The history of optical coatings is a long one with many observations and publications but little industrial activity until a period of explosive growth began in the 1940s. The trigger was World War II and the need on all sides for improved optical instruments ranging from binoculars to periscopes and bombsights. After the war the growth continued, partly because of military needs, but much more because of other factors such as the continuing growth in general optics, the enormous expansion of the chemical industry and its need for infrared and visible analytical tools, the need for narrowband contrast enhancing filters in astronomy, and then, very significantly, the laser. Nowadays, optical coatings are indispensable features of virtually all optical systems (Macleod, 1999).

Early in the nineteenth century, Fraunhofer, investigated firstly an antireflection coating. At the same time, the combined efforts of first Young and then Fresnel finally succeeded in gaining acceptance for the wave theory. Then Poisson, in correspondence with Fresnel derived the multiple-beam interference in a thin film and explained the absentee effect of a half-wave thickness and the perfect antireflection action of a quarter-wave layer with an index of the square root of the product of the two surrounding indices. In 1936, John Strong produced antireflection coatings by evaporation of fluorite to give inhomogeneous films which reduced the reflectance of glass to visible light by 89%. In 1939, Walter Geffcken constructed the first thin-film metal-dielectric interference filters. A fascinating account of Geffcken's work is given by Thelen who describes Geffcken's search for improved antireflection coatings and his creation of the famous quarter-half-quarter design (Macleod, 1999).

Philip Baumeister drove the use of digital computers to design and analyze multilayer thin films, and led research across a broad range of optical coating application areas including synthesis and design, metrology and instrumentation and fabrication, especially UV filters and materials. George Dobrowolski established an international reputation developing mathematical techniques for thin film synthesis (Refermat, 2004).

It is clear that there was a good understanding of interference effects both in single layers and in multilayers the end of the nineteenth century. Turner's paper contains multilayer antireflection coatings, cold mirrors, narrow-band transmission filters, selective reflectors and frustrated total reflectance filters all of which were well advanced. Today there is still incredible progress in optical coatings (Macleod, 1999).

Many hundreds of papers for the design of multilayer, antireflection coatings, its computer programming, and industrial applications have been investigated in the past. It is considered some under heading as follows. In many researches it was used generally glass as a substrate, thick films for multilayer systems, different types of techniques and methods in infrared or ultraviolet region of electromagnetic spectrum, in laser investigations, and materials which its optical characteristics is destroyed and found with difficulty in terms of technologic. In order to satisfy of this lack, our investigation is improved. In our research it is not disrupted characteristics of optical system. It is selected more sensitive materials like ferroelectric materials to external effects, temperature and/or external electrical field; and these selected materials is easily found and cheap technologically.

2.1. Multilayer Thin Film Coatings

In all investigations, the various multilayer systems were considered. The optical constants of thin-film coating materials are determined. The principle of the new thin-film which was designed different infrared coatings is demonstrated. A new type of thin-film that is based on the effects of light interference is proposed. Theoretical analysis is discussed with experimental analysis. The basic results of these studies are described, and their applications to the synthesis are considered.

A generalized design method for an optical filter consisting of a dielectric multilayer structure is proposed. Fourier transform technique with frequency filtering for optical thin-film design is investigated.

Recent developments in thin-film coatings for optical communication systems are reviewed. Multilayer thin-film coatings are a proven technology that is employed in many areas of optical communication systems.

The equipment and methods used to produce antireflection coatings based on various materials are described. It has been discussed some novel concepts of designing broadband AR coatings. A new procedure of broadband multilayer antireflection coatings for semiconductor optoelectronic devices is designed. Antireflection coatings for both visible and far-infrared spectral regions are investigated. Antireflection coatings are calculated theoretically and practically on various devices. A number of equations relating to the multilayer antireflection coatings for a given wavelength are indicated.

Arndt et al. (1984) determined the optical constants of thin-film coating materials. The seven participating laboratories received films of two different thicknesses of scandium oxide (Sc_20_3-the dielectric coating material) and rhodium (Rh-the metal coating). All samples of each material were prepared in a single deposition run. Brief descriptions are given of the various methods used for determination of the optical constants of these coating materials. It is used Wideband Spectrophotometric Method, Modified Valeev Turning Point Method, The Nestell and Christy Method, Algebraic Inversion Method, Inverse Synthesis Method, Bennett and Booty Method, and Envelope Method in this paper. The measurement data are presented, and the results are compared. The mean of the variances of the Sc_20_3 refractive-index determinations in the 0.40-0.75 nm spectral region was 0.03. The corresponding variances for the refractive index and absorption coefficient of Rh were 0.35 and 0.26 respectively. It is very likely that different starting materials and preparation conditions contributed to the large departure of the optical constants published in this paper

Borgogno et al. (1984) investigated refractive index and inhomogeneity of thin films. The fact that the optical characteristics of thin-film materials are generally different from those of the same materials in bulk form is well known. The differences depend very much on the conditions in which the deposition has been carried out. A good understanding of these differences, their causes, and the

influence of deposition parameters is vital if it was to be able to improve coating quality. It has been developed two complementary methods with the objective of deriving information on the index of refraction and its variation throughout the thickness of the film. Perceptible optical inhomogeneity is normally present and appreciable inhomogeneity is frequently present in thin films. Such inhomogeneity is usually associated with layer microstructure. The first is a postdeposition technique. This technique makes use of measurements in air of the transmittance and reflectance of the layer under study over a wide wavelength region. The second, in contrast, makes use of in situ measurements that is measurements made under vacuum and during the actual deposition of the layer. It was shown with the help of several examples that the two methods lead to results which are consistent and demonstrate the existence in deposited materials of an inherent variation of the index of refraction normal to the surface. The thermal sensitivity of the layer properties and their tendency to adsorb atmospheric moisture must be taken into account before the residual differences between the two techniques can be explained.

The principal focus of Tikhonravov (1993) report is on the theoretical study of the properties of spectral coefficients in a complex wave-number plane. The basic results of the study are described. Their applications to the synthesis of a rugate filter and to inhomogeneous layer recognition problems are considered. General results concerning the existence of solutions to synthesis problems are also presented. The close analogy between synthesis problems in thin-film optics and optimal control problems is outlined, and some applications of Pontryagin's maximum principle are considered.

Analytical transformations of the refractive index open new possibilities in the experimental study of inhomogeneous layers with complicated refractive index profiles. Sophisticated mathematical methods elaborated for the solution of inverse problems can be readily implemented. It hopes that software based on these methods will be available shortly.

In connection with the question of the solvability of synthesis problems, the maximum principle was considered. This principle leads to the conclusion that optimal solutions are generally based on two materials with the highest and lowest

possible refractive indices. It should be noted that this mathematical principle expresses deep physical grounds. The desired spectral properties of optical coatings are obtained through properly arranged interference effects that are due to multiple reflections at the layer boundaries. With the increase in the refractive-index ratio, the average amplitudes of the reflected waves increase. This leads to an increase in the importance of the interference effects and makes it easier to achieve the desired spectral properties.

It should be mentioned that the conclusion about the optimality of two-material coatings was made without consideration of the total number of layers. When the reduction of the number of layers is important, the use of more than two materials will likely be preferable. The maximum principle does not impose any limitations on the possible values of the layer thicknesses. This means that rather thin layers may be required in optimal designs. However, it was shown by Sullivan and Dobrowolski that with up-to-date coating technology it is possible to produce quite complicated two-material coatings that consist of many layers, some of which are very thin.

Li and Dobrowolski (2000) investigated high-performance thin-film polarizing beam splitter (PBS) operating at angles greater than the critical angle. A new type of thin-film polarizing beam splitter is proposed that is based on the effects of light interference and frustrated total internal reflection. This PBS has a significantly better performance than conventional thin-film PBS's. It is nonabsorbing, broadband, and wide angle and has high extinction ratios in both the transmitted and the reflected beams. The principles and theory of this PBS are described in detail. Several PBS's designed for the visible and the infrared spectral regions are described. The measured results for a prototype visible PBS of this type are presented as well.

This new PBS is based on the effects of frustrated total internal reflection (FTIR) and of light interference in thin films. It is nonabsorbing, broadband, and wide angle and has high extinction ratios in both reflection and transmission. Compared with that of conventional thin-film polarizers and PBS's, the performance of the new PBS is several times or several orders of magnitude better.

Todorović et al. (2001) defined thermoelastic and electronic deformation components of photoacoustic signal in two-layer system. A model was derived in order to study the dependence of the photoacoustic signal on the thermal, elastic and carrier transport properties of two-layer samples. The various systems were considered: the conductor-semiconductor, the insulator-semiconductor and the semiconductor- semiconductor system. The semiconductor- semiconductor system is possible to take in consideration as a general configuration, where the other two are the special classes. In the theoretical analysis, thermodiffusion, thermoelastic and electronic deformation contributions have been used in order to interpret the photoacoustic effect in a two-layer system.

Results are presented for the second Optical Society of America's Optical Interference Coatings Manufacturing Problem by Dobrowolski et al. (2006b). The participants were asked to produce multilayer coatings which, in the 450–650 nm spectral regions and for light incident at 60°, would have transmittances of 0.7 and 0.3 for p- and s-polarized light, respectively. Three different teams each submitted four solutions. Three different deposition processes were used to produce these coatings. The smallest average departure from the target transmission values was 0.79%.

This paper describes the second Manufacturing Problem. The first was held in conjunction with the 2001 Banff Topical Meeting on Interference Coatings. The main aim of that problem was to see how closely it was possible, using different deposition methods, to produce a filter with quite complex spectral transmittance and reflectance curves specified for the 0.4–0.7 μm spectral region and for a near-normal angle of incidence. By specifying that (T+R) be equal to unity, the use of only nonabsorbing materials in the solutions was imposed. Six teams submitted a total of 11 different samples, most of which had a rms deviation from the target values that was less than 1.5%, with the best being 0.98%.

The aim of the present Manufacturing Problem was to find out how precisely a multilayer coating specified for an oblique angle of incidence could be produced experimentally. Furthermore, the implicit requirement that only nonabsorbing materials be used was removed. The intent was to encourage unusual solutions; to

that end, coatings on the second surface could also contribute to the solution. However, the evaluation of the samples became more difficult as a consequence of the specified highly oblique angle of incidence.

The optical parameters of a SiO_2 thin-film coating determined from the spectral reflectance and transmittance measurements at various incidence angles, including the normal incidence and the Brewster's angle, are compared in this paper by Lamminpää et al (2006). The high-accuracy measurements were carried out through visible near-infrared spectral regions by using our purpose-built instruments. The optical parameters obtained from the reflectance and the transmittance data are consistent over the angles of incidence and agree within 0.2%. The effect of important systematic factors in the oblique incidence spectrophotometric measurements is also discussed.

An interesting finding was that the optical thicknesses determined from the reflectance and the transmittance data were in a slightly worse agreement than the derived physical thicknesses and the refractive indices of the layer, if considered separately. However, taking into account that two different instruments were utilized in the reflectance and the transmittance measurements, this could be possibly attributed to a small discrepancy between the wavelength calibrations of these instruments.

2.1.1. Optical Filters

Verly (1995) developed Fourier transform technique with frequency filtering for optical thin-film design. A Fourier analysis of existing and potentially complex refractive index profiles is often useful in the resolution of thin-film design problems. Applications of a frequency-filtering technique, which consists of the suppression of undesired spatial frequencies from the refractive index profiles, are described. A new, extremely simple antireflection coating synthesis method based on this concept is proposed.

An increasing number of rugate filters (in principle a rugate filters is an interference coating based on a refractive index that varies continuously in the

direction perpendicular to the film plane), wavelets, or minus filters (an interference filter referred to as a minus filter, of the type that reflects a narrow wavelength band while transmitting the wavelength bands from both sides of the spectrum.) are progressively combined until a design with the desired optical performance is found. Viewed from a Fourier perspective, frequency components are gradually added to the Fourier spectrum of the refractive index profiles. The reflectance is also modified because the two types of spectra, Fourier and reflectance, are closely related.

A different and, in a sense, opposite approach is considered here. Given an existing and potentially complex thin-film solution, a Fourier domain analysis is performed and arbitrary frequency regions are examined separately. It is seen that this permits useful unconventional interpretations, gives insight into the problem, and produces interesting results. The concept of frequency filtering, already well known in signal and image processing, is applied to thin-film design. It consists of removing broad arbitrary frequency regions from the Fourier spectrum of the refractive index profile. Results obtained with this useful technique are described. In particular, a new method of AR coating design is proposed.

A generalized design method for an optical filter consisting of a dielectric multilayer structure is proposed to get an arbitrary profile of the wavelength dispersion of reflectivity or transmittance by Yamada and Yamane (1996). The basic concept of the method lies in the fact that the wavelength dispersion of the reflectivity is approximately determined by taking the inverse Fourier transformation of the refractive index profile of the multilayer structure. Construction of a filter with only three different values of refractive index is described.

An optical filter is a fundamental device in optoelectronics. Filters with a dielectric multilayer structure have been applied as, for examples, antireflecting coating facets and distributed Bragg reflectors (DBR) in a surface emitting laser. Most design methods for dielectric multilayer filters, however, are based on empirical knowledge of a given structure. Few general designs to obtain an arbitrary profile on the wavelength dispersion of reflectivity or transmittance have developed.

A gain-flattening filter (GFF) for minimum manufacturing errors (12 designs submitted) and dense wavelength-division multiplex (DWDM) filters for low group-

delay (GD) variation (9 designs submitted) was the subject of a design contest held in conjunction with the Optical Interference Coatings 2001 topical meeting of the Optical Society of America. Results of the contest are given and evaluated by Thelen et al. (2002). It turned out that the parameter space for GFFs with optimum performance when manufacturing errors are not considered is much different from that when manufacturing errors are considered. DWDM filter solutions with low GD variation are possible. The results are: (1) There appears to be no standard design technique for high manufacturing yield. (2) Gain-flattening filters designed for good merit function without consideration of manufacturing errors can have a manufacturing yield that is lower by as much as a factor of 5. (3) Gain-flattening filters designed for high yield that consider relative manufacturing errors do not automatically also have high yield when absolute manufacturing errors are considered. (4) An optimization technique that uses low layer sensitivities as targets would be a desirable component in the design of gain-flattening filters. (5) No contestant was able to design a single narrow-band filter with both good transmission intensity shape and low group-delay ripple. (6) By using two interference filters in series, one in transmission and one in reflection, one can design a filter combination with both good transmission intensity shape and low group-delay ripple.

2.1.2. Optical Communication Systems

Recent developments in thin-film coatings for optical communication systems are reviewed by Gerken and Miller (2004). Particular emphasis is given to thin-film designs with dispersion related to the photonic crystal superprism effect. A single dispersive coating may be used for multiplexing or demultiplexing several wavelength channels by spatial beam shifting.

Multilayer thin-film coatings are a proven technology that is employed in many areas of optical communication systems. New developments include the design of filters with a higher tolerance towards fabrication errors, tunable filters, and dispersive filters for dispersion compensation and wavelength multiplexing and demultiplexing. It was introduced an empirical model for estimating how many

wavelength channels can be demultiplexed using the spatial dispersion of a single thin-film coating. Eight to sixteen channels seem possible in the near future making this a promising component for cost-effective coarse wavelength division multiplexing (CWDM) systems.

2.1.3. Antireflection Coatings

Plasma-polymerized coatings of perfluorobutene-2 (PFB-2;CF_3-CF═CF-CF_3) were found to be effective single-layer antireflection coatings for polymethylmethacrylate (PMMA) by Wydeven and Kubacki (1976). In the range of 400-700 nm, light transmittance of these lenses, when coated on both sides with PFB-2, was about 4% higher than with uncoated lenses. Also, the transmittance curve of the coated lenses was essentially flat from 400 nm to 700 nm.

It was shown that plasma-polymerized PFB-2 coatings are effective single-layer antireflection coatings for PMMA substrates. Some advantages of the plasma technique for depositing antireflection coatings are (a) both sides of the substrate can be coated simultaneously, (b) the coatings are uniform in thickness for curved and flat surfaces, (c) it is a low temperature process, and (d) the deposition times required are short.

Mouchart (1977) developed thin film optical coatings. This study indicates a number of equations relating to the three-layer antireflection coatings for a given wavelength. The notation of coating stability is applied to define stable solutions with respect to film thicknesses or wavelength. As an example, an antireflection coating obtained independently of the central layer is discussed.

McLachlan (1978) investigated two-layer low-absorption antireflection coating for potassium chloride (KCI). This investigation reports the design, preparation, and performance of antireflection coatings on KCl laser windows for 10.6 μm wavelength that use the chalcogenide glasses As_2S_3 and $Ge_{45}Se_{55}$ as the coating materials. Absorption in the coatings was determined by laser calorimetry at a wavelength of 10.6 μm and found to be ~0.1%. Reflectance of the coatings was

also measured and found to be ~0.1%. The laser-induced damage threshold for pulsed $C0_2$-laser radiation was also determined.

Soileau (1980) analyzed mechanisms of laser-induced failure in antireflection-coated $LiNbO_3$ crystal. Substrate preparation before coating and coating cleanliness are the dominant factors affecting laser induced damage to antireflection-coated $LiNbO_3$. Careful control of these factors resulted in an order of magnitude improvements in the damage threshold to 15-20 GW/cm^2 at 30 nsec across the entire surface. In this work the mechanisms for laser-induced damage to AR-coated $LiNbO_3$ at 1.06 μm were studied. The experimental results indicate that the laser-induced failure limits for these coatings were determined by (a) substrate cleanliness, (b) linear absorption in the coating, and (c) cleanliness of the outer surface of the coating.

A method of forming a laser damage resistant wide-spectrum antireflective coating on fused silica and other glasses has been developed by Yoldas and Partlow (1984). The single-layer graded-index coating is deposited from a specific polymer solution which is converted to a porous SiO_2 film. The size of the pores in the film is first reduced by heat treatment to prevent eventual UV scattering. Refractive-index gradation is achieved by grading this non-scattering porosity using a mild etching agent to a depth which is sufficient to smooth the density transition from air to the substrate glass. The resultant coating provides antireflectivity over the entire transmission range of silica extending to wavelengths as short as 250 nm. Laser-damage thresholds as high as 9 J/cm^2 at 350 nm have been demonstrated for this coating on fused silica substrates, which makes it particularly suitable for the optics of high-power lasers.

Vassallo (1990) calculated theoretically and practically antireflection coatings on semiconductor laser diode optical amplifiers. The reflectivity of the end facet of a 3-D dielectric waveguide can be easily calculated, in case of weak guidance, by replacing the waveguide with a homogeneous medium of refractive index n_{eq} while the incident electric (or magnetic) field remains that of the guided mode. The calculation is done through a plane-wave expansion of the incident field; a practical algorithm is given to cope with multidielectric coatings. This process naturally

emerges when exact equations are expanded in terms of powers of the weak guidance parameter and it leads to a 1st-order approximation of the reflectivity (i.e. within 2nd-order error) when n_{eq} is suitably chosen. The facet can be normal or angular with respect to the waveguide axis.

Rancourt et al. (1991) have formulated a new design for an antireflection (AR) coating for use on the outside surface of solar cell covers and other devices. It is superior in both environmental durability and optical performance to the single layer magnesium fluoride (MgF_2). It can not be degraded by atomic oxygen since it consists entirely of stoichiometric oxide materials which have already been space qualified. Theoretical calculations show that the output of a silicon cell with this new AR coating on a silica cover can be increased by about 0.5% over that of a cover with a single layer AR coating.

Li et al. (1992) investigated antireflection coatings for both visible and far-infrared spectral regions. Two methods are described for the design of antireflection coatings that act in two widely separated spectral regions. One is based on the elimination of interface reflections, and the other is based on the use of extended buffer layers. Design results are presented for coatings on ZnS, ZnSe, and Ge substrates that reduce the reflectance in a broad region at ~10 μm, as well as in a band of wavelengths in the visible or near infrared part of the spectrum.

It has been shown theoretically and experimentally that it is possible to construct AR coatings on infrared substrate materials that operate in widely separated spectral regions. Fairly wide AR regions in the visible and in the infrared can also be achieved simultaneously. This improves the chances of a successful manufacture of the coating. The use of these more complex designs does not materially affect the overall deposition time and therefore should not substantially increase the cost of infrared AR coatings. Equations for the thicknesses of two-layer AR subsystems have been presented that are suitable for substrate and infrared coating materials with large extinction coefficients in the visible part of the spectrum. The starting design needs only a little refinement to achieve the desired performance.

Hellmich and Deimel (1992) improved optimal AR-coating for optical waveguide devices. The optimal index of refraction and thickness of an antireflection

coating layer for optical modes (TE/TM) had calculated in semiconductor laser devices. It has been taken into account various correction factors concerning the two-dimensional carrier gas, i.e., the change in photonic energy depending on the width of the quantum well, the resulting change in refractive indexes, and the change in effective masses of the carriers. The value $\sqrt{n_{eff}^{*}} - n_{eff}^{*}$ is the effective optical mode index–is compared to the exact calculated value for the optimal coating index.

It has been simplified an existing theory on optimal refractive indexes and thicknesses of an AR-coating layer on semiconductor laser devices. It has been considered various corrections resulting from the two-dimensional nature of the electron and hole gas for narrow active layers. The calculations show that for TE modes the optimal value for n_c, and the 'square root $n_{eff}^{'}$' value are astonishingly close, i.e., knowing the propagation constant β allows for a good guess of the AR-coating index. This is not true for TM modes. The normalized coating thickness for TM modes varies less than 1% over the active layer thicknesses considered-for TE modes this amounts to a maximum of 6%.

Braun and Jungerman (1995) presented broadband multilayer antireflection coating for semiconductor laser facets. Using a triple-layer antireflection coating of Al_2O_3, Si, and SiO_2, it has been achieved a minimum facet reflectivity of 1.10^{-6} and a bandwidth of 90 nm for a reflectivity of 5.10^{-5} or less for 1550 nm center-wavelength InGaAsP semiconductor lasers. A facet reflectivity of 3.10^{-6} and a bandwidth of 30 nm for a reflectivity of 5.10^{-5} were achieved for 1310 nm InGaAsP lasers. This coating is applicable to broadband external-cavity-tuned laser sources, edge-emitting light-emitting diodes, and semiconductor laser amplifiers. Theoretical calculations and measured results from a large number of coating runs are presented.

Lee et al. (1997) designed a new procedure of broadband multilayer antireflection coatings for semiconductor optoelectronic devices. The antireflection coating is the crucially important technology to obtain high performance in semiconductor laser amplifiers or external cavity modelocked lasers. In modern environment of device application to ultra-high bit rate WDM/TDM systems and/or their testing, achievement of ultralow reflectivity ($R \sim 10^{-5}$) at a very wide range of

wavelength is necessary. It was found that the conventional design by the optical admittance matching principle is not adequate to solve this compatibility problem.

An alternative design guideline was investigated here: (i) Rather than seeking for perfect matching, it is maximized the bandwidth that is defined by $R<R_{max}$, where R_{max}, is the maximum tolerable reflectivity; (ii) at the center wavelength, minimization of R is not required, so W-shaped reflectivity spectrum is acceptable. Another important consideration is the choice of dielectric materials. Insufficient controllability of deposition processes easily degrades the performance. Therefore a very careful process control was necessary for three material systems. This assumption is to use only established two materials, TiO_2, and SiO_2. Experimental trials and manufacturing tolerance considerations will also be presented.

Azzam et al. (2001) reported fourth- and sixth-order polarization aberrations of antireflection coated optical surfaces. For single-layer antireflection coated (ARC) optical surfaces, the first five derivatives of reflectance with respect to angle of incidence φ for the p- and s-polarizations are zero at normal incidence, whereas the first three derivatives of differential transmission phase shift $\Delta_t \left(= \Delta_{tp} - \Delta_{ts}\right)$ with respect to φ are also zero at φ=0. Consequently, ARC optical systems with numerical apertures of <0.7 (φ<45^o) exhibit fourth- and sixth-order polarization aberrations owing to retardance and diattenuation, respectively. Results for ARC Ge and ZnS surfaces are presented to illustrate these effects.

The coating of plastics for optical applications is intended to improve the mechanical durability of soft polymers and to serve an antireflection function by Schulz et al. (2002). Usually a classic four-layer antireflection system is added on top of a single-layer hard coating. With needle optimization, an alternative coating design has been developed. The design is characterized by thin high-refractive-index layers that are almost evenly distributed over the whole stack. Plasma ion-assisted deposition (IAD) was used to deposit coatings upon poly (methyl methacrylate) (PMMA), polycarbonate (PC), and cyclo-olefin copolymer (COC). Uniform antireflection and high scratch resistance have been achieved.

In contrast to common antireflection coatings, a new type of antireflection coating consists of a periodic arrangement of thin high-index layers and thicker low-

index layers. The periods may have an optical thickness of ~3λ/4 at the reference wavelength to achieve a broadband antireflective effect. Coatings of the new design type were deposited upon PMMA, COC, and PC by plasma IAD. The hardness of AR-hard coatings corresponds to that of single SiO_2 layers of the same thickness. With coatings on both sides of thermoplastic materials, transmission was increased uniformly to more than 98% in the visible spectral range. Low sensitivity of the AR-hard design type to systematic thickness errors of the high-index layers during deposition was observed. The low volume of high-index material inside coatings of the AR-hard type could be interesting also for use in other spectral regions.

Poitras and Dobrowolski (2004) performed a numerical investigation of antireflection coatings that reduce significantly the reflection over a wide range of wavelengths and angles of incidence, and it was proposed some experiments to demonstrate their feasibility. It is provided a theoretical description of omnidirectional antireflection coatings that are effective over a wide range of wavelengths. It was shown that to obtain a wide-angle AR coating one has to distort the thickness axis of traditional inhomogeneous transition-layer profiles. To obtain a coating that has a good performance for all angles of incidence as great as 89°, one would need the optical thickness of the coating to be of the order of 50λ_0 or more. During fabrication, the performance of such a coating would be especially sensitive to fabrication errors in the refractive index at the ambient side of the coating. If the inhomogeneous layer is approximated by a multilayer system and if interference effects caused by the finite Fresnel coefficients at the layer interfaces are exploited, it has been shown that the number of layers, and the overall thickness of the AR coating, can be significantly reduced, providing that one is willing to reduce the effective bandwidth of the resulting AR coating and accept some deterioration in its performance at angles close to 89°. The applicability of the multilayer AR coatings in cases of solid–solid and air–solid interfaces has been numerically studied. In the case of an air–solid interface, it was shown that it should be possible to fabricate a quasi-omnidirectional AR coating efficient at a specific wavelength, by use of the optical properties of materials around their reststrahlen bands in the mid-IR.

The equipment and methods used to produce wide-angle antireflection coatings based on Reststrahlen materials are described by Dobrowolski et al. (2006a). The optical constants of the coating materials used in the construction of the multilayers were determined by spectrophotometric ellipsometry and are compared with the literature values. The measured performance of an experimentally produced antireflection coating is compared with the expected calculated performance. The reflectance is low over a wide range of angles, but only in the narrow-wavelength region at which the refractive index of the Reststrahlen material is close to unity. Calculated results are presented for two different AR coatings based on this principle for the case of a Si–air interface. The optical constants of materials considered for the manufacture of these coatings are discussed. The design of a SiO_2-based AR coating is reoptimized by using experimentally determined optical constants. Various aspects of the thin-film deposition process are discussed.

Aroutiounian et al. (2006) investigated almost zero reflectance of a silicon oxynitride (SiO_xN_y)/porous silicon (PS) double layer antireflection coating for silicon photovoltaic cells. A reflectance spectrum calculation for a silicon oxynitride–porous silicon double layer antireflection coating is performed using the matrix method. The results are compared with the corresponding spectrum of diamond-like carbon (DLC)/PS and SiO_2/TiO_2 double layer coatings. A lower reflectance in the visible and infrared regions of the solar spectrum for the SiO_xN_y/PS double layer is obtained, especially in the 450–600 nm spectral range (with a flat reflectance response remaining as low as ≈0.01%), which corresponds to the maximum intensity of solar irradiation. These findings are of importance in solar cell applications.

Some novel concepts of designing antireflection (AR) coatings with equivalent layers are presented by Schallenberg (2006). Essential papers concerning thin-film optics and AR designs are cited, and the AR problem and a previously introduced AR-hard design type are discussed. Based on the known matrix formalism, a potential AR region, an equivalent stack index, and an equivalent substrate index are defined to use the theory of stop-band suppression as a starting point for the design of broadband AR coatings. The known multicycle AR design

type is identified as a typical solution to the AR problem if the presented approach is used.

It has been discussed some novel concepts of designing broadband AR coatings, and the progress in this matter can be concluded as follows: It is possible to substitute theoretically each refractive index of a step index profile, regardless of whether it is less than the given lowest refractive index, by using a stack of at least three quarter-wave (QW) layers. The QW stacks (QWS) of each step of the step-index concept can be identified with the cycles of the known multicycle AR coatings. The required AR bandwidth can be directly connected with the number of layers within the QWS approach. The performance of the residual reflectance within the AR bandwidth is determined by the number of the QWSs and profile steps. The theory of stop-band suppression serves as a basis of broadband AR design, but it can give only a starting point for realizing potential AR designs because asymmetrical QWS have to be used. An equivalent stack index (ESI) and the equivalent stack substrate (ESS) have to be used to synthesize the needed refractive indices. It seems possible to derive a straightforward algorithm to design broadband AR coatings analytically.

2.2. Computer Programming

The various methods for the synthesis of optical thin film systems are reviewed by Dobrowolski in 1960s. He and his colleague are described a computer program for the completely automatic design of optical thin film systems in many papers. Some basic properties of the main approaches to the determination of the optical constants of coating materials are discussed by Nilsson in 1968. Optical multilayer systems with different optimization procedures are demonstrated in 1990s. In the same year several types of multilayer coatings have been investigated in recent years using the computer programming by Verly and his associate. Tikhonravov et al. presented a new optimization algorithm for the synthesis of various optical coatings in 2006.

Antireflective coatings were simulated since 1990. A design algorithm based on a various technique is applied to design antireflection coating and the thin film design software is developed by Tikhonravov, Dobrowolski, Liou, Lee, and Lorch. Lee et al. proposed a novel design procedure of broad-band multilayer antireflection coatings for optical and optoelectronic devices in 1998. Asghar and his colleague has modeled multilayer antireflection coatings in visible and IR bands to reduce reflectance from various substrates in 2000s.

2.2.1. Computer Programming of Multilayer Coatings

The various methods for the synthesis of optical thin film systems with prescribed properties are reviewed by Dobrowolski (1965). One general approach is to refine numerically the properties of an initial system. In many problems, however, the choice of a suitable starting design for refinement is not at all obvious. The present paper describes a computer program for the completely automatic design of optical thin film systems by evolution which does not require a starting design. Apart from the specification of the desired optical properties of the system, the only input data necessary are the refractive indexes of the substrate, the medium, and the thin film materials that may be employed for the construction of the coating. Optical properties that may be specified at present include transmittance, reflectance, phase changes on transmission and reflection, and the first and second derivatives of these quantities with respect to wave number and angle of incidence. Several examples are given to illustrate the performance of this program. Ways are indicated in which this automatic design program was improved further in the future papers. The program was written in the Fortran language to facilitate its use on as many different computers as possible and to safeguard it from the obsolescence of computing equipment. It consists of a main program and a merit function subroutine program. The function of the former is to control the input/output of data and to direct the flow of the calculations. The subroutine program analyzes a multilayer coating and evaluates the merit function.

The reflection-transmission method for determining the optical constants of a film on a substrate has been examined and a computer program for the solution of the equation system has been written by Nilsson (1968). A new method involving only transmittance data in a limited wavelength region has been worked out and has been found to give accurate results. The computer program for this method gives directly n and k curves from the transmission curve. In this paper only the intensity methods at normal incidence is considered. The advantage of normal incidence is that nonflatness and contamination of the surface do not greatly influence the result. Further, those methods are non-sensitive to polarization effects of the optical system. The functional dependencies of n and k on R, R', and T for a film on a transparent substrate have been examined. Computer programs which compute the optical constants from various combinations have been worked out. It has been found that the combination of R and T is the best one. A method using only transmission data has been described and a computer program worked out. It shows that the optical constants obtained in this way are very accurate. This method gives results even when the other methods do not converge.

Dobrowolski and Lowe (1978) investigated optical thin film synthesis program based on the use of Fourier transforms. In Sossi's formulation of the Fourier transform (FT) method of optical multilayer design the refractive-index profile is derived for an inhomogeneous layer of infinite extent having the desired spectral transmittance. This layer is approximated by a finite system of discrete homogeneous layers. Because it does not make any assumptions about the refractive indices, thicknesses, or number of layers, it is the most powerful analytical method proposed so far. The method has been programmed for a computer and combined with other numerical design procedures. With the program it is possible to design filters with almost any desired transmittance characteristics using realistic refractive indices. This has been accomplished in the computer program developed at the National Research Council of Canada.

Dobrowolski and Piotrowski (1982) investigated refractive index as a variable in the numerical design of optical thin film systems. The role of the refractive index in the design of optical multilayer coatings is discussed. The theory

of the Herpin equivalent-index concept is reviewed. New results are presented for an extension of this concept. A computer program is described which automatically transforms a multilayer design utilizing many refractive indices into a system based on the use of two materials only. Experimental results are given to illustrate this. It is shown how, by the use of Herpin equivalent indices, computation time during thin film synthesis can be drastically reduced. It has been shown in this paper that the use of Herpin equivalent-index layers during the method of synthesis by gradual evolution leads to a reduction in computation time and therefore makes possible solutions that could not be obtained otherwise. The behavior of quasi-symmetric Herpin systems has been also investigated. A program has been described which for normal incidence of light converts a multilayer system consisting of many materials into a system made of two materials only but having equivalent spectral characteristics. It is quite possible that most filters will be made this way one day. The advantages of such an approach would be that one could employ material pairs whose optical constants are stable and well-known, that have a low porosity, that adhere well to the substrate, and, most important of all, are compatible with one another by having stresses that are similar in magnitude but opposite in sign. It is true that multilayer coatings of this type consist of more layers, some of which may be quite thin, but it is certain that ways will be found soon to produce such systems accurately.

A versatile method for determination of the optical constants is described that can be applied to a variety of coating materials by Dobrowolski et al. (1983). It is based on the use of an optical thin film synthesis program to adjust the constants of dispersion equations until a good fit is obtained between measured and calculated spectral transmittance and/or reflectance curves. The sensitivity of the determination can be increased by a suitable combination of measurement quantities. Because more than the minimum amount of data can be used, sensitivity to measurement errors and the chances of obtaining multiple solutions can both be reduced. To illustrate the method optical constants are determined of MgF_2, ZnS, MgO, Inconel, and Si films in the visible part of the spectrum and of indium tin oxide (ITO) films in the 0.4-12.0

μm range. It is used Single-Wavelength Methods, Multi-wavelength Methods, and Present Method for dielectric films, metal films, and semiconducting films.

The inverse-Fourier-transform and flip-flop thin-film synthesis methods are compared and contrasted by Dobrowolski (1986). Modifications to the flip-flop method are described which make it useful even for the solution of problems that require a large overall film thickness. The two methods were applied to a number of difficult problems. They yielded solutions that were different but of equivalent performance. When the inverse Fourier transform method is used to design a filter with complex spectral reflectance characteristics, no assumption need be made about the overall thickness of the filter. The method yields solutions based on thick and thin systems with equal facility. The solution can consist of an inhomogeneous film, or of multilayer based on many, or just two refractive indices. For best results the primary solution should be refined. The use of several starting designs and refractive index change directions in the flip-flop method reduces the chances of not finding a solution to a problem. Nevertheless, of the two methods described in this paper, it appears to be somewhat easier to foil. For example, the target curve corresponds to a stack of nine alternate $7\lambda/4$ layers of indices 2.35 and 1.35. The best result obtained with the flip-flop method falls short of that specification. This was despite the fact that the individual layers were $\lambda/4$ layers.

Dobrowolski and Kemp (1990) refined of optical multilayer systems with different optimization procedures. Ten different optimization methods, representing both local and global minimum seeking algorithms, were applied to the solution of three different optical thin film design problems. Because all methods were incorporated in the same thin film design program, and because a routine was invoked that reads CPU time, the relative efficiencies of the various methods could be compared directly. Name of used methods are: Adaptive Random Search, Damped Least Squares, Modified Gradient, Golden Section, Hooke and Jeeves Pattern Search, Basic Powell's Conjugate Search, Rosenbrock's Rotating Coordinates, Generalized Simulated Annealing, Monte Carlo Simulated Annealing, and Revised Nelder-Mead Simplex.

Several errors inherent to the Fourier transform method for optical thin film synthesis, including the inaccuracy of the spectral functions $\tilde{Q}(\sigma)$ used in the Fourier transform, are compensated numerically by using successive approximations by Verly and Dobrowolski (1990). It is shown that the complex phase of $\tilde{Q}(\sigma)$ is a key parameter which can be exploited to reduce significantly the thickness of the synthesized films and to control the shape of the refractive index profiles without affecting the spectral performance. This method is compared to other well established thin film design techniques. It is briefly reviewed the basic Fourier transform method and Sossi's correction process. It is described the modifications implemented in this version and the flow of the calculations in this computer program. Numerical examples are tested. The effects of several optional parameters are illustrated, and some limitations are pointed out. The performance of the process is compared with that of other well established techniques.

Li and Dobrowolski (1996) designed visible wide-angle, broadband polarizing beam splitters based on thin-film interference. A method is described for the design of a thin-film all-dielectric polarizing beam splitter in which the transmittances for p- and s-polarized light are greater than 0.96 and less than 0.03, respectively, throughout the spectral region extending from 0.40 to 0.70 μm, and for an angular field of 12° measured in air. The performances of known devices of this type are briefly reviewed. Some results obtained with this method are then presented. Finally, comments are made on the design of other, similar systems.

It has been shown that the method makes it possible to design wide-band, wide-angle polarizing beams splitters. It should be possible to apply the same method to find solutions to problems in which the spectral and angular properties required and the degree of polarization are intermediate to the ones presented here and to those of the MacNeille and Mouchart systems. Solutions based on other materials should also be possible. In particular, better performances are expected with prisms made of higher refractive index materials. When two identical beam-splitting prisms of the type are placed in series, they form an efficient wideband, wide-angle polarizer. A device of this type would therefore probably be of interest only for use

with high intensity lamps, with which heat absorption is a concern. Although the multilayer systems presented here are complicated, experience with monitoring techniques that employ real-time reoptimization leads to believe that the manufacture of such beam splitters is entirely feasible. The dispersion of the optical constants of the coating materials would have to be allowed for in the final designs. Numerical deposition simulations also indicate that there should be no problems in producing such systems by quartz crystal monitoring. The results of such calculations for the 72-layer system for p- and s-polarized light are shown on an expanded scale. The average merit function of the perturbed systems was 1.74, which represents a small increase over the1.43 value for the original system.

An efficient first-order algorithm with an exact calculation of the gradients is described and applied to the refinement of inhomogeneous dielectric thin films by Verly et al. (1997). Numerical results calculated at normal and oblique angles of incidence are correlated with an important mathematical theorem. It is shown that, when appropriate conditions are satisfied, the synthesis process generates binary-type solutions based on two materials, including classical multilayer.

Tikhonravov et al. (2006a) proposed new optimization algorithm for the synthesis of rugate optical coatings, an interference coating based on a refractive index that varies continuously in the direction perpendicular to the film plane. A model of a rugate coating that takes into account production potentialities of the Leybold Syrus Pro 1100 deposition system is presented. An efficient algorithm for the synthesis of rugate coatings is proposed. Numerical results are also presented. This algorithm does not imply any preliminary restriction on the shape of the rugate refractive-index profile except for the restrictions connected with the range of feasible refractive-index values. The algorithm enables one to perform a synthesis procedure with regularization to obtain smoothly varying rugate refractive-index profiles. It has been provided several examples to demonstrate that the proposed algorithm can be used successfully for the synthesis of rugate coatings with quite different target spectral characteristics. Classical rugate design problems can also be solved by using the proposed synthesis approach.

New optical coating design algorithm with the equivalent layers theory is presented by Tikhonravov et al. (2006b). The algorithm is based on the merit-function-constrained optimization in the accessible domain of equivalent phase thicknesses and equivalent refractive indices. It allows for creation of design coatings with sophisticated narrowband spectral characteristics. A core part of the proposed algorithm is the replacement of a prototype design with equivalent phase thicknesses and indices from the accessible domain by a two-component design with alternating high- and low-refractive-index values. It was shown that in general this replacement is a non-unique procedure. It is believed that this non-uniqueness can be used as a positive factor.

2.2.2. Computer Programming of Antireflection Coatings

An iterative correction process, recently incorporated into the National Research Council of Canada Fourier-transform thin-film synthesis program, is applied to the design of wideband antireflection coatings by Verly et al. (1992). This type of problem is different from those solved in the past by this method. It cannot be handled in a practical way without a correction process. It is considered in detail the effects-critical for this application-of constraints on the refractive indices and overall thicknesses of the solutions. This graded-index and multilayer designs have a remarkable resemblance in performance and refractive-index structure to results obtained by more conventional techniques. The Fourier-transform method is of interest because of its speed and versatility. It is discussed the effect of several important practical considerations on the Fourier-transform method: the constraints imposed by the refractive-index range available for the film materials, and the adjustment of the overall optical thicknesses. It is described the incorporation in the numerical correction process of a subroutine that yields multilayer directly.

A new method for the design of antireflection coatings is described by Tikhonravov and Dobrowolski (1993). A linearly constrained quadratic programming optimization procedure is used to find an inhomogeneous layer solution in the method. Because of a given overall thickness of the layer solution, it

corresponds to the global optimum for the problem. The refractive-index profile of this solution is then approximated by a two-material multilayer system that serves as a starting design for further numerical refinement. It was presented the theoretical basis for this method and discussed the effect of the various approximations made on the solution. Four different antireflection problems are solved to illustrate this new method.

There are many different methods for the design of AR coatings, including the use of exact analytical expressions for the thickness or refractive indices of one-, two-, or three-layer coatings for a single wavelength and angle of incidence. Other approaches include vector methods, analytical methods based on series expansions, numerical refinement and synthesis methods, and methods based on the inverse Fourier transform. Here it is sufficient to state that the question of how close a given AR coating is to the best possible coating has not been answered. This paper is a contribution toward deriving an answer to this interesting question.

Tikhonravov et al. (1996) experience with the application of the needle optimization technique to the design of optical coating is summarized. A physical interpretation of the technique is provided, and its main features are identified. Guidelines on the application of the needle optimization technique to various types of design problems are given. Examples presented in this paper demonstrate that the needle optimization technique is a universal synthesis technique applicable to the design of all types of optical coatings. It is interesting to note that the mean-square form of the merit function allows us to obtain results in the spectral region of interest that have only small deviations in the desired spectral characteristics. It was found that in all cases the reduction of ripples could be achieved by an increase in the wavelength grid density beyond a certain level. For wide spectral bands it is usually better to use nonuniform wavelength grids that are denser for shorter wavelength values (uniform in frequency space).

Dobrowolski and Sullivan (1996) investigated a universal antireflection coatings for substrates the visible spectral region. It is possible to design normal incidence antireflection coatings that reduce the reflectance of any substrate with a refractive index that lies in the range of 1.48 to 1.75. The performance of such

coatings depends on the width of the spectral region over which the reflectance is to be suppressed, on the coating materials used for their construction, and on the overall optical thickness of the layer system. For example, the calculated average spectral reflectance of a set of six different substrates with refractive indices 1.48, 1.55, 1.60, 1.65, 1.70, and 1.75 when coated with a 0.56-μm-thick, eight-layer antireflection coating designed for the 0.40-0.80-μm spectral region, was 0.34%. This is higher than the average reflectance that is accessible with a conventional antireflection coating of similar optical thicknesses designed for a particular refractive index. However, it is an acceptable value for most applications. With the universal type of antireflection coating described, it is thus possible to coat a number of different refractive-index substrates in one deposition run, and it can result in considerable cost and time savings.

Mathematical and computational evidence that strongly suggests that optimal solutions exist to single-band, normal-incidence antireflection coating problems is presented by Dobrowolski et al. (1996). It is shown that efficient synthesis and refinement techniques can quickly and accurately find such solutions. Several visible and infrared antireflection coating examples are presented to support this claim. Graphs that show the expected optimal performance for different representative substrates, refractive-index ratios, wavelength ranges, and overall optical thickness combinations are given. Typical designs exhibit a pronounced semiperiodic clustering of layers, which has also been observed in the past. Explanations of this phenomenon are proposed.

A novel design procedure of broad-band multilayer antireflection (AR) coatings for optical and optoelectronic devices is proposed by Lee et al (1998). The design algorithm is based on the optical admittance detuning, with the bandwidth of finite reflectivity as a new merit function. Coating structures consist of only two materials with nonquarter-wave thicknesses. Numerical mappings on the optimization of the four-layer AR coating using TiO_2 and SiO_2 showed that there are four candidate regions realizing broad bandwidths. Specifically for a 1.55-μm GaInAs/AlGaInAs MQW semiconductor laser facet, the bandwidth as broad as 106nm for $R<10^{-5}$ was predicted. Preliminary experiments on the four-layer AR

coating on glass and InP substrates showed the broad-band performance of the new design. For the glass and InP substrates, the bandwidths of about 217 and 185 nm were estimated for $R<10^{-4}$ by curve fitting the spectrophotometrically measured data. Although further refinements of the evaluation technique is needed, the results obtained here indicate that this design procedure is a promising approach to high-quality AR coatings.

A digital search technique based on the flip–flop method was applied to design a broadband antireflection coating using very thin high-, middle- and low-index layers by Liou (2002a). The optical performance of the average reflectivity over the visible region (from 400 to 750 nm) was 0.19%, which yielded a better result than the design using only very thin high- and low-index layers.

Liou (2002b) have designed broad-band normal-incidence antireflection coatings over the visible spectral region for a set of eight various substrates with indices 1.45, 1.50, 1.55, 1.60, 1.65, 1.70, 1.75 and 1.784. It is shown that the calculated average reflectance of the eighty-layer flip–flop antireflection coating design for substrates over the 400–750 nm spectral region can be reduced to less than 0.34%.

A design procedure of a broadband multiplayer antireflection coating is proposed by Liou (2003). The design algorithm based on the flip-flop operation of the indices of layers is used first, and the tuning operation of the thickness of layers is applied afterward to improve the performance and to simplify the structure of the final solution. The final design, obtained by the flip-flop tuning search technique of a three-material 100-layer system starting with low indices for all layers, is a nine-layer structure, and the average reflectivity over the visible spectral region is reduced to lower than 0.16%. It is shown that the structure designed by three-material flip-flop tuning is much simpler and its performance is better compared with the AR coating design obtained by the flip-flop synthesis method.

Lorch (2003) investigated theory and measuring of antireflection coatings. The characterization of antireflection (AR) coatings is not trivial. A preferred measurement method is the Hakki-Paoli method. But for broad-area lasers, an advanced method has to be used. One way is the measurement of the spectrally

resolved far-field; another is the use of single-mode ridge-waveguide lasers. Different AR coatings in the range of 10^{-1}–10^{-4} (fabricated by ion-beam sputter deposition) have been deposited on single-mode lasers and characterized successfully.

Asghar et al. (2003a) analysed modeling high performance multilayer antireflection coatings for visible and infrared (3-5 μm) substrates. Multilayer antireflection coatings have been modeled in visible and IR (3-5 μm) bands to reduce reflectance from glass, germanium (Ge), silicon (Si) and zincselenide (ZnSe) substrates. The transmittance of bare glass substrate is around 95% whereas for Ge 64%, Si 70%, ZnSe 84%. These values are enhanced reasonably by the application of multilayer films. Starting from a single layer, the layers have been added systematically forming multilayer structures to reduce reflectance considerably with each increasing layer. The designed layers are optimized for their performance by varying their thickness and refractive indices. The analysis of these modals has shown that the proposed multilayer structures are very effective in reducing the reflectance for all the substrates in two spectra.

Multilayer antireflection coatings have been designed and analyzed computer aided in visible spectrum by Asghar et al. (2003b). Multilayer antireflection coatings have been designed in visible spectrum (0.4-0.7 μ) to reduce the reflectance from a glass substrate (n=1.52). The transmittance of bare glass substrate is around 95%, which can be enhanced to ~99% for each optical component over the entire spectrum, for specific applications. Starting from a single layer, the layers have been added systematically to reduce the reflectance by the addition of each layer. A software code has been developed based upon the complex matrix calculation theory to design and analyze the multilayer thin film configurations on glass substrate. Care has been taken in the selection of coating material to ensure the use of materials, which are common in thin film industry world over. The designed layers are optimized for their performance by varying their thickness and refractive indices. The analysis of designed multilayer coatings has shown that the performance of these coatings has been considerably improved by an appreciable amount with an increase in the number of layers in a systemic manner.

Reflective and antireflective coatings were designed and simulated by Duyar and Durusoy (2004). Optical transmission and reflection values were deduced with a matrix formulation via a personal computer. It was found that the number of layers affects the optical performance. The width of the high-reflectance region in the reflectance curves decreases, while its height increases with the increasing number of layers for the reflective coating design. The antireflection coatings transmit about 99.89% in a broad high-pass band at the central wavelength of λ_0=450 nm. In addition, simulated Fabry-Perot filters result in a single sharp transmittance peak at the desired central wavelength. The half-width of the transmission band at central wavelength decreases and its peak height increases with the increasing number of the coated layers.

A search algorithm based on tuning iteration has been applied to design the normal-incidence broadband visible antireflection coating for crown glass substrates by Liou (2004a). It was shown that the average visible spectral reflectivity of the 40-layer tuning iteration designs was reduced to within approximately 0.067–0.077% with the structure of the final solutions reduced to about 10–12 layers.

A design procedure, based on the flip-flop tuning search algorithm, is applied to design universal visible antireflection coatings for various substrates with indices 1.45, 1.50, 1.55, 1.60, 1.65, 1.70, 1.75 and 1.784 by Liou (2004b). The universal broadband antireflection coating designs obtained by the flip-flop tuning method for a two-material and a three-material system with 80 sublayers of 300 nm thickness starting at high index and middle index lead to 10-layer structures, and the average reflectivity of these designs for the eight different substrates over the entire visible spectral region (400–750 nm) decrease to lower than 0.199% and 0.201%, respectively. Although the antireflection performance for each substrate is somewhat less than the optimum, it is acceptable for most applications.

A simple straightforward design algorithm based on the tuning iteration search is applied to design universal visible antireflection coatings for substrates with indices in the range of 1.45 to 1.784 by Liou (2004c). The method uses a two-material multilayer system starting with a binary code of alternating high and low indices and with all sublayers initially set at equal physical thickness. The

thicknesses of all layers are subsequently tuned one by one and one at a time to improve the average reflectivity over the visible spectral region until the antireflection performance stabilizes. It is found that the 30-layer tuning iteration designs for visible antireflection coating for a set of eight different substrates with indices 1.45, 1.50, 1.55, 1.60, 1.65, 1.70, 1.75 and 1.784 lead the final designs to 10–12 layer structures and the average visible spectral reflectivities for the substrates are reduced to approximately 0.173–0.190%. The visible AR performances for each substrate are less than the optimum values but are acceptable.

A design algorithm based on the minimizing search technique was proposed for designing the normal-incidence wideband visible or wideband infrared multilayer antireflection coating by Liou (2004d). The method utilized a tuning operation of the thickness of sublayers first, and then refined the antireflective performance and simplified the design by a layer minimizing operation. It was shown that the average visible spectral reflectivity of three-material thirty-layer and two-material thirty-layer minimizing search antireflection coating designs for glass substrates were reduced to less than 0.054% and 0.056% with a 12-layer structure, and the average infrared reflectivity of a two-material forty-layer minimizing search antireflection coating design for a germanium substrate over the broadband spectral region of 7.7–12.3 μm was reduced to less than 0.488% with a 22-layer structure.

A design method based on the minimizing search algorithm was applied to create universal wideband visible antireflection coating designs for commonly used substrates with refractive indices ranging from 1.45 to 1.784 by Liou (2004e). The minimizing search algorithm consists of a tuning operation of sublayer thickness and an eliminating operation of sublayers, which can refine the mean visible antireflection performance and simplify the design structure of the desired solution. It was shown that the two material 30-layer minimizing search for universal wideband visible antireflection coating designs of a set of eight different substrates with refractive indices of 1.45, 1.50, 1.55, 1.60, 1.65, 1.70, 1.75 and 1.784 were reduced to 12-layer structures and the average reflectivity for the eight different substrate systems over the visible spectral region were very coincident and were reduced to lie between 0.172–0.173%.

A simple straightforward method for achieving a wideband antireflection coating design over the visible spectral region was proposed by Liou (2004f). The design procedure utilized the tuning operation of the thickness of a two-material multilayer system first, and the exchanging operation of layers was applied afterward to refine the visible antireflection performance and simplify the design structure. An additional iteration process was used for the further improvement of the antireflection performance. It was shown that the two-material 30-layer iteration exchanging search for an antireflection coating design over the 400–750 nm spectral region was reduced to 16–20 layer structures, and their average visible spectral reflectivity were very good and reduced to approximately 0.032–0.033%.

A design algorithm based on a modified minimizing search technique is applied to design a visible antireflection coating for a wide angular incidence with an angle up to 30^{o} from the normal by Liou and Liu (2005a). The design approach consisting of tuning and minimizing operations is effective in refining the antireflective performance and simplifying the design structure of the desired solution. It is shown that the maximum wide angular visible spectral reflectance of minimizing search antireflection coating designs for a three-material 60 layer system is reduced to less than 0.490% with 15-21 layered structures, and the average visible spectral reflectance for each incident angle is reduced to below 0.137%.

A design algorithm, based on the exchanging search technique, was used for optimizing the visible antireflection coating design of substrates with refractive indices ranging from 1.45 to 1.784 by Liou and Liu (2005b). In this method, a tuning operation for the layer thicknesses of a two-material multilayer assembly was first carried out, followed by an exchanging operation for further refining the visible antireflection performance and simplifying the design structure. The average visible reflectivity of two-material thirty-layer exchanging search universal antireflection coating designs for a set of eight different substrates with indices 1.45, 1.50, 1.55, 1.60, 1.65, 1.70, 1.75 and 1.784 were reduced to approximately 0.172–0.174% with 12-14 layer structures.

A jumping search method is applied to the design of a normal-incidence antireflection coating for the 400-750 nm spectrum regions by Liou (2005). A search

algorithm that includes jump turning and optimal elimination is successively used to optimize the visible antireflection performance and to simplify the design structure. This method first makes use of layer-thickness jump tuning to reduce the visible-spectrum reflectivity and second uses an optimal elimination operation to reduce the layer number in order to simplify the design structure and further refine the AR performance of the system. The dispersion of optical constants and/or the slight aborting of the coating materials and substrate medium are taken into account in the calculations of the search process. It is shown that the average visible reflectivity of the jumping search antireflection coating designs of a two-material 40 layer system is reduced to approximately 0.064-0.079%, and the final designs are reduced to 14-16 layered structures.

Antireflection coatings (ARC) have been modeled and experimentally prepared for optical and electro-optical applications in the visible spectrum (0.4-0.7 μm) to reduce reflections from the surface of glass by Asghar et al. (2005). Reflection of BK7 bare glass substrate varies from 3.5 to 6.0% over the desired spectrum. This value is reduced reasonably by integrating multilayer thin films, based on dielectric materials, behaving as ARC. Three different three-layer configurations are deposited on glass substrate. The reflection profiles of theoretical and experimental curves are compared and analyzed to demonstrate the use of these multilayered structures. The physical parameters and deposition conditions of the three configurations are optimized before multilayer deposition. Matrix calculations determine the spectral transmittance and reflectance profile for multilayered structures on a substrate. Based on the matrix theory, it has been developed a software program to design and simulate the performance of multilayer coatings. The software is developed in visual C++. Basic parameters like individual layer thickness, design wavelength, refractive index of the layer, extinction coefficient, incident angle and spectral range are given as input to the software. The program then generates the out put in tabular and graphical form in terms of transmittance, reflectance and absorptance profiles. These input parameters can be varied to optimize the results and to carry out necessary variations in the design.

A jumping search algorithm is applied to achieve a broadband visible antireflection coating design for a wide-angular-incidence with an incident angle of up to 45^o from the normal by Liou (2006). It is shown that by the jumping search, the wide-angular visible AR coating designs of a two-material 20 layer system are reduced to 14 layer structures and their visible AR performances for the wide-angular-incidence range are highly comparable to each other. The maximum visible spectral reflectance of the final designs for incident angles lying in the range of 0-45^o is reduced to less than 0.869% and the maximum average visible spectral reflectance for every incident angle is suppressed to lower than 0.646%.

Two challenging optical thin-film filter design problems were devised for the 2004 Optical Interference Coatings topical meeting of the Optical Society of America by Tilsch et al. (2006). A total of 25 submissions were evaluated in the OIC 2004 Optical Filter Design Contest. A manufacturable, broadband, broad-angle antireflection (AR) coating for the visible (13 designs submitted) and a minimum-shift immersed short-pass filter (12 designs submitted) were the subjects of the design contest held in conjunction. Under the specified constraints, the broadband, broad-angle AR coating could be made more than 65 nm wide. The statistical stability of manufacturing simulations is discussed. The short-pass filter could operate up to a ±5.5° angular range. The submitted designs are described and evaluated.

2.3. Applications Towards Image Converter

In this review the characteristics of a coherent IR image converter for different materials are given. New models of incoherent-to-coherent IR image converter based on variant materials are discussed. Some recent results are summarized.

An experimental procedure is described by Schow et al. (1983). This procedure involves measurement of threshold values of infrared and upconverted powers for evaluating the quantum efficiency of a parametric upconverter. The threshold method is employed to determine the efficiency of a dye laser proustite

upconversion system. A new procedure of measuring efficiency with higher sensitivity is presented i.e., there are no requirements for using focused or high intensity beams. Furthermore, this technique can be used for determining the efficiency of systems designed for single beam or image upconversion. Such systems preferably employ image intensifiers rather than photomultiplier tubes for detection of the upconverted light. A threshold technique for measuring the quantum efficiency of a parametric upconversion system had illustrated. The method is particularly useful since the theoretical efficiency may be different from the actual value by several orders of magnitude.

Notni et al. (1992) reported a novel scheme for an incoherent-to-coherent converter by means of the selective erasure of the random dynamic gratings created by the beam-fanning process in $BaTiO_3$. Furthermore, the spatial resolution properties of a two-wave mixing incoherent-to-coherent converter are discussed in the geometrical limit, and using the two-dimensional two-wave mixing theory. Compared with using four-wave mixing (FWM) or two-wave mixing (TWM) this configuration is simpler. In order to investigate the resolution limits and degradation mechanisms of a TWM the photorefractive incoherent-to-coherent converter (PICOC), two-dimensional (2D) coupled-wave theory of TWM was used. A strong image distortions (asymmetric peaking) in the case of gain coefficients $\Gamma_0 d>4$ is founded. It is demonstrated that the resolution of a TWM PICOC is limited by a geometrical factor (inclination of the incoherent to the coherent beam) and by the erasure-contrast ratio.

A photorefractive incoherent-to-coherent optical converter (PICOC) is demonstrated by Sun et al. (1998); conversion is accomplished by anisotropic self-diffraction in $BaTiO_3$. The set up of the PICOC is easy, and only two writing beams are required. The diffraction efficiency reaches 50%, and resolution is 22 line pairs (lp)/mm in a typical-size crystal. Further, the resolution reaches 40 lp/mm when a $BaTiO_3$: Rh crystal of thickness 1.2 mm is used, and the diffraction efficiency is as high as 51%. The resolution of the PICOC can be increased effectively by reduction of the crystal thickness with no penalty for low diffraction efficiency.

Zhang et al. (1999) proved that high-resolution incoherent-to-coherent conversion can be carried out in an incoherent-to-coherent converter based on the photorefractive fanning effect. It was improved the resolution in two ways; one was to use a high-quality imaging system, and the other was to use a heavy doping crystal. Because the output coherent image has the same direction as the incident coherent beam, and thus the resolution is not limited by the grating diffraction. A resolution as high as 90.5 line pairs/mm in this experiment was obtained. The transmittance of the coherent beam relative to the intensity of the incoherent beam was measured. When the intensity ratio β of the incoherent beam to the coherent beam was less than 3, the noise and instability increased and the resolution decreased. It has been also demonstrated the ability of the method to convert an image with gray levels. From the experimental results it is believed that this method is effective for incoherent-to-coherent image conversion with gray levels. The resolving power with respect to the interaction length was also estimated theoretically by the Fourier optics method. The numerical results agree well with the experiments.

Wang et al. (1999) presented a new approach to incoherent-to-coherent optical conversion by means of azobenzene liquid-crystalline films. A new approach to incoherent-to-coherent optical conversion based on the erasing locally of the photo-induced birefringence is reported. The employed sample is an azobenzene liquid-crystalline film. This film possesses photoinduced birefringence of large magnitude and the characteristic of long-term optical storage. A steady birefringence is induced in the sample by linearly polarized light and then erased locally by an incident incoherent image. The coherent image is read from the film placed between two crossed polarizers with a He-Ne laser beam. The obtained coherent image is a negative replica of the incident scene. The incoherent-to-coherent image conversion by means of azobenzene liquid-crystalline films was realized. The spatial resolution of the readout coherent image is 31 lines/mm.

Salamov and Günen (2001a) researched the mechanisms of non-silver image recording in an infrared image converter with a semiconductor photodetector. In this study the influence of a low pressure discharge on the mechanisms of the image

recording on metallic Bi film (i.e. non-Ag photography) in an infrared image converter with a GaAs semiconductor photodetector is investigated. A part of the discharge energy is transferred to the electrodes of the system by the bombardment of the electrodes surface due to electron-ion flow. This process leads to the sputtering mechanisms of the electrode surface material. The analysis showed that the image formed on Bi film during discharge exposure was due to the formation of Bi_2O_3 on the surface. It is shown that, for the first time, the image recording on Bi film was primarily due to the effectiveness of sputtering and physicochemical interactions in the discharge gap during the transition from the Townsend discharge to the glow discharge type. Scanning electron microscopy analysis of the sputtering pits showed that the density of the sputtered material depends on the energy of the bombarding charged particles. This dependence can be explained by the assumption that effectiveness of sputtered process is proportional to the densities of both the electron and ion current and the stream of sputtered particles leaving the electrode surface.

Salamov et al. (2001b) developed coherent infrared image converter based on GaAs and $Bi_{12}SiO_{20}$ (BSO) crystals. A new model of incoherent-to-coherent IR image converter based on a GaAs photoconductor joined to an electro-optic (EO) BSO crystal has been analyzed theoretically and experimentally. The possibility of field transfer from the photoconductor to the EO crystal under infrared (IR) radiation sufficient for realization of the EO (Pockels) effect in the EO crystal was assessed. Based on the electric field parameters and parameters of the photoconductor and EO crystal, the threshold sensitivity of the converter was estimated. The experimental photoconductor-EO crystal structure by which IR radiation (0.9-1.5 μm) was converted into coherent visible radiation was obtained on the basis of theoretical calculations. The measured threshold sensitivity of the converter, 510^{-4} W/cm^2, was found to be in the limits of theoretical estimation. The good recognition results suggest that the advantages of this device, such as good grey-level reconstruction, make it an effective coherent infrared image converter.

Kurt et al. (2001) made an analysis of the image homogeneity in an ionization-type infrared image converter using the fractal dimension. This paper analyses the image homogeneity realized by recording the spatial distribution of the

gas discharge light emission in an ionization-type infrared (IR) image converter with a gallium arsenide semiconductor photodetector. The image of the photodetector material which contains the internal inhomogeneities is studied thoroughly at the optimum converter condition in order to image the large-diameter photodetector plates (100 mm) for nondestructive analysis. The analysis of the image homogeneity is determined by the fractal dimension of the gas discharge light emission when a current is passed through a converter cell. The images are analyzed using both the profile and spatial distribution light emission intensity data showing the internal inhomogeneity in the photodetector plate. Thus, by using the fractal concept, the image quality of the high resistivity photodetector plate can be assessed exactly and the size and location of the internal inhomogeneity in the photodetector plate can be ascertained. With the advent of sophisticated computer technology, conventional inspection methods can be replaced with imaging system. An effective imaging system must be compact and reasonably economic and have good contrast resolution, simple operation and routine availability. Relating to advances an image production, determination of the image quality is vital in defining the most appropriate physical parameter of the imaging system, making it possible to obtain, for instance, better contrast resolution, a less hazy image and a homogeneous appearance. Thus, in addition to the conventional image analysis methods, the fractal dimension method has been applied to identify the surface inhomogeneity of a photodetector plate. The fractal dimension method has been used to analyse quantitatively the image structure in an ionization-type IR image converter with a gallium arsenide semiconductor photodetector.

Incoherent-to-coherent conversion by use of the photorefractive beam-fanning effect and amplification by two-wave coupling have been demonstrated experimentally in a photorefractive $Ba_{1-x}Sr_xTiO_3$ crystal by Qiu et al. (2001). The converted coherent image is amplified by 60× for a coherent coupled beam of an average intensity of 300 mm/cm^2. The resolution of the amplified coherent image is ~28 line pairs/mm for an incoherent beam with an intensity of a few milliwatts per square centimetre. A notable advantage of the method is that incoherent-to-coherent conversion and coherence amplification of the converted coherent image are realized

simultaneously in a photorefractive crystal. In this method there are three beams: an incoherent beam and two uniform coherent beams (a coherent read beam and a coherent coupled beam). When the extraordinarily polarized coherent read beam is incident upon a photorefractive $Ba_{1-x}Sr_xTiO_3$ crystal, the intensity of its transmitted beam is very weak because of the photorefractive beam-fanning effect. When the incoherent beam is incident into the coupled region of the beam fanning, this coupled region is modulated by selective erasure. This results in the generation of a coherent positive replica of the incoherent image in the transmission of the coherent read beam. At the same time, if an extraordinarily-polarized coupled beam is directed into the region behind the coupled region of the beam fanning and interacts with the converted coherent image, the converted coherent image is enhanced by two-wave coupling.

Salamov et al. (2002) has analyzed theoretically and experimentally the new model of incoherent-to-coherent infrared (IR) image converter based on a GaAs photoconductor joined to an electro-optic (EO) $Bi_{12}SiO_{20}$ crystal. The possibility of field transfer from the photoconductor to the EO crystal under the IR radiation sufficient for realization of the EO (Pockels) effect in the EO crystal was assessed. Based on the electric field parameters and the parameters of the photoconductor and EO crystal, the threshold sensitivity of the converter was estimated. IR radiation (0.9-1.5 μm) was converted into the coherent visible radiation by the experimental photoconductor–EO crystal structure. This photoconductor–EO crystal structure was obtained on the basis of theoretical calculations. The measured threshold sensitivity of the converter, 510^{-4} Wcm^{-2}, was found to be in the limits of theoretical estimation.

Kurt et al. (2002) investigated filamentation of light emission in an infrared-visible image converter with a semiconductor photodetector. This work studies the light emission patterns associated with the spatial modulation of the transversal distribution of the current density in a converter cell with a GaAs semiconductor cathode. Such light emission exhibits spatial structures of current filaments depending on the feeding voltage, illumination intensity, gas pressure and the surface treatment of the electrodes. When the current is increased above the stable limit, breakdown or small current filamentations begin. However, *n*-GaAs exhibits an S-

shaped current-density-field relation due to impact ionization of carriers from shallow donors into the conduction band under high electric fields. The assessment of the filament formation is then based on analysis of the discharge light emission, recorded through a transparent anode. The filamentation was primarily due to the formation of a space charge of positive ions in the discharge gap. This changed the discharge from the Townsend to the glow type. Studies of the characteristics of such systems showed that current and light emission filamentation are strongly affected by the resolution of the IR images. By irradiating the semiconductor cathode with IR light it is possible to displace the filaments spatially. The width and the light density of the filaments are almost the same for a certain parameter set. The filament shape does not change with the system parameters. The results obtained can be used to improve the output characteristics of converters.

Salamov (2003) discussed dependence of the characteristics on the structure of a coherent infrared image converter. The characteristics of a coherent IR image converter that uses electro-absorption in a GaAs photoconductor (PC) and the electro-optic (EO) Pockels effect in a $Bi_{12}SiO_{20}$ (BSO) crystal has been analyzed theoretically and experimentally. An experimental PC-EO crystal structure was obtained on the basis of theoretical calculations. IR-radiation (0.9-1.7 μm) can be converted into coherent visible radiation by this PC-EO crystal structure. The measured threshold sensitivity of the converter, 510^{-4} W/cm^2, was found to be comparable to theoretical estimates. The limiting resolution of the readout image was about 10 lp/mm. The contrast ratio depends strongly on the change in the absorption coefficient and on the thickness of the GaAs PC. The change in the absorption coefficient is estimated by use of the quadratic equation of an applied electric field that is not excessively strong. Under this condition, an optimum thickness of the GaAs PC that will yield the maximum contrast ratio can be determined.

A new model of incoherent-to-coherent IR image converter based on a GaAs photoconductor (PC) joined to an electro-optic (EO) $Bi_{12}SiO_{20}$ (BSO) crystal has been analyzed theoretically and experimentally by Salamov B.G. et al. (2003a). The possibility of field transfer from the PC to the EO crystal under the infrared (IR) radiation sufficient for realization of the EO (Pockels) effect in the EO crystal was

assessed. Based on the electric field parameters and the parameters of the PC and EO crystal, the threshold sensitivity of the converter was estimated. The experimental PC-EO crystal structure was obtained on the basis of theoretical calculations. IR radiation (0.9-1.5 μm) was converted into the coherent visible radiation by this PC-EO crystal structure. The limiting resolution of readout image was about 10 lp/mm. The measured threshold sensitivity of the converter, 510^{-4} W/cm^2, was found to be in the limits of theoretical estimation. The results indicate that this device has the potential for use in a high-speed, high-contrast optically addressed spatial light modulators.

Salamov et al. (2003b) searched the spatial homogeneity of a large-diameter (100 mm) photodetector surface realized by recording the spatial distribution of the gas discharge light emission (DLE) in an ionization-type infrared image converter (ITIIC) with a GaAs photodetector. Analysis of the surface homogeneity is determined by the fractal dimension of the gas DLE when a current is passed through a converter cell. Fractal dimension estimation is found to be a powerful method because it enables both a non-destructive testing facility and use of the whole surface area of the photodetector surface in three dimensions. The effect on the roughness of the photodetector surface through plasma chemical processes at different experimental conditions was established. The effectiveness of the desorption process is proportional to the densities of bombarding particles as well as the stream of desorpted particles leaving the cathode surface. The surface images of the etched photodetector are analysed using both the profile and spatial distribution DLE intensity data showing the surface inhomogeneity in the photodetector plate. It is quantitatively concluded that plasma etching at certain experimental conditions can cause an improvement in surface homogeneity of the photodetector and spatial distribution DLE and ITIIC.

3. MATERIAL AND METHOD

3.1. Material

3.1.1. Principles of Ferroelectrics

We have to choose a material that is sensitive to temperature in this study. This type of material is pyroelecric [polar] material which is responsive to temperature. This material possesses a spontaneous electric polarization, P_s. The permanent electric dipole moment possessed by all pyroelectric materials may be reoriented by the application of an electric field. Internal electric field continues very long and do not vanish in a short time. Material is to be nonconductive, that is, internal electric field must be different from zero. Such materials are called ferroelectric. All ferroelectric crystals are necessarily both pyroelectric and piezoelectric. All pyroelectric materials are also piezoelectric. Many lose these polar properties at the transition or at Curie temperature, T_c. A nonpolar phase above T_c is the so-called paraelectric phase. Phase transition is very high in this type of materials i.e. ferroelectric materials pass from ferroelectric phase to paraelectric phase at very high temperatures. In summary, our material must be perfect insulator, be permanent and possess high polarization (spontaneous polarization is different from zero). $LiNbO_3$ possesses all these characteristics. In other words, $LiNbO_3$ is pyroelectric at room temperature, possess high transition temperature (1480 K), and possess high saturation polarization (50 $\mu C/cm^2$); and permanent polarization value of $LiNbO_3$ is P_s=70 $\mu C/cm^2$.

All features of ferroelectric materials are described in details below.

3.1.1.1. Characteristic Properties of Ferroelectrics

Ferroelectrics are materials which possess a spontaneous electric polarization P_s which can be reversed by applying a suitable electric field E. This process is known as switching, and is accompanied by hysteresis (Figure 3.1). In many ways

these materials are electrical analogues of ferromagnetics, in which the magnetization (*I*) may be reversed by a magnetic field (*H*). In some practical ways ferroelectrics differ from ferromagnetics, and in their fundamental mechanisms they are totally different (Burfoot, 1967).

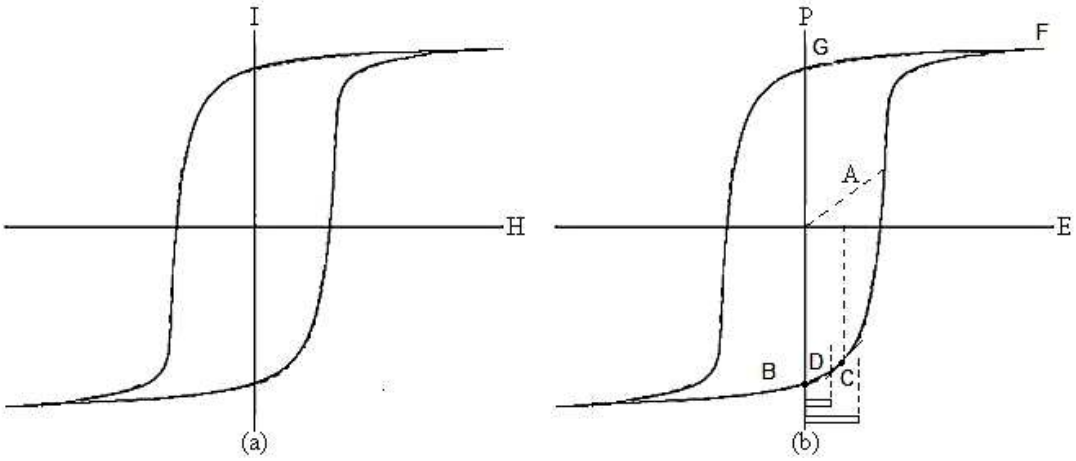

Figure 3.1. (a) Ferromagnetic and ferroelectric hysteresis loops, schematic.
(b) shows also the half-pulse and the full read-pulse used in matrix stores (Burfoot, 1967).

Ferroelectrics are all solids, and all are non-metallic. The properties of a ferroelectric are most simply studied when the material is in 'single-crystal form'.

Three properties of ferroelectrics are their reversible polarization, their 'anomalous' properties and their non-linearities. Most ferroelectrics cease to be ferroelectric above a temperature T_0 known as the 'transition temperature' (The characteristic temperature appearing in Curie-Weiss Law is written T_c, while T_0 means the transition temperature, and is not called 'Curie temperature'). The anomalous behaviour near T_0 is probably as significant as the reversible polarization, but it is not definitive of a ferroelectric. The permittivity ε rises sharply to a very high peak value at the temperature T_0; the very high values in this neighbourhood are referred to as anomalous values (See Figure 3.2). The permittivity values of most ferroelectrics are high even in temperature regions not close to T_0. The permittivity can be found by putting a pair of electrodes on the crystal and using any suitable a.c.

method of measuring the crystal capacity. The corresponding susceptibility η is given by the slope of the short, thick line B in Figure 3.1 (b). The relation is

$$\varepsilon=1+4\pi\eta \qquad \text{(CGS units)}$$
$$[\varepsilon=\varepsilon_0+\eta \qquad \text{(MKS units)}]$$

where ε_0, the permittivity of free space, has the value $8.85.10^{-12}$. These are incremental values, not to be confused with the value of a slope such as A in Figure 3.1 (a slope A would give the value of P/E; its value would depend very strongly on E, and would embrace negative values) (Burfoot, 1967).

Above the transition temperature T_0, the anomaly is frequently of the Curie-Weiss form

$$\varepsilon = \frac{4\pi C}{T - T_c}$$
$$[\varepsilon = \frac{C}{T - T_c} \qquad \text{MKS}]$$

to a good approximation. C is known as Curie constant. ε falls off rapidly below T_0. The value T_c usually coincides with T_0 in materials with first-order transition. In other materials T_c is a few degrees below T_0. In some cases (for example, alums), the ε values are not so high, and in others (for example, ammonium sulphate) the form of the anomaly above T_0 is not even approximately Curie-Weiss.

The dotted line in Figure 3.2 (a) gives an example of anisotropic dielectric behaviour. In some cases not all components of ε exhibit anomalies. That is, there may be no anomaly when the electroded faces of the crystal are in certain directions relative to the crystal axes (Burfoot, 1967).

The anomalous peak does not demonstrate conclusively that a particular material is ferroelectric. There are many other possible causes of such peaks. Figure 3.2 (a) and (c) show transitions which are first-order and second-order respectively. In practice it is not easy to distinguish first-order from second-order transitions; it is

difficult to say experimentally to what extent the transition is isothermal. Figure 3.2 shows the associated peaks in permittivity. If there is any out-of-phase response of the polarization to the measuring a.c., this implies dielectric loss (Burfoot, 1967).

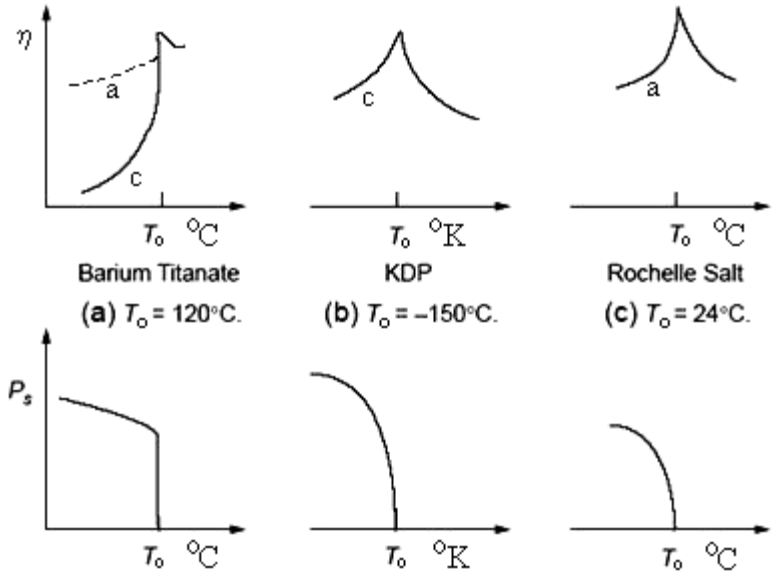

Figure 3.2. Susceptibility (upper diagram) and polarization (lower diagram), to show the electric anomaly and the order of transition, respectively. The letter on the curves shows the crystal direction in which the susceptibility was measured; there may be no anomaly in other directions. The diagram shows the logarithmic value. η_a is in the direction perpendicular to the spontaneous polarization (Burfoot, 1967).

The dielectric non-linearity is a significant characteristic of ferroelectrics. If the polarization created by an applied field E does not remain proportional to E as it increases, then an a.c. measurement of the permittivity will differ as the magnitude of the measuring voltage changes. Another practical expression of this concerns measurements made with sufficiently small measuring voltages, but with superimposed bias voltage. The measured permittivity changes with change of bias, because the slope c in Figure 3.1 (b) differs from the slope b. Examples of this change, above T_0, are shown in Figure 3.3. In studies of the underlying physics it is of more concern to express the non-linearity as a function of P. The non-linearity turns out to be very fundamental to ferroelectricity (Burfoot, 1967).

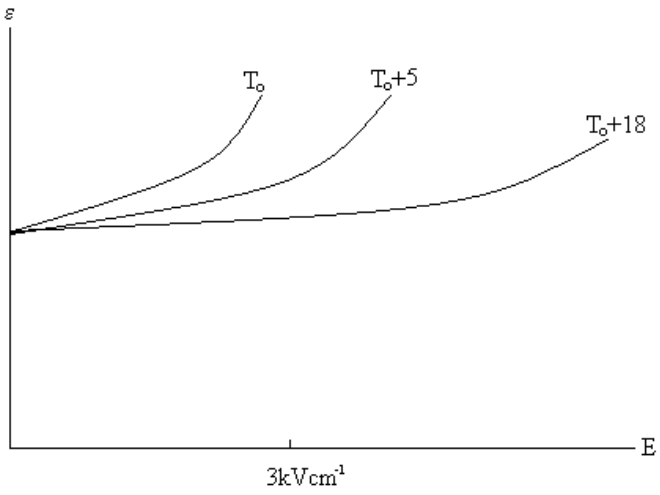

Figure 3.3. Non-linear permittivity in barium titanate, theoretical. The permittivity falls again for bias exceeding on $kVcm^{-1}$ (Burfoot, 1967).

Figure 3.1 above shows the process of switching. This hysteresis loop is usually displayed on an oscilloscope by means of a Sawyer Tower circuit (1930), (Figure 3.4). The most convenient specimen is a wafer-shaped crystal in which the polarization is directed through the thickness. Electrodes are evaporated on to the faces. The applied a.c. signal must be large enough to switch the crystal. The field is $E = V / d$, where V is the applied voltage and d is the crystal thickness (Burfoot, 1967).

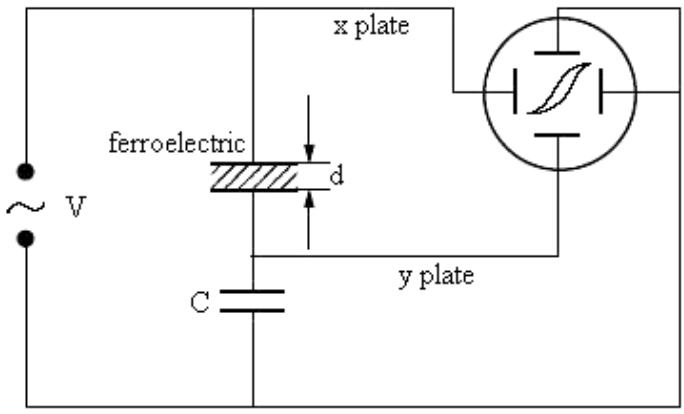

Figure 3.4. Sawyer Tower circuit for the display of the hysteresis loop. C may be $100\mu f$ (Burfoot, 1967).

The small impedance of the capacitor *C* scarcely reduces the signal applied across the crystal, so that the signal on the x-plates of the oscilloscope is proportional to *E*. Polarization, which is defined as the dipole moment per unit volume, is also equal to the surface charge per unit area if the electrodes are perpendicular to the polarization. Therefore, during switching, the charge released on the crystal surface at any instant is AΔ, where A is the electrode area and Δ is the change of *P* which has taken place at that instant. The instantaneous current, per unit area of each electrode, is $i = dP/dt$. The capacitor integrates this current so that the voltage on the y plates at any instant is $A\Delta/C$. The oscilloscope display is then a loop such as that shown in Figure 3.1 (b) (Burfoot, 1967).

If the series capacitor is replaced by a small series resistor *r*, the voltage across *r* will represent the switching current transient *i(t)*, which can be displayed on the oscilloscope, a convenient time base being used for the x signal. This function *i(t)* depends on the field value, so that the transient produced by a sinusoidal applied voltage is not very informative. Instead, a field is used which rises instantaneously to a fixed value *E*. The 'square' wave shown in Figure 3.5 (b) will give repetitive switching as shown, each transient being characteristic of the value *E*. The transient can then easily be displayed, as in Figure 3.5 (a), for detailed study (Burfoot, 1967).

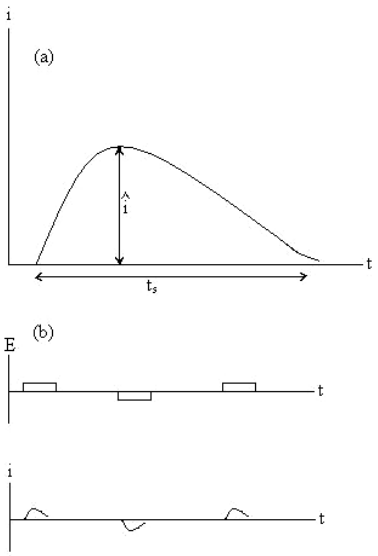

Figure 3.5. Switching transients. Showing characteristic parameters *i* and t_s. The current density is *i* (Burfoot, 1967).

The switching time t_s (Figure 3.5 (a)) are defined rather arbitrarily. For example, it is often taken to be the time at which the current i falls to 10 per cent of its maximum value i, or some similar criterion. When the value of E is changed, the value of the maximum current i increases, and the switching time t_s decreases. The shape of the switching transient $i(t)$ usually remains unaltered within wide limits. Such switching currents are referred to as having an affine form. Figure 3.6 shows Mertz's results (1956) for barium titanate. This field dependence has been expressed as

$$i \propto \frac{1}{t_s} \propto e^{-\alpha/E}$$

where α is of order 10 kVcm^{-1} (10^6 Vm^{-1}).

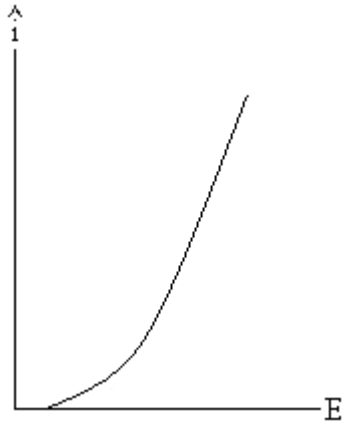

Figure 3.6. Dependence of switching current on field. The diagram shows the maximum value, i (Burfoot, 1967).

The value of spontaneous polarization can most easily be determined by examining the switching loop when it is displayed by means of a Sawyer Tower circuit. Values of P_s may also be determined from pyroelectric currents, which give a measure of dP_s/dT; if such currents can be measured in the neighbourhood of a number of temperatures T, up to T_0, the function $P_s(T)$ can be found. The pyroelectric current is a transient current passing through a suitable circuit connected between the electrodes on the crystal, when the crystal temperature is made to fluctuate about T.

The temperature fluctuation may be produced, for example, by means of a light-flash falling on the crystal or in other ways (Burfoot, 1967).

Spontaneous polarization is usually compensated by external charges, and its presence is only manifested when it is changed by field or temperature changes as described above.

3.1.1.1.(1). Properties of Piezoelectricity

Piezoelectricity is the property possessed by some crystals of acquiring electric polarization under external mechanical stresses, or the converse property of changing size or shape when subject to external electric fields E. The latter effect must be distinguished from electro-striction, which refers to deformations depend on E^2 rather than E (Burfoot, 1967).

There are many piezoelectric materials which are not ferroelectric, but all ferroelectrics are piezoelectric. In some ferroelectrics, the spontaneous polarization creates part of the piezoelectric effect. A possible classification of ferroelectrics is a division into those which are still piezoelectric above T_0, where they are no longer ferroelectric, and those which are not. One of the piezoelectric coefficients, b, gives the rate of change of strain with polarization (Burfoot, 1967).

Crystals (barium titanate, potassium dihydrogen phosphate, triglycine sulphate, Rochelle salt) are not still piezoelectric above T_0, the coefficient b is not constant, but is proportional to polarization. Therefore in this type of ferroelectric the piezoelectric effect would be zero if the spontaneous polarization vanished. The polarization 'creates' the piezoelectric coefficient b (Burfoot, 1967).

3.1.1.1.(2). Materials Properties

When it is possible to substitute one group of atoms, B, for another group, A, in a lattice, or to make extra groups B occupy interstitial positions in the crystal lattice A without breaking up the crystal lattice structure, B is said to be dissolved in A, and the resulting solid is a solid solution. The numbers of atoms of the solvent A

and solute B need not be in special integral ratios to achieve this; a whole range of concentrations is often possible. Then a continuous variation in the values of certain properties may be obtained by varying the concentration. An enormous variety is possible; cases of interest in a study of ferroelectrics include some where only one of the pure materials A and B is ferroelectric, and some where both are ferroelectric (Burfoot, 1967).

Many properties in ferroelectrics are observed not to have the form which would be expected in homogeneous material. This is often because there are domains. A ferroelectric domain is a macroscopic region in which the direction of the spontaneous polarization differs from that in adjacent domains.

The domain walls separating domains can move, inside each-single crystal, so that the domains grow or shrink.

A ferroelectric domain is a homogeneous region in a ferroelectric crystal. In each domain the polarization is in a different direction. The demarcation between two domains is called a domain wall and a wall is usually thought of as being so thin that it has a much smaller volume than the bulk material in the domains. A domain is an ordered region, the extent of the order in different domains often being the same, so that the magnitude of the polarization is the same in different domains, even though the direction is not. It is quite possible, however, for the magnitude also to differ, because of stresses and fields set up by neighbouring domains (Burfoot, 1967).

A single-crystal specimen may contain more than one domain, although by definition it cannot contain more than one crystallite. The single-crystal specimen has domain walls, but no grain boundaries. This distinction was illustrated in Figure 3.7. A domain wall does not interrupt the crystal lattice. The crystal lattice remains coherent through a wall, although it may be distorted by the wall. Yet in spite of this coherence, even the directions of the crystal axes can change in passing through a wall. Whether the directions do change, with walls of a particular type, depends on the crystal symmetry. It is not easy rigorously to define a single domain and a single crystal. Domains are related in a manner which is quite analogous to the relationship of crystallographic ‘twins’ (Burfoot, 1967).

In a polycrystalline material there may be several domains in each crystallite. The distinction between a crystallite interface and a domain wall is illustrated schematically in Figure 3.7. A domain wall does not interrupt the crystal lattice. Figure 3.7 (b) is over simplified, since it shows the lattice sites in no way modified by the presence of the wall. The differing polarizations, in fact, involve slightly differing sites for some ions within the lattice cell, and in many cases also a change of the cell shape. The latter effect will also occur in ferromagnetic materials (Burfoot, 1967).

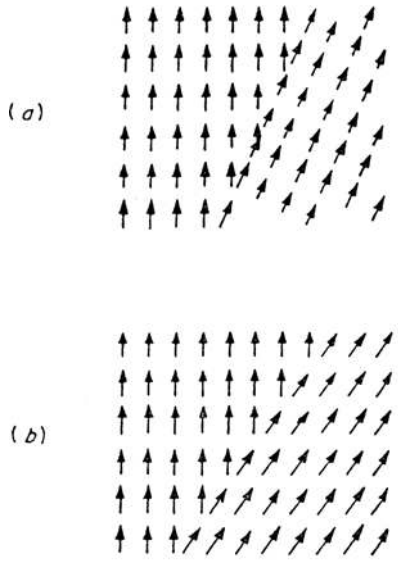

Figure 3.7. (a) A grain boundary and (b) a domain wall, respectively (schematic) (Burfoot, 1967).

Ceramic forms of solid materials are frequently used. The case of barium titanate may be given as an example of the manufacturing process. Ceramic specimens of barium titanate are made by grinding barium titanate, together with any required additive, and extruding or pressing it. This produces a complicated polycrystalline material, in which there are spaces known as pores; often, many of the crystallites will have grown together at their corners through a process of diffusion. The additives may be required to modify the properties, reducing the permittivity or the transition temperature, or may be used for technical reasons, for example, as fluxes to alter the growth-rate of the crystallites. Ceramics are hard, and

can be made any reasonable size and shape–blocks, discs or hollow cylinders–and up to several inches in size (Burfoot, 1967).

Some of the properties of a ceramic will differ from those of the corresponding single-crystal material. This is because the crystallites are randomly oriented, because many of them are under stress even when no external stress is applied and because of the porosity. A simple density factor will usually describe the property changes which are due to porosity. The transition temperature is usually not different in the ceramic form of the material, and this is true also of the specific heat and the Curie constants, except possibly for a porosity correction. In barium titanate, each of the crystallites has six possible directions for the polarization relative to its crystal axes, which themselves may lie in all directions. The actual polarization directions in the ceramic will be distributed at random among these six. But these may not always be so; special processing will produce special orientations. For example, an electric field applied at a suitable stage of the manufacture, or even, in some cases, applied to the cold product, will affect the distribution. This process is known as poling. It tends to encourage in each crystallite that direction which is nearest to the field direction. Such a process can not produce an overall polarization as large as that of the single crystal. It can be shown that, in principle, a maximum value of 84 per cent in barium titanate is possible. Stresses and porosity prevent this figure being reached; in practice a typical figure is 55 per cent whilst the field is applied and less when it is removed (Burfoot, 1967).

Similarly, values of piezoelectric coefficients occur which are about one-quarter of the single-crystal values, after suitable poling fields have been applied.

The direct effect of poling on the permittivity of a ceramic should be to change the permittivity towards the values appropriate to the single-crystal form. For example, in barium titanate a decrease would be expected in the permittivity value measured parallel to the poling field, since the single-crystal permittivity is smallest in the direction of P_s (See Figure 3.2). However, it seems there is also an opposite effect due to changes in the stresses acting on the crystallites, and this may well predominate (Burfoot, 1967).

It is easy to see that some crystal properties will be much affected by the different conditions existing in ceramics; other will not. For example, the overall P_s is an average over the various crystallites; if they are randomly oriented, the value will average out to zero. Similarly, an overall piezoelectric effect will be small, since a field lengthens some crystallites but shortens others. But the permittivity may not be much affected, because the measuring a.c. field (in a particular half-cycle) causes an increase of the polarization in some crystallites, but a decrease in others. The latter are those crystallites in which the polarization is oriented at an angle greater than 90^o to the field, so that the polarization change in the direction of the field is positive in all crystallites. That is, the quantity $\boldsymbol{\Delta}=\mathbf{P}-\mathbf{P_s}$ may be negative in some crystallites, but $\boldsymbol{\Delta}.\mathbf{E}$ is positive in all. If the single-crystal material is isotropic, $\boldsymbol{\Delta}$ is always parallel to **P**, and there should be no difference in permittivity, between ceramic and crystal, attributable directly to the orientations (Burfoot, 1967).

The properties of ceramics can be controlled. Desired values may be obtained by altering internal stresses through control of the state of sub-division (crystallite sizes) or by means of different annealing processes. In ceramic barium titanate, the permittivity increases as the crystallite size decreases. Additives can also alter the stresses. The addition of antimonates to barium titanate in preparing a ceramic reduces the permittivity peak. When strontium titanate is added to barium titanate, certain regularities of arrangement of the ions occur if the temperature conditions allow, because the strontium ions is 11 per cent smaller than the barium ion. A consequence is that T_0 differs according to the heat treatment given to the ceramic during manufacture (Burfoot, 1967).

3.1.1.2. Polarization in Crystals

3.1.1.2.(1). Polarization

Polarization P defined as dipole moment per unit volume. Polarization P may be measured in debyes per structural unit if the volume υ per structural unit is known. The polarization P is equal to the charge per unit area on any crystal surface

which happens to be perpendicular to the vector **P**. Therefore *P* is often quoted in microcoulombs per square centimeter (μcoul cm^{-2}). One microcoulomb is approximately 3000 e.s.u. (CGS unit) (Burfoot, 1967).

Ferroelectric materials are a subgroup of the pyroelectric materials. There are no ferroelectrics which are not pyroelectrics, just as there are no pyroelectrics which are not piezoelectrics. Polarization may be altered by changes in the external conditions. The terms dielectric, piezoelectric and pyroelectric refer to polarization changes which result from small changes of applied field, of stress, or of temperature respectively. These changes may be detected as currents in a suitable circuit attached to electrodes on the crystal (Burfoot, 1967).

Changes in the applied electric field *E* produce dielectric currents. The electric displacement **D** is given by

$$\mathbf{D} = \varepsilon_0 \mathbf{E} + \mathbf{P}$$
$$\varepsilon = \varepsilon_0 + \eta$$

where ε_0 is the permittivity of free space, $d\mathbf{D}/d\mathbf{E}$ is the permittivity ε, and dP/dE is the susceptibility η (Burfoot, 1967).

When the polarization is altered by a small change in the electric field *E*, the material is exhibiting its dielectric property. When the polarization is altered by a small change in the external stress *X*, including any changes in shear stress, the material is exhibiting its piezoelectric property. When the polarization is altered by a small change in the temperature *T*, the material is exhibiting its pyroelectric property. Pyroelectrics have finite polarization even at zero external fields *E* and stresses *X*, and this polarization is referred to as spontaneous polarization P_s. It is assumed that if P_s exists, then the material is pyroelectric, that is, that P_s will change with temperature. This is why materials with spontaneous polarization are called pyroelectrics (Burfoot, 1967).

Those piezoelectrics which are not also pyroelectrics must have zero polarization when both field *E* and stress *X* are zero. Dielectrics which are neither piezoelectric nor pyroelectric have zero polarization when the field *E* is zero.

Larger changes in the external conditions may change the crystal class. When a spontaneous polarization P_s exists, changes of temperature insufficient to change the crystal class will, in general, alter the value of P_s. Changes of stress X will also alter the polarization; changes of field E will also alter the polarization. Thus some dielectric crystals are piezoelectric, and some of the piezoelectric crystals are pyroelectric (Burfoot, 1967).

In some pyroelectrics, changes of field can reduce the polarization to zero and reverse it. This is switching the crystal, and these crystals, relatively few in number, are the ferroelectrics. Thus some of the pyroelectric crystals are ferroelectrics.

All crystals are classified according to their symmetry. Not all the crystal classes can possess spontaneous polarization. Only the polar classes may do so. In general, the non-polar classes have higher symmetry. It is not possible to tell which pyroelectrics can be switched, but if, under some more extreme change of conditions, a pyroelectric leaves the polar classes, and thus becomes more symmetric, it must then cease to be ferroelectric (Burfoot, 1967).

3.1.1.2.(2). Crystal Symmetry

There are 230 possible configurations for a crystal structure, which are based on the symmetry elements of translational position and orientation. These are known as the 230 space groups. If the translational repetitions are ignored, these 230 possibilities break down into 32 classes known as the 32 point groups. Therefore the points groups are based on the orientations only. A point group is a combination of symmetry elements (Burfoot, 1967).

An n-fold rotation axis may be taken as an example of a symmetry element. A crystal possessing this as one of its symmetry elements has an axis about which a rotation of $2\pi/n$ causes no recognizable difference. The term centro-symmetric provides another example. Any point may be described by coordinates x, y, z, with respect to the origin of symmetry. A centrosymmetric crystal is one in which a hypothetical operation which moves each point x, y, z, to −x, −y, −z, causes no recognizable difference. The symmetry of the macroscopic external form and

properties of a crystal is determined by the point group, and this is the basis of the classification into 32 crystal classes (Burfoot, 1967).

Symmetry considerations alone can show that some of the 32 crystal classes can not possess certain properties. For example, no crystal which is centro symmetric can possess a finite polarization. Any **P** vector would be inverted by the symmetric operation; this would give a recognizable difference, which is contrary to the postulated symmetry requirements. Therefore a crystal belonging to a centrosymmetric class can not be polar (Burfoot, 1967).

This is one example of Neumann's Principle, which may be stated: "The symmetry elements of any physical property of a crystal must include the symmetry elements of the point group of the crystal." The Principle does allow the symmetry elements of a physical property to include symmetry elements extra to those of the class of the crystal. Therefore a knowledge of the class of the given material may be sufficient to show that the material can not possess a certain property (such as coefficients of piezoelectricity), but it can never show that the material must possess a certain property. For example, any crystal belonging to a polar class can be a pyroelectric crystal, but pyroelectric property could, in principle, be of vanishing magnitude (Burfoot, 1967).

A ferroelectric unit is a microscopic component of the crystal. Although a microscopic component may possess certain symmetry elements, crystal class is defined as a macroscopic symmetry class; it is measurable macroscopically if it is found those special directions in the crystal in which a physical property takes identical values. Therefore in a given material, changes of crystal class are conceivable which do not involve alteration of the component. For example, the components may each possess a permanent dipole moment p_0, even in a non-polar crystal class. This can occur because, if the dipole moments are randomly oriented, then the macroscopic polarization P is zero. If a degree of orientation of the microscopic dipole moments sets in, a polarization P now exists. This may happen through a transition or phase change, without change of the magnitude p_0. The macroscopic crystal symmetry must have become lower; the crystal class has changed to a polar class. A material may changed its crystal class in this way under

changes of temperature, stress or field. For example, the ferroelectric mechanism in Rochelle salt is apparently related to the existence of two possible equilibrium positions for certain hydrogen atoms, which may be equivalent to a reversible microscopic dipole p_0 (Burfoot, 1967).

A point group is a combination of symmetry elements through the origin of symmetry. Table 3.1 shows the 32 point groups in Maguin-Hermann notation. The symbols given are the 'short' international symbols. The operations of rotations, etc., indicated cause no recognizable difference in the crystal. The key to the symbols is as follows:

For leading symbol:

- for *n* (=2, 3, 4, 6) read '*n*-fold rotation axis'.
- for $\bar{n}$ read '*n*-fold rotation (about the rotation axis) followed by inversion about the origin of symmetry'.
- *m* is equivalent to $\bar{2}$.

For non-leading symbol:

- for /*m* read 'with a mirror plane normal to the axis referred to before the oblique stroke'.
- for 2 (or *n*) read 'with a diad (or *n*-fold) axis normal to the axis which precedes the stroke'.
- for *m* read 'with a mirror plane parallel to the preceding axis'.

The Table shows also the further classification into seven crystal systems. For convenience, column 1 in Table 3.1 shows a further classification into three optical groups (Burfoot, 1967).

Table 3.1. The 32 Point Groups (Burfoot, 1967)

		Centrosymmetric		Non-Centrosymmetric				
				Polar		Not Polar		
Biaxial	Triclinic	$\bar{1}$		1				
	Monoclinic	2/*m*		2	*m*			
	Orthorhombic	*mmm*		*mm*2		222		
Uniaxial	Tetragonal	4/*m*	4/*mmm*	4	4*mm*	$\bar{4}$	$\bar{4}$2*m*	422
	Trigonal	$\bar{3}$	$\bar{3}$ *m*	3	3*m*		32	
	Hexagonal	6/*m*	6/*mmm*	6	6*mm*	$\bar{6}$	$\bar{6}$ *m*2	622
Optically isotropic	Cubic	*m*3	*m*3*m*			432	$\bar{4}$ 3*m*	23

The optical group refers to certain symmetry properties of the Indicatrix, an ellipsoid describing optical properties. It is possible for the ellipsoid to become more symmetrical at high frequencies, without any change in the macroscopic symmetry of the crystal. Therefore, strictly, column 1 describes the minimum symmetry of the optical property in the crystal system of column 2. An example is the orthorhombic crystal of Rochelle salt which becomes uniaxial (but of course still orthorhombic) at wavelengths shorter than 1.4 micron. That is, it is biaxial at some infrared wavelengths, but becomes optically more symmetric in the visible region (Burfoot, 1967).

3.1.1.2.(3). Crystal Classes

Twelve of the thirty-two crystal classes can be neither piezoelectric nor pyroelectric; these twelve are the centrosymmetric classes and class 432. A further ten can not be pyroelectric, and these are included in the last column of the Table 3.1; class 432 can not be pyroelectric either. The remaining ten are called the polar classes (Burfoot, 1967).

The word polar is used in many terms such as polar crystal, polar class, polar molecule or polar unit, and polar direction, and the meanings are not all quite obvious. A few examples will clarify these terms (Burfoot, 1967).

The example of Rochelle salt, above, shows that polar molecules or polar units do not necessarily form crystals in polar classes. Below T_0 the Rochelle salt crystal is monoclinic, class 2, which is one of the polar classes. There are reasons for supposing that, above T_0, the dipoles p_0 still effectively exist, but the lattice has now undergone a slight change to the more symmetric orthorhombic class 222, which is not one of the polar classes. Triglycine sulphate is also class 2 below T_0, and it seems probable that, again, permanent dipoles p_0 effectively exist, both below and above T_0. Yet, in triglycine sulphate above T_0 the macroscopic symmetry is even more striking. Triglycine sulphate above T_0 is monoclinic, class 2/*m*, which is one of the centrosymmetric classes, and therefore most certainly could not be polar, despite the existence of p_0 (Burfoot, 1967).

Polar class is a macroscopic concept. But the randomly arrangement of microscopic dipole units is nevertheless sometimes called polar, and polar crystal is often used to mean ionic crystal. An ionic crystal is one in which the microscopic units possess a charge q rather than a dipole moment. Both these usages refer to microscopic concepts. Use of the term 'polar crystal' to describe ionic crystals arose because of the nature of the bond between a pair of opposite charges; but the bonds in ionic crystals are not arranged in pairs (Burfoot, 1967).

Furthermore, there can be polar directions in non-polar classes. A polar direction is such that none of the symmetry operations appropriate to the crystal class will interchange the ends of this direction.

For example, the non-polar class 32 is that which has the following symmetry elements: a threefold rotation axis and three twofold rotation axes in the perpendicular plane, at 120^{o} intervals. Any of these three is a polar direction; that is, none of the rotations in the symmetry class 32 will interchange the ends of this direction (Burfoot, 1967).

It must not be supposed that non-centrosymmetric materials must at least have polar directions. For example, the class 222 has three perpendicular two-fold rotation axes. This class has no polar directions. But it certainly has no centre of symmetry, because under the symmetry operations implied by the three twofold axes a general point (x, y, z) moves successively to ($+x, -y, -z$) and then to ($-x, -y, +z$) but never to ($-x, -y, -z$) as a centre of symmetry would require it to do (Burfoot, 1967).

The symmetry principles discussed above apply to properties and to transitions in crystals in general, not only in ferroelectric crystals. However, ambiguities have been glossed over which are shown up rather well in the case of ferroelectric materials. Some of these can be seen from a closer look at Neumann's Principle (Burfoot, 1967).

Neumann's Principle refers to physical properties. A physical property may be defined as the response resulting from a given stimulus; elastic compliance is the physical property which is a measure of the strain resulting from a given applied stress; susceptibility is the polarization resulting from a given applied electric field,

and so on. Thus, according to this definition, strain and polarization are not physical properties in this sense. Therefore the strain and the polarization in a crystal do not have to conform to the crystal symmetry if they are caused by a stress, or by a field which does not conform. The spontaneous strain and polarization, however, do conform to the crystal symmetry, because this is defined when they already exist (Burfoot, 1967).

The value of a physical property is measured about specified values of temperature, stress and field. The crystal symmetry referred to in Neumann's Principle is the symmetry which exists before application of the stimulus, when temperature, stress and field have the values about which the property is to be measured. The crystal symmetry may be different during application of the stimulus (Burfoot, 1967).

The ferroelectric transition is accompanied by a change of symmetry, and takes place under specified conditions; usually zero external stress and field are specified. Two points arise which are of considerable interest and merit further discussion. They are the operational meaning of polarization and the defining symmetries in a ferroelectric crystal (Burfoot, 1967).

As so often happens, conceptual definitions and operational definitions are here ill-matched. Stress is defined by reference to a zero which is chosen for convenience, but polarization is defined with a zero which is apparently inflexible and unambiguous. However, although the concept is unambiguous, it would, in practice, be difficult or impossible to measure a polarization which could not be made to vary, and indeed it is only changes of polarization that it is able to be measured (Burfoot, 1967).

Ferroelectrics are a sub-group of the polar crystals, but relatively few polar crystals are ferroelectrics. Each ferroelectric structure is a slight distortion of a related non-polar structure, namely that structure which exists above the transition temperature T_0. Some materials exhibit a whole series of ferroelectric structures at different temperatures. Barium titanate is non-ferroelectric above 120 ^{o}C, but it becomes a tetragonal ferroelectric below 120 ^{o}C, an orthorhombic ferroelectric below 5 ^{o}C and a rhombohedral ferroelectric below –90 ^{o}C (Burfoot, 1967).

3.1.1.3. Structure and Ferroelectricity of $LiNbO_3$

Lithium niobate ($LiNbO_3$) possess a high Curie temperature (1210 ^oC). It is chemically stable and insoluble in water and in organic solvents. It has high mechanical Q_m and low acoustic losses, and has turned out to be excellent materials for high frequency transducer and surface acoustic wave (SAW) devices (Xu, 1991).

Lithium niobate ($LiNbO_3$) and lithium tantalate ($LiTaO_3$) have similar structures.

Currently, many devices, such as SAW devices, high-frequency and high-temperature transducers, infrared detectors, laser modulators, laser frequency multipliers, optical parameter oscillators, optical waveguides, high-frequency band-with filters, etc., are routinely being made with $LiNbO_3$ or $LiTaO_3$. Just for SAW devices in color TV's, several tons of $LiNbO_3$ single crystals are required every year (Xu, 1991).

$LiNbO_3$ is a colorless or light yellow crystal with a melting point of 1240±5 ^oC, a density of 4.64 g/cm^3 and with hardness 6 on Moh's hardness scale.

The structures of both $LiNbO_3$ and $LiTaO_3$ are displayed in Figure 3.8. The crystal structure of ABO_3 is composed of oxygen octahedra, and the neighboring oxygen octahedra are connected to each other through an oxygen ion that serves as a common 'tie-end'. In Figure 3.8 (a), lightly deformed oxygen octahedral aligned along the *c*-axis (threefold-axis) are shown. The cation arrangement follows the sequence Nb (or Ta), vacancy, Li, Nb (or Ta), vacancy, Li,…. A unit cell in a hexagonal lattice with the c-axis perpendicular to the paper is shown in Figure 3.8 (b). The symmetry of both crystals belongs to the point group 3*m* in the trigonal ferroelectric phase at room temperatures. The symmetry changes to the point group $\bar{3}m$ in the paraelectric phase above Curie temperature. At room temperature, the lattice parameters of the trigonal unit cell are a=5.4944 Å, α=55^{o}52' in $LiNbO_3$. Sometimes, it is more convenient to choose a hexagonal cell for description of its structure. In this case, the lattice parameters are a_H=5.1483 Å, c_H=13.8631 Å, (the subscript 'H' denotes hexagonal cell) in $LiNbO_3$.at 23 ^oC (Xu, 1991).

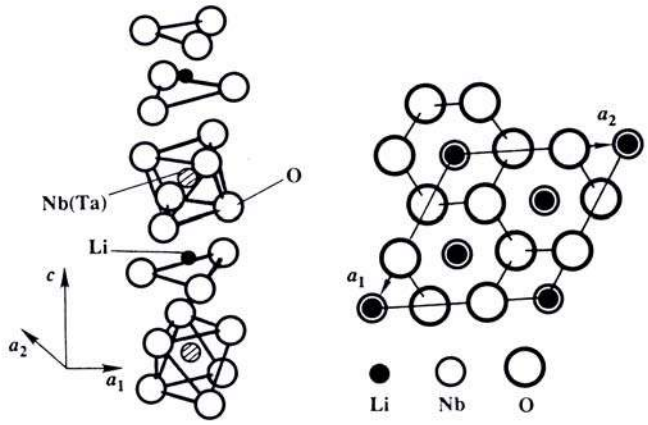

Figure 3.8. The structure of $LiNbO_3$: (a) Sequence of distorted oxygen octahedral along the polar c-axis; (b) one unit cell viewed from the top of the c-axis (Xu, 1991).

Ferroelectric-paraelectric phase transitions in $LiNbO_3$ are found to be second-order transitions, or to be 'very close to second-order' transitions, as seen from their dielectric, pyroelectric and thermal properties. The temperature dependence of their spontaneous polarization is just characteristic of second order phase transitions, in other words, P_s is proportional to $(T_c - T)^{1/2}$. However, in the vicinity of the Curie temperature, the variation of the dielectric constant obeys Curie-Weiss law, i.e., ε is proportional to $|T - T_c|^{-1}$. Curie-Weiss constants of magnitude 10^5K have been observed. This indicates that these phase transitions apparently have characteristics of displacement-type phase transitions (Xu, 1991).

In $LiNbO_3$, the direction of spontaneous polarization is the same as that of ion displacement, which coincides with the *c*-axis. As the temperature approaches the transition temperature of $LiNbO_3$ from below, Nb^{5+} ions move towards the centers of the oxygen octahedra, and Li^+ ions towards the nearest oxygen planes. Therefore, in the paraelectric phase, Nb^{5+} ions are just at those median positions between to nearest oxygen planes and spontaneous polarization disappears in the crystal. As the temperature comes down from the Curie point, observable cation displacements occur relative to the oxygen layer along the *c*-axis. An illustration of the displacements of Nb^{5+} and Li^+ ions before and after the ferroelectric phase transition

is shown in Figure 3.9. The direction of displacement of Nb^{5+} ions coincides with that of Li^{+} ions. At room temperature, the distance between a Nb^{5+} ion and its nearest oxygen plane is 0.9 Å, and that between a Nb^{5+} ion and its next-nearest neighbor oxygen plane is 1.41 Å. The corresponding distances for Li^{+} ions are 0.71 Å and 1.60 Å, respectively.

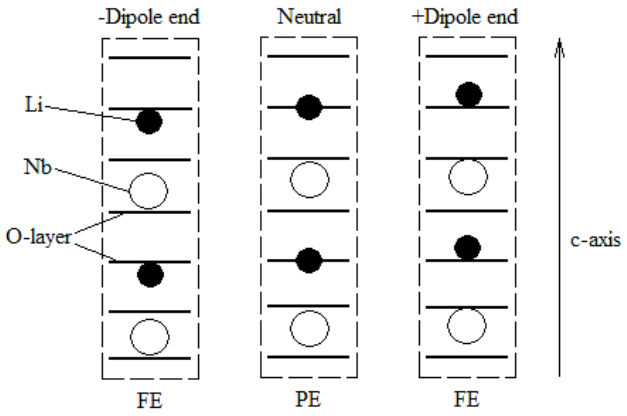

Figure 3.9. Oxygen layers and cations in the ferroelectric phase and the paraelectric phase of $LiNbO_3$: A full period along c-axis is shown (Xu, 1991).

From this data it can be calculated the relative ion displacements with respect to the mass center in a cell, between the structure at room temperature and that above the Curie point. This implies that a spontaneous polarization with a larger value occurs at room temperature. $LiNbO_3$, however, was considered a frozen ferroelectric, whose ferroelectric domains will not switch under and electric field in the conventional manner. The spontaneous polarization in $LiNbO_3$ was estimated to be at least of the order 50 $\mu C/cm^2$ from pyroelectric measurements and preliminary data on the temperature dependence of the non linear optical coefficient d_{33}. In fact, a P_s value of 70 $\mu C/cm^2$ has been observed at room temperature (Xu, 1991).

3.1.2. Theoretical Background

There is no systematic method for the design of antireflection coatings. Fundamentally, all the performance curves have been computed by application of the matrix method (Macleod, 1986).

We first reviewed basis principles and mathematical foundation of thin films. The reflectance, the transmittance and the absorptance of thin films are shown below in details. Then, antireflection coatings on high and low-index substrates features were reviewed by the matrix method.

3.1.2.1. Basic Theory of Optical Thin-Film

Basic theory is necessary in order to make calculations of the properties of multilayer thin-film coatings. A simple extension of the analysis occurs in the case of a thin, plane parallel film of material covering the surface of a substrate. The presence of two or more interfaces means that a number of beams will be produced by successive reflections and the properties of the film will be determined by the summation of these beams. It is said that the film is thin when interference effects can be detected in the reflected or transmitted light, that is, when the path difference between the beams is less than the coherence length of the light, and thick when the path difference is greater than the coherence length (Macleod, 1986).

3.1.2.1.(1). The Reflectance of a Thin-Film

The arrangement is illustrated in Figure 3.10. It is denoted waves in the direction of incidence by the symbol + (that is, positive-going) and waves in the opposite direction by – (that is, negative-going) (Macleod, 1986).

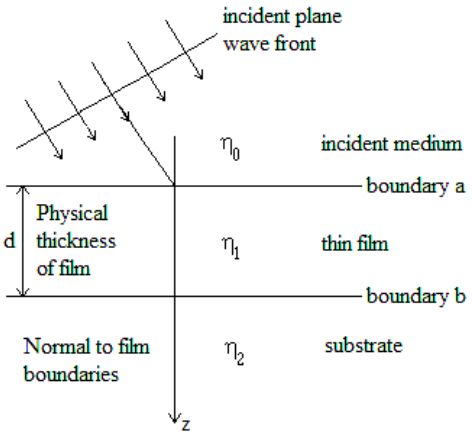

Figure 3.10. Plane wave incident on a thin film (Macleod, 1986).

The interface between the film and the substrate was denoted by the symbol *b*. It is considered the tangential components of the fields. There is no negative-going wave in the substrate and the waves in the film can be added into one resultant positive-going wave and one resultant negative-going wave (Macleod, 1986). At this interface the tangential components of **E** and **H** are

$$E_b = E_{1b}^{+} + E_{1b}^{-} \tag{3.1}$$

$$H_b = \eta_1 E_{1b}^{+} - \eta_1 E_{1b}^{-} \tag{3.2}$$

where it is being neglecting the common phase factors and where E_b and H_b represent the resultants. Hence

$$E_{1b}^{+} = \frac{1}{2}\left(H_b/\eta_1 + E_b\right) \tag{3.3}$$

$$E_{1b}^{-} = \frac{1}{2}\left(-H_b/\eta_1 + E_b\right) \tag{3.4}$$

$$H_{1b}^{+} = \eta_1 E_{1b}^{+} = \frac{1}{2}\left(H_b + \eta_1 E_b\right) \tag{3.5}$$

$$H_{1b}^{-} = -\eta_1 E_{1b}^{-} = \frac{1}{2}\left(H_b - \eta_1 E_b\right). \tag{3.6}$$

The fields at the other interface *a* at the same instant and at a point with identical *x* and *y* coordinates can be determined by altering the phase factors of the waves to allow for a shift in the *z* coordinate from 0 to *–d*. The phase factor of the positive-going wave will be multiplied by $\exp(i\delta)$ where

$$\delta = 2\pi N_1 d \cos\theta_1 / \lambda \tag{3.7}$$

and θ_1 may be complex, while negative-going phase factor will be multiplied by $\exp(-i\delta)$ (Macleod, 1986). The values of *E* and *H* at the interface are using equations (3.3)-(3.6),

$$E_{1a}^{+} = E_{1b}^{+} e^{i\delta} = \frac{1}{2}\left(H_b/\eta_1 + E_b\right)e^{i\delta}$$
$$E_{1a}^{-} = E_{1b}^{-} e^{-i\delta} = \frac{1}{2}\left(-H_b/\eta_1 + E_b\right)e^{-i\delta}$$
$$H_{1a}^{+} = H_{1b}^{+} e^{i\delta} = \frac{1}{2}\left(H_b + \eta_1 E_b\right)e^{i\delta}$$
$$H_{1a}^{-} = H_{1b}^{-} e^{-i\delta} = \frac{1}{2}\left(H_b - \eta_1 E_b\right)e^{-i\delta}$$

so that

$$\begin{aligned} E_a &= E_{1a}^{+} + E_{1a}^{-} \\ &= E_b\left(\frac{e^{i\delta} + e^{-i\delta}}{2}\right) + H_b\left(\frac{e^{i\delta} - e^{-i\delta}}{2\eta_1}\right) \\ &= E_b \cos\delta + H_b \frac{i\sin\delta}{\eta_1} \end{aligned}$$

$$\begin{aligned} H_a &= H_{1a}^{+} + H_{1a}^{-} \\ &= E_b \eta_1 \left(\frac{e^{i\delta} - e^{-i\delta}}{2} \right) + H_b \left(\frac{e^{i\delta} + e^{-i\delta}}{2} \right). \\ &= E_b i\eta_1 \sin\delta + H_b \cos\delta \end{aligned}$$

This can be written in matrix notation as

$$\begin{bmatrix} E_a \\ H_a \end{bmatrix} = \begin{bmatrix} \cos\delta & \left(i\,\mathrm{s}in\delta\right)/\eta_1 \\ i\eta_1\,\mathrm{s}in\delta & \cos\delta \end{bmatrix} \begin{bmatrix} E_b \\ H_b \end{bmatrix}. \tag{3.8}$$

Since the tangential components of **E** and **H** are continuous across *a* boundary, and since there is only a positive-going wave in the substrate, this relationship connects the tangential components of **E** and **H** at the incident interface with the tangential components of **E** and **H** which are transmitted through the final interface. The 2×2 matrix on the right-hand side of equation (3.8) is known as the characteristic matrix of the thin film (Macleod, 1986).

The input optical admittance of assembly is defined as

$$Y = H_a / E_a \tag{3.9}$$

The reflectance of a simple interface between an incident medium of admittance η_0 and a medium of admittance Y is i.e.

$$\rho = \frac{\eta_0 - Y}{\eta_0 + Y}$$

$$R = \left(\frac{\eta_0 - Y}{\eta_0 + Y} \right) \left(\frac{\eta_0 - Y}{\eta_0 + Y} \right)^{*}. \tag{3.10}$$

Equation (3.8) can be written

$$E_a \begin{bmatrix} 1 \\ Y \end{bmatrix} = \begin{bmatrix} \cos\delta & (i\,\mathrm{s}in\delta)/\eta_1 \\ i\eta_1\,\mathrm{s}in\delta & \cos\delta \end{bmatrix} \begin{bmatrix} 1 \\ \eta_2 \end{bmatrix} E_b \tag{3.11}$$

which gives

$$Y = \frac{\eta_2 \cos\delta + i\eta_1 \sin\delta}{\cos\delta + i(\eta_2/\eta_1)\sin\delta}$$

Normally, Y is the parameter which is of interest and the matrix product on the right-hand side of equation (3.11) gives sufficient information for calculating it:

$$\begin{bmatrix} B \\ C \end{bmatrix} = \begin{bmatrix} \cos\delta & (i\,\mathrm{s}in\delta)/\eta_1 \\ i\eta_1\,\mathrm{s}in\delta & \cos\delta \end{bmatrix} \begin{bmatrix} 1 \\ \eta_2 \end{bmatrix} \tag{3.12}$$

where

$$\begin{bmatrix} B \\ C \end{bmatrix}$$

is defined as the characteristic matrix of the assembly . Clearly, $Y = C/B$.

3.1.2.1.(2). The Reflectance of an Assembly of Thin-Films

Let another film be added to the single film so that the final interface is denoted by *c*, as shown in Figure 3.11. The characteristic matrix of the film nearest the substrate is

$$\begin{bmatrix} \cos\delta_2 & (i\sin\delta_2)/\eta_2 \\ i\eta_2 \sin\delta_2 & \cos\delta_2 \end{bmatrix}$$

and from equation (3.4)

$$\begin{bmatrix} E_b \\ H_b \end{bmatrix} = \begin{bmatrix} \cos\delta_2 & (i\sin\delta_2)/\eta_2 \\ i\eta_2 \sin\delta_2 & \cos\delta_2 \end{bmatrix} \begin{bmatrix} E_c \\ H_c \end{bmatrix}. \tag{3.13}$$

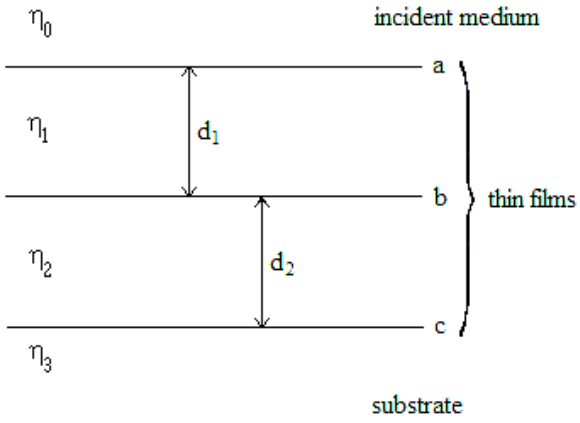

Figure 3.11. Notation for two films on a surface (Macleod, 1986).

It can be applied equation (3.4) again to give the parameters at interface *a*, i.e.

$$\begin{bmatrix} E_a \\ H_a \end{bmatrix} = \begin{bmatrix} \cos\delta_1 & (i\sin\delta_1)/\eta_1 \\ i\eta_1 \sin\delta_1 & \cos\delta_1 \end{bmatrix} \begin{bmatrix} \cos\delta_2 & (i\sin\delta_2)/\eta_2 \\ i\eta_2 \sin\delta_2 & \cos\delta_2 \end{bmatrix} \begin{bmatrix} E_c \\ H_c \end{bmatrix} \tag{3.14}$$

and the characteristic matrix of the assembly is

$$\begin{bmatrix} B \\ C \end{bmatrix} = \begin{bmatrix} \cos\delta_1 & (i\sin\delta_1)/\eta_1 \\ i\eta_1 \sin\delta_1 & \cos\delta_1 \end{bmatrix} \begin{bmatrix} \cos\delta_2 & (i\sin\delta_2)/\eta_2 \\ i\eta_2 \sin\delta_2 & \cos\delta_2 \end{bmatrix} \begin{bmatrix} 1 \\ \eta_3 \end{bmatrix}. \tag{3.15}$$

Y is C/B, and the amplitude reflection coefficient and the reflectance are, from equation (3.10),

$$\rho = \frac{\eta_0 - Y}{\eta_0 + Y}$$

$$R = \left(\frac{\eta_0 - Y}{\eta_0 + Y}\right)\left(\frac{\eta_0 - Y}{\eta_0 + Y}\right)^* .$$

This result can be immediately extended to the general case of an assembly of q layers, when the characteristic matrix is simply the product of the individual matrices taken in the correct order, that is,

$$\begin{bmatrix} B \\ C \end{bmatrix} = \left(\prod_{r=1}^{q} \begin{bmatrix} \cos\delta_r & (i\,\mathrm{s}in\delta_r)/\eta_r \\ i\eta_r\,\mathrm{s}in\delta_r & \cos\delta_r \end{bmatrix} \right) \begin{bmatrix} 1 \\ \eta_s \end{bmatrix} \tag{3.16}$$

i.e.

$$\begin{bmatrix} B \\ C \end{bmatrix} = \mathrm{M} \begin{bmatrix} 1 \\ \eta_s \end{bmatrix}$$

where M is a product matrix given by

$$\mathrm{M} = [\mathrm{M}_1][\mathrm{M}_2]...[\mathrm{M}_a][\mathrm{M}_b][\mathrm{M}_c]...[\mathrm{M}_p][\mathrm{M}_q]$$

and where

$$\delta_r = \frac{2\pi N_r d_r \cos\theta_r}{\lambda}$$

$\eta_r = \mathscr{Y} N_r \cos\theta_r$ for s-polarization (TE)

$\eta_r = \mathscr{Y} N_r / \cos\theta_r$ for p-polarization (TM)

and where it has been used the suffix s to denote the substrate or exit medium (Macleod, 1986).

$$\eta_s = \mathscr{Y} N_s \cos\theta_s \qquad \text{for s-polarization (TE)}$$
$$\eta_s = \frac{\mathscr{Y} N_s}{\cos\theta_s} \qquad \text{for p-polarization (TM)} .$$

If θ_0, the angle of incidence, is given, the values of θ_r can be found from Snell's law, i.e.

$$N_0 \sin\theta_0 = N_r \sin\theta_r = N_s \sin\theta_s . \tag{3.17}$$

A useful property of the characteristic matrix of a thin film is that the determined is unity. This means that the determinant of the product of any number of these matrices is also unity (Macleod, 1986).

It avoids difficulties over signs and quadrants if, in the case of absorbing media, the scheme used for computing phase thicknesses and admittances is:

$$\delta_r = \left(2\pi/\lambda\right) d_r \left(n_r^2 - k_r^2 - n_0^2 \sin^2\theta_0 - 2in_r k_r\right)^{1/2} \tag{3.18}$$

the correct solution being in the fourth quadrant. Then

$$\eta_{rs} = \mathscr{Y} \left(n_r^2 - k_r^2 - n_0^2 \sin^2\theta_0 - 2in_r k_r\right)^{1/2} \tag{3.19}$$

and

$$\eta_{rp} = \frac{y_r^2}{\eta_{rs}} = \frac{\mathscr{Y}^2 \left(n_r - ik_r\right)^2}{\eta_{rs}} \tag{3.20}$$

It is useful to examine the phase shift associated with the reflected beam. Let $Y = a + ib$. Then with η_0 real

$$\rho = \frac{\eta_0 - a - ib}{\eta_0 + a + ib} = \frac{\left(\eta_0^2 - a^2 - b^2\right) - i\left(2b\eta_0\right)}{\left(\eta_0 + a\right)^2 + b^2}$$

i.e.

$$\tan\phi = \frac{\left(-2b\eta_0\right)}{\left(\eta_0^2 - a^2 - b^2\right)} \tag{3.21}$$

where ϕ is the phase shift (Macleod, 1986).

3.1.2.1.(3). Reflectance, Transmittance and Absorptance

Sufficient information is included in equation (3.16) to allow the transmittance and absorptance of a thin film assembly to be calculated. To have a physical meaning, the incident medium should be transparent, that is, η_0 must be real.

First of all, it is calculated the net intensity at the exit side of the assembly, which it is taken as the k^{th} interface (Macleod, 1986). This is given by

$$I_k = \frac{1}{2}\mathrm{Re}\left(E_k H_k^*\right) \tag{3.22}$$

where it is being dealt with the component of intensity normal to the interfaces.

$$\begin{aligned} I_k &= \frac{1}{2}\mathrm{Re}\left(E_k \eta_s^* E_k^*\right) \\ &= \frac{1}{2}\mathrm{Re}\left(\eta_s\right) E_k E_k^* \end{aligned} \tag{3.23}$$

If the characteristic matrix of the assembly is

$$\begin{bmatrix} B \\ C \end{bmatrix}$$

then the net intensity at the entrance to the assembly is

$$I_{\mathrm{a}} = \frac{1}{2}\mathrm{Re}\left(BC^*\right) E_k E_k^* . \tag{3.24}$$

Let the incident intensity be denoted by I_i; then equation (3.24) represents the intensity actually entering the assembly, which is $\left(1-R\right) I_i$:

$$\left(1-R\right) I_i = \frac{1}{2}\mathrm{Re}\left(BC^*\right) E_k E_k^*$$

i.e.

$$I_i = \frac{\mathrm{Re}\left(BC^*\right) E_k E_k^*}{2\left(1-R\right)} \tag{3.25}$$

Equation (3.23) represents the intensity leaving the assembly and entering the substrate and so the transmittance T is

$$T = \frac{I_k}{I_i} = \frac{\mathrm{Re}\left(\eta_s\right)\left(1-R\right)}{\mathrm{Re}\left(BC^*\right)} . \tag{3.26}$$

The absorptance A in the multilayer is connected with R and T by the relationship

$$1 = R + T + A$$

so that

$$A = 1 - R - T = (1 - R)\left(1 - \frac{\mathrm{Re}(\eta_s)}{\mathrm{Re}(BC^*)}\right). \tag{3.27}$$

In the absence of absorption in any of the layers it can readily be shown that the above expressions are consistent with $A = 0$ and $T + R = 1$, for the individual film matrices will have determinants of unity and the product of any number of these matrices will also have a determinant of unity. The product of the matrices can be expressed as

$$\begin{bmatrix} \alpha & i\beta \\ i\gamma & \delta \end{bmatrix}$$

where $\alpha\delta + \gamma\beta = 1$ and, because there is no absorption, α, β, γ and δ are all real (Macleod, 1986).

$$\begin{bmatrix} B \\ C \end{bmatrix} = \begin{bmatrix} \alpha & i\beta \\ i\gamma & \delta \end{bmatrix} \begin{bmatrix} 1 \\ \eta_s \end{bmatrix} = \begin{bmatrix} \alpha + i\beta\eta_s \\ \delta\eta_s + i\gamma \end{bmatrix} \tag{3.28}$$

$$\begin{aligned} \mathrm{Re}(BC^*) &= \mathrm{Re}\left[(\alpha + i\beta\eta_s)(\delta\eta_s^* - i\gamma)\right] = (\alpha\delta + \gamma\beta)\,\mathrm{Re}(\eta_s) \\ &= \mathrm{Re}(\eta_s) \end{aligned}$$

and the result follows.

It can be manipulated equations (3.26) and (3.27) into slightly better forms. From equation (3.10)

$$R = \left(\frac{\eta_0 B - C}{\eta_0 B + C}\right)\left(\frac{\eta_0 B - C}{\eta_0 B + C}\right)^* \tag{3.29}$$

so that

$$(1-R) = \frac{2\eta_0\left(BC^* + B^*C\right)}{\left(\eta_0 B + C\right)\left(\eta_0 B + C\right)^*}.$$

Inserting this result in equation (3.26) it is obtained

$$T = \frac{4\eta_0 \,\mathrm{Re}(\eta_s)}{\left(\eta_0 B + C\right)\left(\eta_0 B + C\right)^*} \tag{3.30}$$

and in equation (3.27)

$$A = \frac{4\eta_0 \,\mathrm{Re}\left(BC^* - \eta_s\right)}{\left(\eta_0 B + C\right)\left(\eta_0 B + C\right)^*}. \tag{3.31}$$

Equations (3.29), (3.30) and (3.31) are the most useful forms of the expressions for *R, T* and *A* (Macleod, 1986).

3.1.3.1. Antireflection Coatings

3.1.3.1.(1). Antireflection Coatings on High-Index Substrates

The term high-index can not be defined precisely in the sense of a range with a definite lower bound. It simply means that the substrate has an index sufficiently higher than the available thin-film materials to enable the design of high-performance antireflection coatings consisting entirely, or almost entirely, of layers with indices lower than that of the substrate. These high-index substrates are principally of use in the infrared. Semiconductors are common, and it would be completely impossible to use them in the vast majority of applications without some form of antireflection coating. For many purposes, the reduction of a 30% reflection loss to one of a few percent would be considered adequate. It is only in a limited number of applications where the reflection loss must be reduced to less than one percent (Macleod, 1986).

3.1.3.1.(1).(a). The Single Layer Antireflection Coatings

The simplest form of antireflection coating is a single layer (Macleod, 1986). Consider Figure 3.12. If the incident medium is air, provided the index of the film is lower than the index of substrate, the reflection coefficient at each interface will be negative, denoting a phase change of 180^o. The resultant locus is a circle with a minimum at the wavelength for which the phase thickness of the layer is 90^o, that is, a quarter-wave optical thickness, when the two vectors are completely opposed. Complete cancellation at this wavelength, that is, zero reflectance, will occur if the vectors are of equal length (Macleod, 1986).

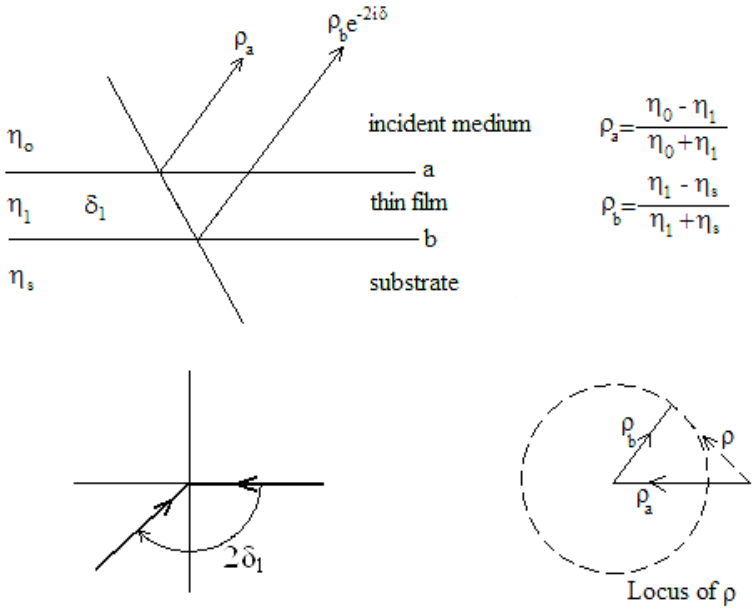

Figure 3.12. Vector diagram of a single-layer antireflection coating (Macleod, 1986).

This condition in the notation of Figure 3.12 is,

$$\rho_a = \rho_b$$

$$\frac{\eta_0 - \eta_1}{\eta_0 + \eta_1} = \frac{\eta_1 - \eta_s}{\eta_1 + \eta_s} \tag{3.32}$$

which requires

$$\frac{\eta_1}{\eta_0} = \frac{\eta_s}{\eta_1} \tag{3.33}$$

or

$$\eta_1 = \left(\eta_0 \eta_s\right)^{1/2} \tag{3.34}$$

which can also be written for normal incidence.

The condition for a perfect single layer antireflection coating is, therefore, a quarter-wave optical thickness of material with optical admittance equal to the square root of the product of the admittances of substrate and medium (Macleod, 1986).

The optical admittance of a substrate coated with a quarter-wave optical thickness of material is,

$$Y = \eta_f^2 / \eta_s \tag{3.35}$$

where η_f is the admittance of the film material and η_s that of the substrate. Therefore the reflectance is given by

$$R = \left(\frac{\eta_0 - Y}{\eta_0 + Y} \right)^2 = \left(\frac{\eta_0 - \eta_f^2 / \eta_s}{\eta_0 + \eta_f^2 / \eta_s} \right)^2 . \tag{3.36}$$

It is used the matrix method. The characteristic matrix of a single film on a substrate is given by

$$\begin{bmatrix} B \\ C \end{bmatrix} = \begin{bmatrix} \cos\delta_1 & (i \sin\delta_1)/\eta_1 \\ i\eta_1 \sin\delta_1 & \cos\delta_1 \end{bmatrix} \begin{bmatrix} 1 \\ \eta_s \end{bmatrix} \tag{3.37}$$

i.e.

$$\begin{bmatrix} B \\ C \end{bmatrix} = \begin{bmatrix} \cos\delta_1 + i(\eta_s/\eta_1)\sin\delta_1 \\ \eta_s \cos\delta_1 + i\eta_1 \sin\delta_1 \end{bmatrix} \tag{3.38}$$

where

$$\left.\begin{aligned}\eta_p &= \eta/\cos\theta \\ \eta_s &= \eta\cos\theta\end{aligned}\right\} \text{ for each material}$$
$$\delta_1 = 2\pi\eta_1 d_1\cos\theta_1/\lambda$$

where θ is the angle of incidence, η_s is optical admittance for s-polarization (TE), η_p is optical admittance for p-polarization (TM) and

$$\eta_0\sin\theta_0 = \eta_1\sin\theta_1 = \eta_s\sin\theta_s \tag{3.39}$$

If λ_0 is the wavelength for which the layer is a quarter-wave optical thickness at normal incidence, then $n_1 d_1 = \lambda_0/4$ and

$$\delta_1 = \frac{\pi}{2}\left(\frac{\lambda_0}{\lambda}\right)\cos\theta_1 \tag{3.40}$$

so that the new optimum wavelength is $\lambda_0\cos\theta_1$ (Macleod, 1986).

The amplitude reflection coefficient is

$$\rho = \frac{\eta_0 - Y}{\eta_0 + Y} = \frac{\eta_0 - C/\mathrm{B}}{\eta_0 + C/B} = \frac{(\eta_0 - \eta_s)\cos\delta_1 + i\left[(\eta_0\eta_s/\eta_1) - \eta_1\right]\mathrm{s}\,in\delta_1}{(\eta_0 + \eta_s)\cos\delta_1 + i\left[(\eta_0\eta_s/\eta_1) + \eta_1\right]\mathrm{s}\,in\delta_1} \tag{3.41}$$

and the reflectance

$$R = \frac{(\eta_0 - \eta_s)^2\cos^2\delta_1 + \left[(\eta_0\eta_s/\eta_1) - \eta_1\right]^2\mathrm{s}\,in^2\delta_1}{(\eta_0 + \eta_s)^2\cos^2\delta_1 + \left[(\eta_0\eta_s/\eta_1) + \eta_1\right]^2\mathrm{s}\,in^2\delta_1} \tag{3.42}$$

3.1.3.1.(1).(b). Double Layer Antireflection Coatings

A vector diagram of one possibility is shown in Figure 3.13. It is used the matrix method. The characteristic matrix of the assembly is

$$\begin{bmatrix} B \\ C \end{bmatrix} = \begin{bmatrix} \cos\delta_1 & (i\sin\delta_1)/\eta_1 \\ i\eta_1 \sin\delta_1 & \cos\delta_1 \end{bmatrix} \begin{bmatrix} \cos\delta_2 & (i\sin\delta_2)/\eta_2 \\ i\eta_2 \sin\delta_2 & \cos\delta_2 \end{bmatrix} \begin{bmatrix} 1 \\ \eta_s \end{bmatrix}$$
$$= \begin{bmatrix} \cos\delta_1\left[\cos\delta_2 + i(\eta_s/\eta_2)\sin\delta_2\right] + i\sin\delta_1\left(\eta_s\cos\delta_2 + i\eta_2\sin\delta_2\right)/\eta_1 \\ i\eta_1\sin\delta_1\left[\cos\delta_2 + i(\eta_s/\eta_2)\sin\delta_2\right] + \cos\delta_1\left(\eta_s\cos\delta_2 + i\eta_2\sin\delta_2\right) \end{bmatrix} \quad (3.43)$$

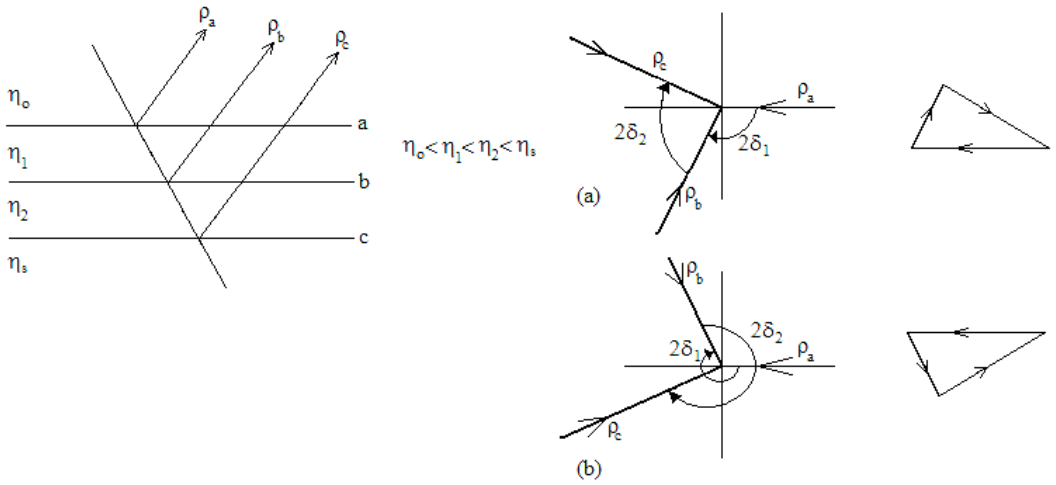

Figure 3.13. Vector diagram for double-layer antireflection coating. The thickness of the layers can be chosen to close the vector triangle and give zero reflectance in two ways, (a) and (b) (Macleod, 1986).

The reflectance will be zero if the optical admittance Y is equal to η_0, i.e.

$$i\eta_1\sin\delta_1\left[\cos\delta_2 + i(\eta_s/\eta_2)\sin\delta_2\right] + \cos\delta_1\left(\eta_s\cos\delta_2 + i\eta_2\sin\delta_2\right)$$
$$= \eta_0\left\{\cos\delta_1\left[\cos\delta_2 + i(\eta_s/\eta_2)\sin\delta_2\right] + i\sin\delta_1\left(\eta_s\cos\delta_2 + i\eta_2\sin\delta_2\right)/\eta_1\right\} \quad (3.44)$$

The real and imaginary parts of these expressions must be equated separately giving

$$-\left(\eta_1\eta_s/\eta_2\right)\sin\delta_1\sin\delta_2+\eta_s\cos\delta_1\cos\delta_2=\eta_0\cos\delta_1\cos\delta_2-\left(\eta_0\eta_2/\eta_1\right)\sin\delta_1\sin\delta_2$$

$$\eta_1\sin\delta_1\cos\delta_2+\eta_2\cos\delta_1\sin\delta_2=\left(\eta_0\eta_s/\eta_2\right)\cos\delta_1\sin\delta_2+\left(\eta_0\eta_s/\eta_1\right)\sin\delta_1\cos\delta_2$$

i.e.

$$\begin{aligned}\tan\delta_1\tan\delta_2&=\left(\eta_s-\eta_0\right)\Big/\left[\left(\eta_1\eta_s/\eta_2\right)-\left(\eta_0\eta_2/\eta_1\right)\right]\\&=\eta_1\eta_2\left(\eta_s-\eta_0\right)\Big/\left(\eta_1^2\eta_s-\eta_0\eta_2^2\right)\end{aligned}\tag{3.45}$$

and

$$\tan\delta_2/\tan\delta_1=\eta_2\left(\eta_0\eta_s/\eta_1^2\right)\Big/\left[\eta_1\left(\eta_2^2-\eta_0\eta_s\right)\right]\tag{3.46}$$

giving

$$\tan^2\delta_1=\frac{\left(\eta_s-\eta_0\right)\left(\eta_2^2-\eta_0\eta_s\right)\eta_1^2}{\left(\eta_1^2\eta_s-\eta_0\eta_2^2\right)\left(\eta_0\eta_s-\eta_1^2\right)}\tag{3.47}$$

$$\tan^2\delta_2=\frac{\left(\eta_s-\eta_0\right)\left(\eta_0\eta_s-\eta_1^2\right)\eta_2^2}{\left(\eta_1^2\eta_s-\eta_0\eta_2^2\right)\left(\eta_2^2-\eta_0\eta_s\right)}\tag{3.48}$$

The values of δ_1 and δ_2 found from these equations must be paired. The right-hand sides of equations (3.47) and (3.48) must be positive. δ_1 and δ_2 are then real. This requires that, of the expressions

$$\left(\eta_2^2-\eta_0\eta_s\right)\tag{3.49}$$

$$\left(\eta_1^2\eta_s - \eta_0\eta_2^2\right) \tag{3.50}$$

$$\left(\eta_0\eta_s - \eta_1^2\right) \tag{3.51}$$

either all three must be positive, or, any two are negative and the third positive (Macleod, 1986).

An effective coating is one consisting of two quarter-wave layers (Figure 3.14). The appearances of the vector diagram at three different wavelengths are shown (a), (b) and (c). At $\lambda = \frac{3}{4}\lambda_0$ and $\lambda = \frac{3}{2}\lambda_0$ the three vectors in the triangle are inclined at 60^o to each other. Provided the vectors are all of equal length, the triangles will be closed and the reflectance will be zero at these wavelengths (Macleod, 1986). This condition can be written

$$\frac{\eta_1}{\eta_0} = \frac{\eta_2}{\eta_1} = \frac{\eta_s}{\eta_2} \tag{3.52}$$

and solved for η_1 and η_2:

$$\eta_1^3 = \eta_0^2\eta_s \tag{3.53}$$

$$\eta_2^3 = \eta_0\eta_s^2 \tag{3.54}$$

The reflectance at the reference wavelength λ_0 where the layers are quarter-waves is given by

$$\begin{aligned} R &= \left(\frac{\eta_0 - \left(\eta_1^2/\eta_2^2\right)\eta_s}{\eta_0 + \left(\eta_1^2/\eta_2^2\right)\eta_s}\right)^2 \\ &= \left(\frac{1-\left(\eta_s/\eta_0\right)^{1/3}}{1+\left(\eta_s/\eta_0\right)^{1/3}}\right)^2 \end{aligned} \tag{3.55}$$

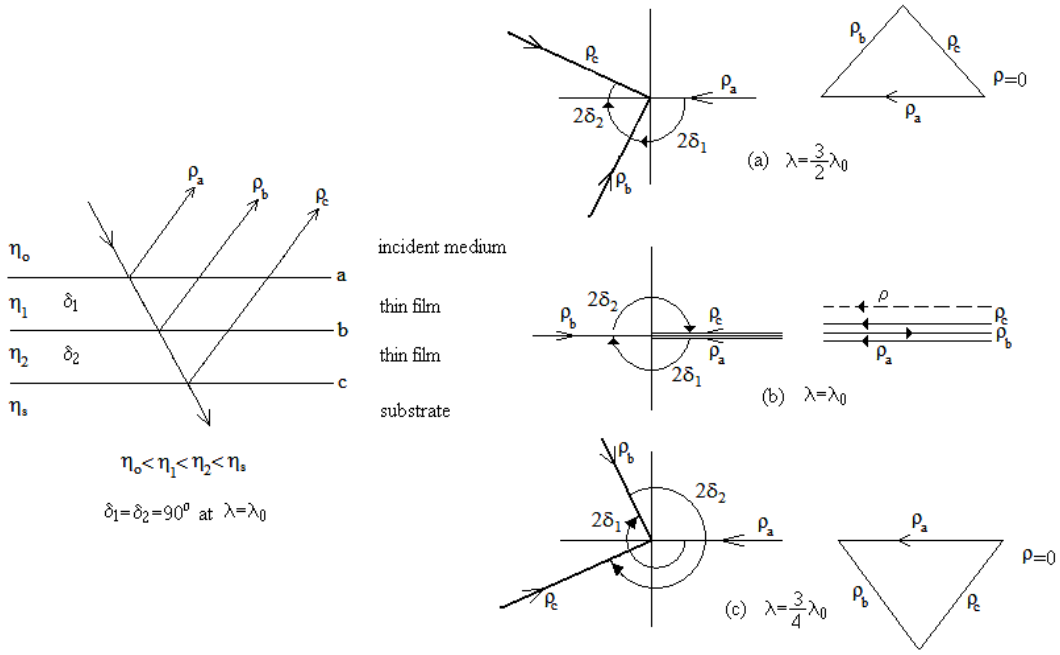

Figure 3.14. Vector diagrams for quarter-quarter antireflection coatings on a high-index substrate (Macleod, 1986).

which is a considerable improvement over the bare substrate (Macleod, 1986).

The coating described is a special case of a general coating where the layers are of equal thickness. To compute the general conditions it is easiest to return to the analysis leading up to equations (3.47) and (3.48) (Macleod, 1986).

Let δ_1 be set equal to δ_2 and denoted by δ, where it is recalled that if λ_0 is the wavelength for which the layers are quarter-waves then

$$\delta = \frac{\pi}{2}\left(\frac{\lambda_0}{\lambda}\right). \tag{3.56}$$

From equation (3.46)

$$\eta_2\left(\eta_0\eta_s - \eta_1^2\right) = \eta_1\left(\eta_2^2 - \eta_0\eta_s\right) \tag{3.57}$$

i.e.

$$\eta_0\eta_s = \eta_1\eta_2 \tag{3.58}$$

which is a necessary condition for zero reflectance (Macleod, 1986).

From equation (3.45) it is found the wavelengths λ corresponding to zero reflectance:

$$\tan^2\delta = \frac{\eta_1\eta_2\left(\eta_s-\eta_0\right)}{\eta_1^2\eta_s-\eta_0\eta_2^2} = \frac{\eta_0\eta_s\left(\eta_s-\eta_0\right)}{\eta_1^2\eta_s-\eta_0\eta_2^2}. \tag{3.59}$$

If δ' is the solution in the first quadrant, then there are two solutions:

$$\delta = \delta' \qquad \text{or} \qquad \pi - \delta'$$

and the two values of λ are:

$$\lambda = \left(\frac{\pi/2}{\delta}\right)\lambda_0. \tag{3.60}$$

In all practical cases, η_s will be greater than η_0 and the above equation for $\tan^2\delta$ will have a real solution provided

$$\eta_1^2\eta_s - \eta_0\eta_2^2 \tag{3.61}$$

is positive or zero. This expression is identical to expression (3.50) (Macleod, 1986).

At the reference wavelength λ_0, $\delta = \pi/2$ and the layers are quarter-waves. The optical admittance is given by

$$\frac{\eta_1^2}{\eta_2^2}\eta_s \tag{3.62}$$

and the reflectance by

$$R = \left(\frac{\eta_0 - \left(\eta_1^2/\eta_2^2\right)\eta_s}{\eta_0 + \left(\eta_1^2/\eta_2^2\right)\eta_s} \right)^2 . \tag{3.63}$$

3.1.3.1.(1).(c). Multilayer Antireflection Coatings

Figure 3.15 shows a vector diagram for a three layer coating. Each layer is a quarter-wave thick at λ_0. If $\eta_s > \eta_3 > \eta_2 > \eta_1 > \eta_0$, then the vectors will oppose each other at $\frac{2}{3}\lambda_0$, λ_0, and $2\lambda_0$ and provided the vectors are all of equal length, will completely cancel at these wavelengths, giving zero reflectance (Macleod, 1986).

This coating is similar to the quarter-quarter coating of Figure 3.14, but where the two zeros of the two-layer coating are situated $\frac{3}{4}\lambda_0$ and $\frac{3}{2}\lambda_0$, those of this three-layer coating stretch from $\frac{2}{3}\lambda_0$ to $2\lambda_0$, a much broader region (Macleod, 1986).

The condition for the vectors to be of equal length is

$$\frac{\eta_1}{\eta_0} = \frac{\eta_2}{\eta_1} = \frac{\eta_3}{\eta_2} = \frac{\eta_s}{\eta_3} \tag{3.64}$$

which becomes with some manipulation

$$\eta_1^4 = \eta_0^3 \eta_s$$
$$\eta_2^4 = \eta_0^2 \eta_s^2 \qquad (3.65)$$
$$\eta_3^4 = \eta_0 \eta_s^3$$

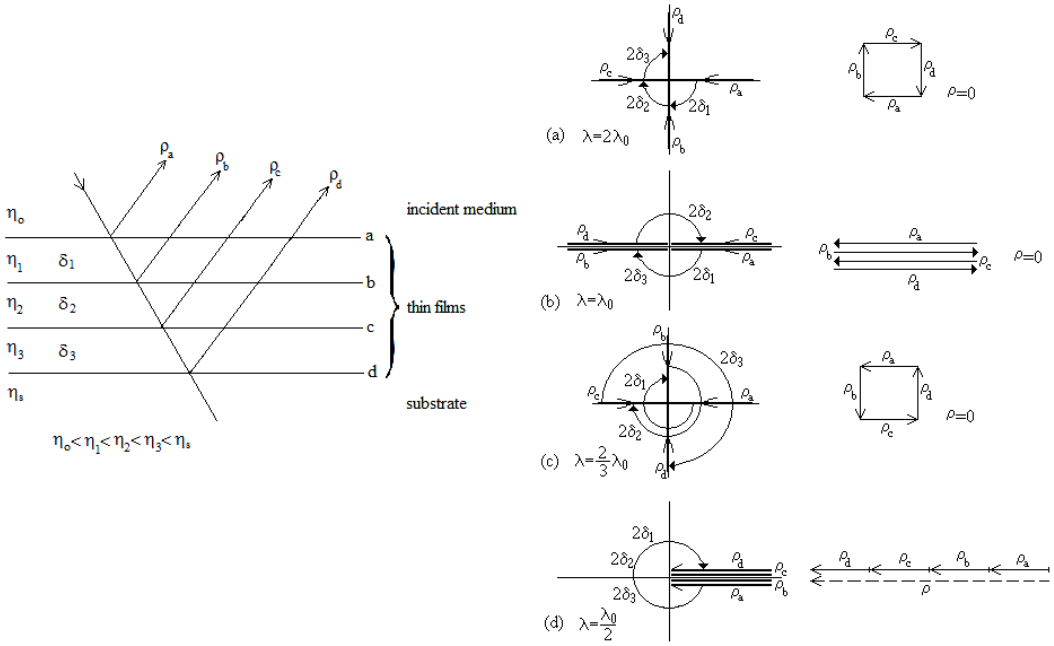

Figure 3.15. Vector diagram for a quarter-quarter-quarter coating on a high-index substrate (Macleod, 1986).

3.1.3.1.(2). Antireflection Coatings on Low-Index Substrates

Although the theory developed for antireflection coatings on high-index material applies equally well to low-index materials, the problem is made much more harsh by the lack of any rugged thin-film materials of very low-index. Design techniques for antireflection coatings on low-index materials are less well organized and involve much more intuition and trial and error than those for high-index materials (Macleod, 1986).

The commonest low-index material is crown glass, and coatings are most frequently required for the visible region of the spectrum, which extends from around 400 nm to around 700 nm (Macleod, 1986).

3.2. Method

There are many different methods for the design of multilayer antireflection coatings. For a good overview of multilayer coatings theory the interested reader is referred to the books by Macleod (1986), Knittl (1976), and Tikhonravov and Furman (1992).

Here some of the commonly used methods in thin film design will be mentioned briefly.

3.2.1. The Vector Method

The vector method is usually associated with the design of antireflection coatings. Two assumptions are involved: first, that the layers are all non-absorbing, and second, that the behaviour of a multilayer can be understood by considering one reflection of the incident wave at each interface.

The reflection coefficient at each interface is represented by $R_r = \frac{n_{r-1} - n_r}{n_{r-1} + n_r}$ and the phase thicknesses of the layers are given by $\delta_r = 2\pi n_r \cos\theta_r d_r / \lambda$, where n_r is the refractive index and d_r is the thickness of the r^{th} layer. The resultant amplitude coefficient of the stack is given by the vector sum of coefficients for each interface. This sum can be found graphically or analytically (Macleod, 1986).

3.2.2. Alternative Method of Calculation

The success of the vector method prompts one to ask whether it can be made more accurate by considering second and subsequent reflections at the various boundaries instead of just one. In fact, an alternative solution of the thin film problem can be obtained in this way. It is simpler to consider normal incidence only. The expression can be adapted for non-normal incidence quite simply when the materials are transparent and with some difficulty when they are absorbing (Macleod, 1986).

3.2.3. Smith's Method

In 1958, Smith formulated a useful design method which is known as the method of effective interfaces. It consists of choosing any layer in the multilayer and then considering multiple reflections within it. The reflection and transmission coefficients at the boundaries of the layer are considered to be the resultant coefficients of the complete structures on either side. This technique can be extended to deal with absorbing layers also. This method provides an insight into the properties of a particular type of filter, but is highly complicated.

A particularly useful technique of this type has been developed by Musset and Thelen (1966). It is based on Smith's method, that is, the method of effective interfaces. This involves the breaking down of the assembly into two subsystems. The conditions for a perfect antireflection coating are called the amplitude condition by Musset and Thelen. The amplitude condition is a function of the two subsystems. The phase condition can be satisfied by adjusting the thickness of the spacer layer. The amplitude condition can, using a method devised by Musset and Thelen, be satisfied for all wavelengths, but it is difficult to satisfy the phase condition except at a limited number of discrete wavelengths. At other wavelengths the performance departs from ideal to a variable degree (Macleod, 1986).

3.2.4. The Smith Chart

The Smith chart is a device which is intended to simplify calculations involved in the design of thin film filters. This chart represents circles of constant amplitude coefficient and circles of constant real part and constant imaginary part of the reduced optical admittance. A scale, calibrated in terms of optical thickness is provided around the outside of the chart. This enables the calculation to be very simply carried out by rotating the point corresponding to the amplitude reflection coefficient of the particular layer, around the center of the chart through the appropriate angle (Macleod, 1986).

3.2.5. Circle Diagrams

In this method, the multilayer is considered to be gradually built up layer by layer, immersed all the time in the final incident medium. As each layer increases from zero to its final value, some parameter of the multilayer at that stage, like reflectance or admittance, is calculated and the locus is plotted. The loci for these dielectric layers take the form of a series of circular arcs or even complete circles, each corresponding to a single layer, which are connected at points corresponding to interfaces between different layers (Macleod, 1986).

4. FORMULATION

4.1. Four-Layer Antireflection Coating

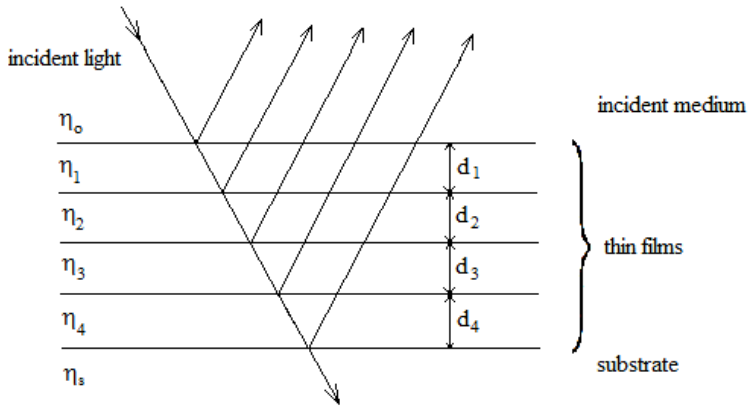

Figure 4.1. The structure of four-layer antireflection coating.

The arrangement is illustrated in Figure 4.1. The characteristic matrix of the assembly is

$$\begin{pmatrix} B \\ C \end{pmatrix} = \left\{ \prod_{r=1}^{4} \begin{bmatrix} \cos\delta_r & i\sin\delta_r / n_r \\ in_r \sin\delta_r & \cos\delta_r \end{bmatrix} \right\} \begin{bmatrix} 1 \\ n_s \end{bmatrix} \tag{4.1}$$

where n_s is substrate admittance, δ_r is the phase thickness of the r^{th} layer, i.e.

$$\delta_r = \frac{2\pi N_r d_r \cos\theta_r}{\lambda} \tag{4.2}$$

where d_r is the physical thickness of the r^{th} layer, and n_r is the optical admittance of the r^{th} layer, i.e.

$$\begin{aligned} \eta_r &= \mathscr{Y} N_r \cos\theta_r \qquad \text{for s-polarization (TE)} \\ \eta_r &= \mathscr{Y} N_r / \cos\theta_r \qquad \text{for p-polarization (TM)} \end{aligned} \tag{4.3}$$

where $\mathscr{Y}$ is the admittance of free space, N_r is the refractive index of the r^{th} layer, θ_0 is the angle of incidence and θ_r which is incidence angle of the r^{th} layer can be found from Snell's Law, i.e.

$$N_0 \sin\theta_0 = N_r \sin\theta_r = N_s \sin\theta_s . \tag{4.4}$$

We can calculate equation (4.1) and found the matrix elements B and C from the result of this calculation:

$$\begin{aligned} B = \Bigg\{ & \cos\delta_1\cos\delta_2\cos\delta_3\cos\delta_4 - \frac{n_4}{n_3}\cos\delta_1\cos\delta_2\sin\delta_3\sin\delta_4 - \frac{n_3}{n_2}\cos\delta_1\sin\delta_2\sin\delta_3\cos\delta_4 \\ & - \frac{n_4}{n_2}\cos\delta_1\sin\delta_2\cos\delta_3\sin\delta_4 - \frac{n_2}{n_1}\sin\delta_1\sin\delta_2\cos\delta_3\cos\delta_4 + \frac{n_2 n_4}{n_1 n_3}\sin\delta_1\sin\delta_2\sin\delta_3\sin\delta_4 \\ & - \frac{n_3}{n_1}\sin\delta_1\cos\delta_2\sin\delta_3\cos\delta_4 - \frac{n_4}{n_1}\sin\delta_1\cos\delta_2\cos\delta_3\sin\delta_4 \\ & + i\Bigg[\frac{n_5}{n_4}\cos\delta_1\cos\delta_2\cos\delta_3\sin\delta_4 + \frac{n_5}{n_3}\cos\delta_1\cos\delta_2\sin\delta_3\cos\delta_4 + \frac{n_5}{n_2}\cos\delta_1\sin\delta_2\cos\delta_3\cos\delta_4 \\ & - \frac{n_3 n_5}{n_2 n_4}\cos\delta_1\sin\delta_2\sin\delta_3\sin\delta_4 - \frac{n_2 n_5}{n_1 n_4}\sin\delta_1\sin\delta_2\cos\delta_3\sin\delta_4 - \frac{n_2 n_5}{n_1 n_3}\sin\delta_1\sin\delta_2\sin\delta_3\cos\delta_4 \\ & + \frac{n_5}{n_1}\sin\delta_1\cos\delta_2\cos\delta_3\cos\delta_4 - \frac{n_3 n_5}{n_1 n_4}\sin\delta_1\cos\delta_2\sin\delta_3\sin\delta_4 \Bigg] \Bigg\} \end{aligned} \tag{4.5}$$

and

$$\begin{aligned} C = \Bigg\{ & -\frac{n_1 n_5}{n_4}\sin\delta_1\cos\delta_2\cos\delta_3\sin\delta_4 - \frac{n_1 n_5}{n_3}\sin\delta_1\cos\delta_2\sin\delta_3\cos\delta_4 - \frac{n_1 n_5}{n_2}\sin\delta_1\sin\delta_2\cos\delta_3\cos\delta_4 \\ & + \frac{n_1 n_3 n_5}{n_2 n_4}\sin\delta_1\sin\delta_2\sin\delta_3\sin\delta_4 - \frac{n_2 n_5}{n_4}\cos\delta_1\sin\delta_2\cos\delta_3\sin\delta_4 - \frac{n_2 n_5}{n_3}\cos\delta_1\sin\delta_2\sin\delta_3\cos\delta_4 \\ & + n_5\cos\delta_1\cos\delta_2\cos\delta_3\cos\delta_4 - \frac{n_3 n_5}{n_4}\cos\delta_1\cos\delta_2\sin\delta_3\sin\delta_4 \\ & + i\Bigg[n_1\sin\delta_1\cos\delta_2\cos\delta_3\cos\delta_4 - \frac{n_1 n_4}{n_3}\sin\delta_1\cos\delta_2\sin\delta_3\sin\delta_4 - \frac{n_1 n_3}{n_2}\sin\delta_1\sin\delta_2\sin\delta_3\cos\delta_4 \\ & - \frac{n_1 n_4}{n_2}\sin\delta_1\sin\delta_2\cos\delta_3\sin\delta_4 + n_2\cos\delta_1\sin\delta_2\cos\delta_3\cos\delta_4 + n_3\cos\delta_1\cos\delta_2\sin\delta_3\cos\delta_4 \\ & - \frac{n_2 n_4}{n_3}\cos\delta_1\sin\delta_2\sin\delta_3\sin\delta_4 + n_4\cos\delta_1\cos\delta_2\cos\delta_3\sin\delta_4 \Bigg] \Bigg\} \end{aligned} \tag{4.6}$$

The amplitude reflection coefficient and the reflectance are, respectively,

$$\rho = \left(\frac{n_0 - Y}{n_0 + Y} \right) = \left(\frac{n_0 B - C}{n_0 B + C} \right) \tag{4.7}$$

$$R = \rho \rho^* \tag{4.8}$$

where the input optical admittance is $Y = C/B$.

The effective coating is one consisting of four quarter-wave layers. Let δ_1 be set equal to δ_2 and denoted by δ, and if λ_0 is the wavelength for which the layers are quarter-waves then

$$\delta = \frac{\pi}{2} \left(\frac{\lambda_0}{\lambda} \right) \tag{4.9}$$

Now $\delta = \delta_1 = \delta_2 = \delta_3 = \delta_4 = 90^\circ$ at $\lambda = \lambda_0$. By substituting $\sin 90^\circ = 1$, $\cos 90^\circ = 0$ into the equations (4.5) and (4.6) to obtain the expression of the optical admittance Y. Using Y, the reflectance of our assembly is written as

$$R_5 = \left(\frac{n_0 - \dfrac{n_1^2 n_3^2}{n_2^2 n_4^2} n_5}{n_0 + \dfrac{n_1^2 n_3^2}{n_2^2 n_4^2} n_5} \right)^2 . \tag{4.10}$$

Inserting the optical admittance into equation (3.30) the transmittance of the assembly is

$$T_5 = \frac{4 n_0 n_1^2 n_3^2 \, \mathrm{Re}(n_5)}{n_2^2 n_4^2 \left(n_0 + \dfrac{n_1^2 n_3^2}{n_2^2 n_4^2} n_5 \right)^2} \tag{4.11}$$

and into equation (3.31) the absorption of the assembly is

$$A_5 = \frac{4n_0 n_1^2 n_3^2 \,\mathrm{Re}\left(BC^* - n_5\right)}{n_2^2 n_4^2 \left(n_0 + \frac{n_1^2 n_3^2}{n_2^2 n_4^2} n_5\right)^2}. \tag{4.12}$$

In ferroelectric materials temperature and polarization dependences of refractive index shows nonlinear characters. The refractive indices of each layer depending on polarization for the ferroelectric based multilayer antireflection coating system is written as follows,

$$n(p) = n(0) + \frac{\partial n}{\partial p}\Delta p + \frac{1}{2!}\frac{\partial^2 n}{\partial p^2}\Delta p^2 + ... \tag{4.13}$$

where $n(p)$ is the refractive index depending on spontaneous polarization in ferroelectric phase, $n(0)$ is refractive index in nonpolar phase, Δp is the polarization difference on ferroelectric phase. For simplicity, we neglect the powers higher than the second. Then reflectance, transmittance and absorptance were calculated again by using equation (4.13). A very long expression was found depending on refractive indices of each layer, derivatives of refractive indices, (Δp) and $(\Delta p)^2$ (Appendix I). So, the reflectance, transmittance and absorptance was theoretically found depending on polarization. We can write the same expression for $n(T)$ too (Appendix II). This means that the optical properties of a system can be changed by external electric or thermal field in the multilayer antireflection coating.

5. NUMERICAL RESULTS

Many numerical methods for the design of all multilayer coatings with prescribed spectral characteristics have been described in the past. When solving various problems in multilayer optics field, it is assumed in most cases that a layered medium consists of a finite number of homogeneous and isotropic layers. In this case, in order to determine the amplitude of transmittance and reflectance, it is mathematically convenient and efficient to employ various recurrent calculating techniques. Depending on the particular problem to be solved, a specific technique is preferred. Mastering various methods expands one's concept of the properties of multilayer coatings. The application of these methods will further permit to obtain a number of significant conclusions for analysis and synthesis (Tikhonravov and Furman, 1992).

The characteristic matrix of a multilayer thin film takes on a very simple form if the optical thickness is an integral number of quarter or half waves. This means,

$$\delta = n(\pi/2) \qquad n = 0,\ 1,\ 2,\ 3.... \tag{5.1}$$

For n even, $\cos\delta = \pm 1$ and $\sin\delta = 0$, so the layer is the integral number of half wavelength thick, and the matrix becomes the unity matrix,

$$\pm\begin{bmatrix} 1 & 0 \\ 0 & 1 \end{bmatrix}. \tag{5.2}$$

This can have no effect on the reflectance or transmittance of an assembly, as if the layer were entirely absent. This result is particularly useful, thus half-wave layers are sometimes referred to as absentee layers.

For n odd, $\sin\delta = \pm 1$ and $\cos\delta = 0$, so that the layer is the odd number of quarter wavelengths thick, and the matrix becomes

$$\pm\begin{bmatrix} 0 & i/\eta \\ i\eta & 0 \end{bmatrix}. \tag{5.3}$$

This is not quite as simple as the half-wave case, but such a matrix is still easy to handle in calculation. In particular, if a substrate or combination of thin films has an admittance of Y, then addition of an odd number of quarter-waves of admittance η alters the admittance of the assembly to η^2/Y. This makes the properties of a succession of quarter-wave layers very easy to calculate. The admittance of a stack of five quarter-wave layers is

$$Y = \frac{\eta_1^2}{\eta_2^2}\frac{\eta_3^2}{\eta_4^2}\frac{\eta_5^2}{\eta_s}. \tag{5.4}$$

Designs are often specified in terms of fractions of quarter-waves at a reference wavelength because of the simplicity of assemblies involving quarter- and half-wave optical thicknesses. Usually only two or possibly three different materials are involved in designs and a convenient shorthand notation for quarter-wave optical thicknesses is H, M or L; where H refers to the highest of the three indices, M the intermediate and L the lowest (Macleod, 1986).

5.1. Design of Multilayer Antireflection Coatings Based on Ferroelectric

Based on the matrix theory, we have developed a Fortran software program to design and simulate the performance of multilayer coatings. Using this software, we have designed and optimized multilayer antireflection coatings which are consisted of insulator thin films for ferroelectric substrate.

There are a lot of systems that can be done for this kind of calculation. These are quite expensive systems. By means of Fresnell formulas, we designed a much simpler program making use of the nearly same process.

We designed an algorithm of two- and three-component optical coatings calculated by matrix method at normal incidence. Two-component optical coatings

are multilayer stacks consisting of layers with alternating low refractive index n_L and high refractive index n_H; three-component optical coatings are consisted of refractive index with the lowest of the three indices n_L, the intermediate n_M and the highest n_H. Our algorithm consists of three main steps schematically shown in Figure 5.1.

During the input stage, the following parameters must be provided: the refractive indices of substrate n_s, air n_a, and the low n_L, intermediate n_M and high n_H index coating materials, a certain wavelength λ_0=550 nm, the angle of incidence θ, a quarter-wave optical thickness $nd = \lambda_0/4$, and a number of sublayers N.

The calculation stage is to solve the problem by matrix method which is mentioned in Section 3. In the current version of our program, the characteristic matrix is firstly calculated at normal incidence, and then reflectance and transmittance are computed in wavelength range from 400 nm to 800 nm.

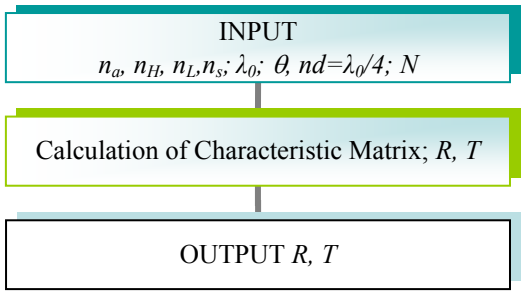

Figure 5.1. Flowchart of the optimization algorithm.

The output of our program routine consisted of 401 reflectance and transmittance values for each planned multilayer structure. As simulated and plotted in the next sections, the reflectance is come to close zero.

5.2. Synthesis of Optical Coating and Presentation of Calculation Results

The geometrical thicknesses of the layers and the wavelength λ enter the calculation formulas for reflection and transmission only in combination $kd = 2\pi d/\lambda$. This means that a simultaneous proportional change of the thicknesses

of all layers and of the wavelength do not change the values of reflection and transmission (providing the refractive indices of all layers remain unchanged). Thus, in a spectral band where the dispersion of the refractive indices can be neglected, proportional changes of the thicknesses of all layers result in a shift of the reflectance and transmittance curves along the spectral band. In this connection, when describing the coating structure, it is convenient to use relative values of layer thicknesses rather than their absolute values (Tikhonravov and Furman, 1992).

When this kind of coatings is done, there must be certain level in which its optical characteristics should not destroy. This means that it should not disrupt characteristics of optical system which is designed in terms of geometrical optics (aberration, coma, dichroism, astigmatism). There must be selected more sensitive materials to external effects, temperature and/or external electrical field, like ferroelectric materials for this type of coatings. Additionally, these selected materials must be easily found and cheap in terms of technology.

5.2.1. Even Folded Multilayer Antireflection Coatings

Most widely recognized is the way of description where the optical thicknesses of the layers $n_j d_j$ are designated as fractions of $\lambda_0/4$, with λ_0 being a certain basic wavelength. Let, for instance, a coating is a two-component one, consisting of alternating layers featuring high n_H and low n_L refractive indices. Table 5.1 shows the general design data of each layer material and thickness.

Changing optical paths range from 0.068784 μm to 0.123318 μm as folds of $\lambda_0/4$, graphs is found in all analysis.

Table 5.1. Design data for layers used in all configuration

Layer number	Material	Refractive Index (*n*)	Thickness (μm)
Layer #1	ZnSe	2.39	0.057531
Layer #2	ZrO_2	2.05	0.067073
Substrate	$LiNbO_3$	2.28	0.060307

5.2.1.1. Analysis of Two-Layer Antireflection Coating

The synthesis process started with a search for a two-layer antireflection coating with HL setting of the starting design. It has already two possibilities, HL and LH. In order to reach a better result, we preferred HL setting. The reflectance of the synthesized coating is provided in Figure 5.2. The optical thicknesses of the layers are equal to $\lambda_0/4$ at certain wavelength λ_0=550 nm.

Figure 5.2. Reflectance profile of two layers antireflection coating.

Considering the two-layer antireflection coating, the structure of such a coating:

a-HL-s

a on the extreme left shows the air, the letter on the right *s* stands for the substrate in the given coating. There is a consecutive list of the optical thicknesses in the direction from the outer space to the substrate. The letters H and L refer to the layers having the refractive indices of n_H and n_L, respectively. The numerical coefficients before them show the optical thicknesses of the layer as fractions of $\lambda_0/4$. If a coefficient is absent, the corresponding layer has a quarter-wave optical thickness.

Thus, the coating described above has layers featuring the refractive index n_H, n_L and the optical thickness $0.25\lambda_0$.

An antireflection coating was designed for the visible spectral band on the basis of materials with the refractive indices of n_L=2.05 (ZrO_2), n_H=2.39 (ZnSe) with ferroelectric featuring n_s=2.28 ($LiNbO_3$) as the substrate and air n_0=1.00 as the outer space. The layer adjacent to the substrate had a low refractive index. Reflectance of each layer approaches the zero when the thickness of each layer equals a quarter-wave thick at λ_0. The reflectance curve between 400 nm and 800 nm visible region of electromagnetic spectrum for this configuration is shown in Figure 5.2. In case of two layer configuration, we had a maximum reflectance of 1.7% and minimum of 0.025%.

5.2.1.2. Analysis of Four-Layer Antireflection Coating

The reflectance profile of four-layer coating comprising ZrO_2 and ZnSe is shown in Figure 5.3. In order to be lower reflection we selected a-HHHL-s setting from probable 16 configurations. All layers have a quarter-wave optical thickness at certain wavelength, λ_0=550 nm.

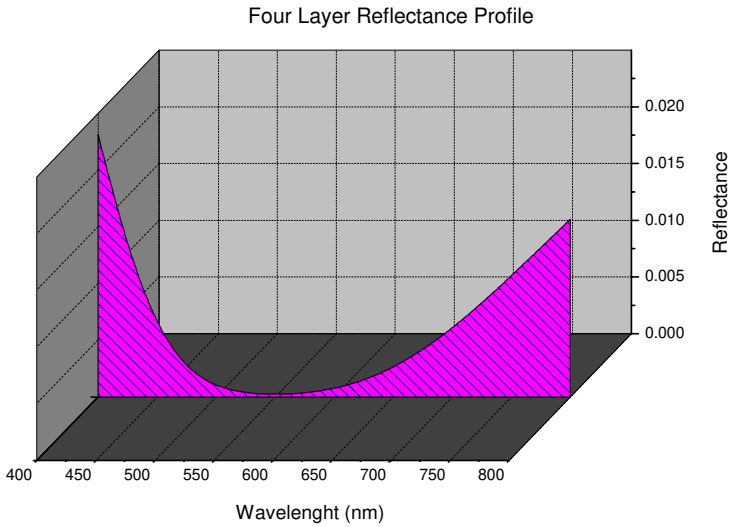

Figure 5.3. Reflectance profile of four layers antireflection coating.

In case of this configuration, the reflection curve is 0.025% the broadband between 500 nm and 600 nm and the curve is seen to increase up to 2.3% excluding this broadband. A slight increase in reflectance can be seen, but this result is so low considering total reflectance results and the important feature of this design is the zero reflectance of multilayer at a spectral point.

5.2.1.3. Analysis of Six-Layer Antireflection Coating

The performance of the six-layer design (a-HHLL HL-s) is shown in Figure 5.4. Each layer is again a quarter-wave thick at λ_0 (550 nm), when it gives zero reflectance. We decided this configuration from 64 probabilities to lower reflectance. The reflection curve is nearly 0.0012% the broadband between 465 nm and 675 nm. The reflectance from the substrate is close to 1.67% when the spectral range approaches to the wings of curve. We can see that the reflectance of the substrate approach to zero with the other of layer. Therefore, the performance of the coating is further improved by the addition of four layers.

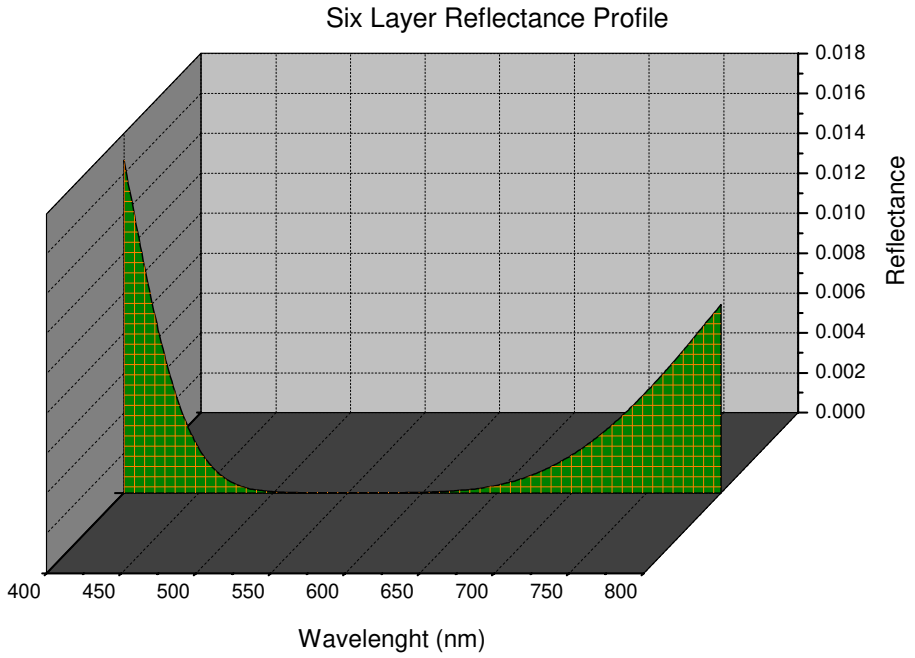

Figure 5.4. Reflectance profile of six layers antireflection coating.

5.2.1.4. Analysis of Eight-Layer Antireflection Coating

The synthesis process continued with an eight-layer antireflection coating with a-LLHH LLHL-s setting. In order to be a lower reflectance we preferred this setting from probable 256 settings. The reflectance curve of eight-layer coating is shown in Figure 5.5. The optical thicknesses of each layer are quarter-wave at certain wavelength, λ_0=550 nm.

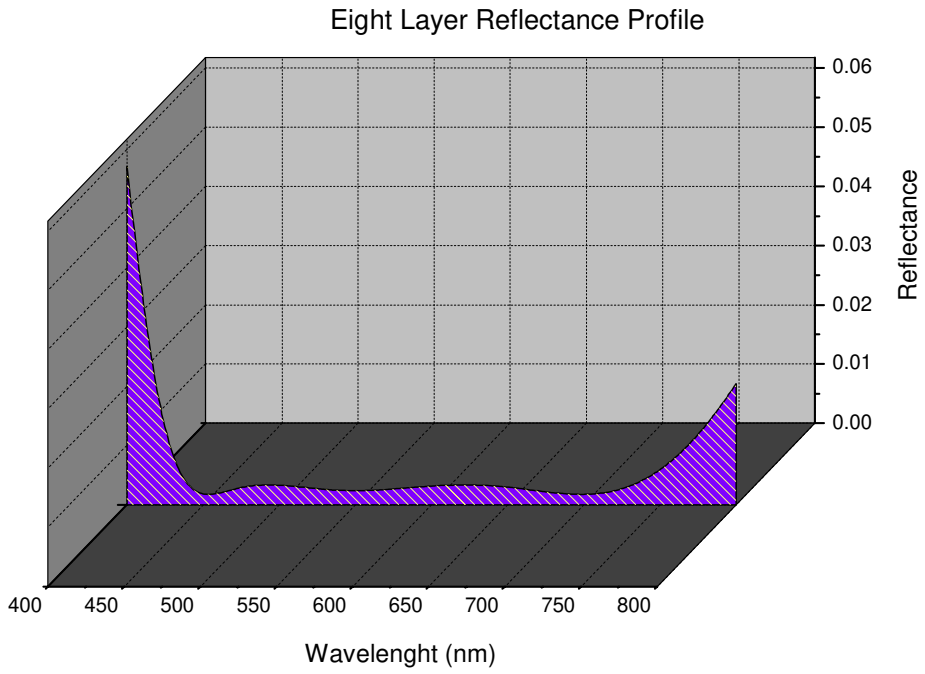

Figure 5.5. Reflectance profile of eight layers antireflection coating.

The reflection curve is nearly 0.0017% the broadband between 440 nm and 740 nm with slight fluctuation but it is seen to increase 5.7% at the wings of the curve in this configuration. A sudden increase in reflectance can be seen, but the important feature of this design is the long scale from 440 nm to 740 nm in visible range.

5.2.1.5. Analysis of Ten-Layer Antireflection Coating

The reflectance curve of ten-layer coating is shown in Figure 5.6. The ten-layer structure of such an antireflection coating is considered as a-HHHHH HHHHL-s. We thought that this configuration has the lowest reflectance from 1024 probabilities. All layers have a quarter-wave optical thickness at certain wavelength once more, λ_0=550 nm. The curve that the minimum reflectance of ten-layer coating has 0.0003% in the band between 515 nm and 590 nm is shown in Figure 5.6. In the spectral range from 400 nm to 800 nm maximum reflectance are approximately to 2.2% when it comes close to the wings of the curve in the range. The performance of a ten-layer is more or less similar to the others.

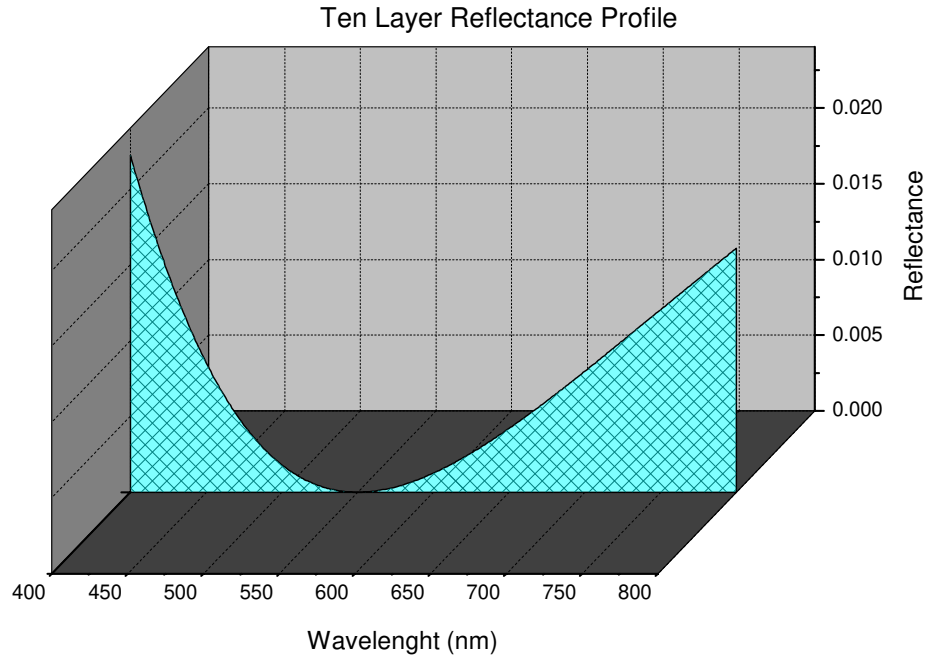

Figure 5.6. Reflectance profile of ten layers antireflection coating.

The reflectance can be plotted multilayer configurations which are explained above to compare with each other in one graph as shown in Figure 5.7. It is represented ten-layer, four-layer, two-layer, eight-layer, and six-layer antireflection coatings as curve B, C, D, E, and F respectively. It is clearly seen that the reflectance can be decreased to lower value by increasing number of layers. This means that the transmittance can be considerably increased. It is seen that the optimum layer number equals six; because the spectral range of reflectance for two-, four-, eight-, and ten-layer is higher than the spectral range of six-layer.

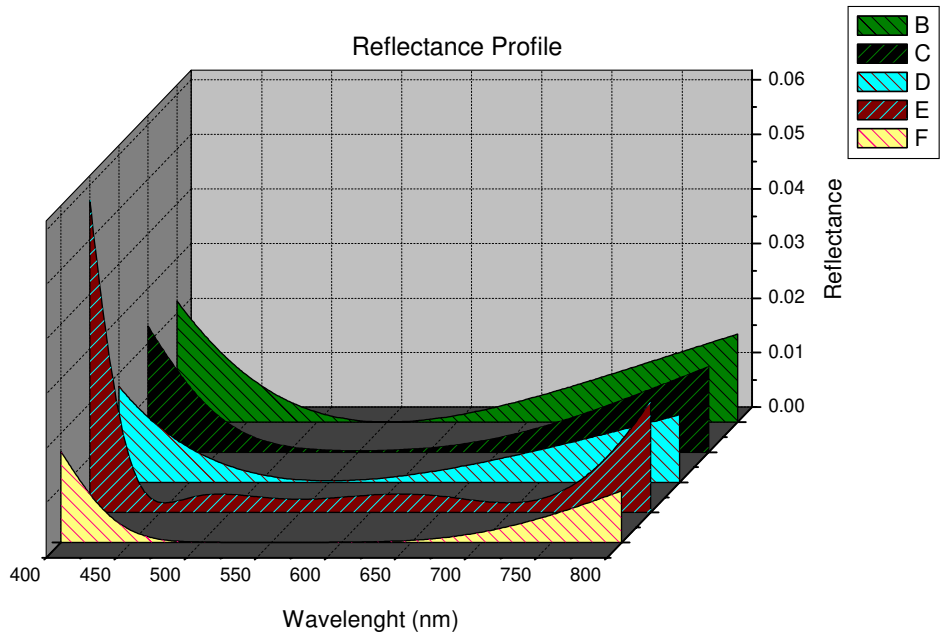

Figure 5.7. Reflectance profile of 2, 4, 6, 8, and 10 layers antireflection coating.

5.2.1.6. Analysis of Twelve-Layer Antireflection Coating

By increasing the number of layers and optimizing their index and thickness, the reflectance from the substrate can be reduced to a reasonably low value. In other words, the transmittance through the substrate can be increased substantially (Asghar et al., 2003b). We have simulated 12 layers for the best performance of multilayer coatings based on the matrix theory. The decrease in reflectance by addition of layers over the substrate can be observed by plotting eight different twelve-layer design configurations in one graph as shown in Figure 5.8.

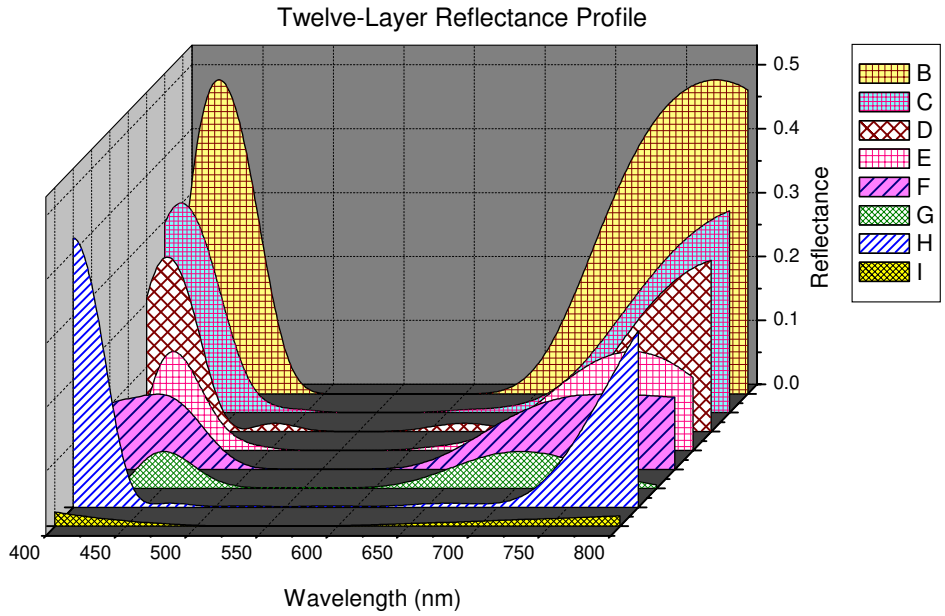

Figure 5.8. Combined reflectance profile for twelve-layer configurations on $LiNbO_3$.

It has totally 4096 possibilities in twelve-layer configuration. The refractive indexes of 12-sublayer system with alternating high and low indices are coded as a-LLHL LHLL LLHL-s, a-LLLL HHLH HLHL-s, a-LLLL HHLL LLHL-s, a-LLHH LLLL LLHL-s, a-HHHH HHLL LLHL-s, a-HHHH LLHH HHHL-s, a-HHLL HHHH LLHL-s, a-HHHH HHHH HHHL-s settings and this codes represents curve B, C, D, E, F, G, H, and I respectively.

The optical thicknesses of the layers are quarter-wavelength thick. In case of these configurations, the reflection curve of B stays almost 0.00016% in the broadband between 500 nm and 600 nm with 49% at the maximum as to the wings of the curve. The reflection curve C is about 0.00012% in the band between 520 nm and 585 nm. With the exception of this band, the C curve sees 32% at the highest between 400 nm and 800 nm range is seen to increase. The reflection curve of D is around 0.0012% in the spectral range from 530 nm to 575 nm and maximum reflection is roughly 27% when it moves towards to the wings of the curve. The minimum reflection curve of E is just about 0.017% in the range from 520 nm to 585 nm. The curve E is seen to rise up to 15% out of in the range. The minimum reflection of curve F is very nearly 0.04% in the broadband between 515 nm and 590 nm with 11% at the maximum as to the wings. The reflection of curve G is about 0.1% in the spectral range from 500 nm to 620 nm. This curve between 400 nm and 800 nm range is seen to increase 5.7% with the exception of this wideband. The reflection of curve H is 0.1% in the broadband between 450 nm and 700 nm and the curve is seen to increase up to 42% excluding this broadband. The minimum reflection of curve I is 0.00049% in the spectral range from 480 nm to 650 nm. This curve is seen to increase up to 2.2% excluding the wideband. A slight increase in reflectance in some wavelengths can be seen, but the important feature of this design is very nearly the zero reflectance at certain wavelength, λ_0=550 nm.

In order to remain constant in the broader optic ranges of quarter-wave layer we got ratio of one of transmission values of curves to another. The transmission values ratios of curves are shown in Figure 5.9, 5.10, 5.11, 5.12, and 5.13. We think that selected materials are suitable to reduce reflection in the visible region since the value of curves ratio one to another at the same optical range in these figures is approximately one.

In Figure 5.9 curve C is the ratios of coded curve as a-LLLL HHLL LLHL-s to coded curve as a-HHLL HHHH LLHL-s and curve B is the ratios of coded curve as a-LLLL HHLL LLHL-s to coded curve as a-HHHH HHHH HHHL-s for 12 layers. The ratio value of curves is fairly one in these curves.

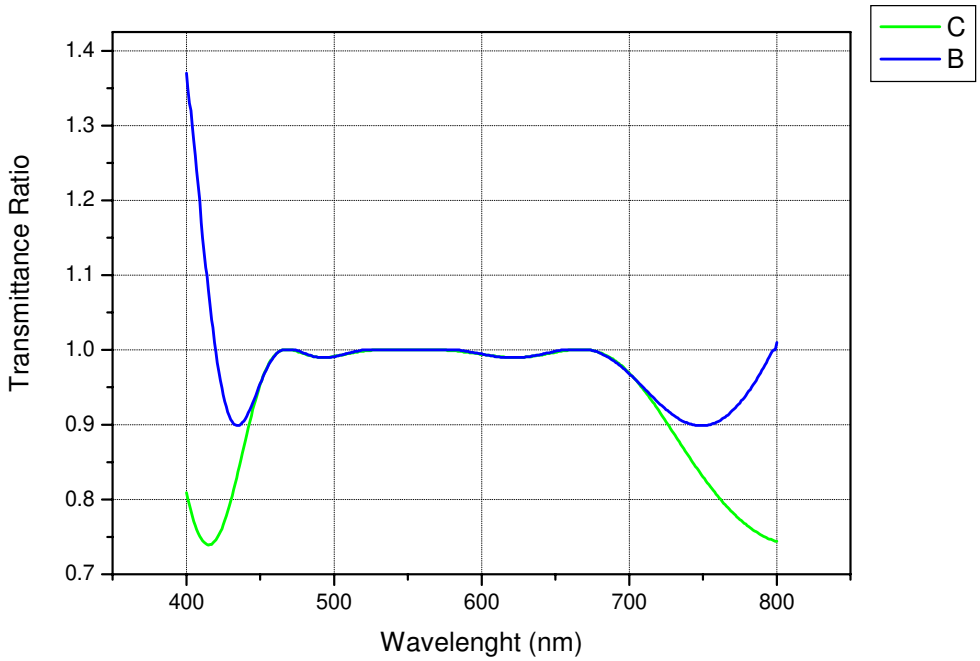

Figure 5.9. The transmittance ratios of three different coded curves for 12 layers.

In Figure 5.10 the transmittance ratios of coded curve as a-LLHL LHLL LLHL-s to coded curve as a-LLLL HHLL LLHL-s, a-LLHH LLLL LLHL-s, a-LLLL HHLH HLHL-s, a-HHLL HHHH LLHL-s, a-HHHH HHLL LLHL-s, a-HHHH LLHH HHHL-s, a-HHHH HHHH HHHL-s is shown as curve B, C, D, E, F, G, and H in that order. The ratio value of curves is closely one in these curves.

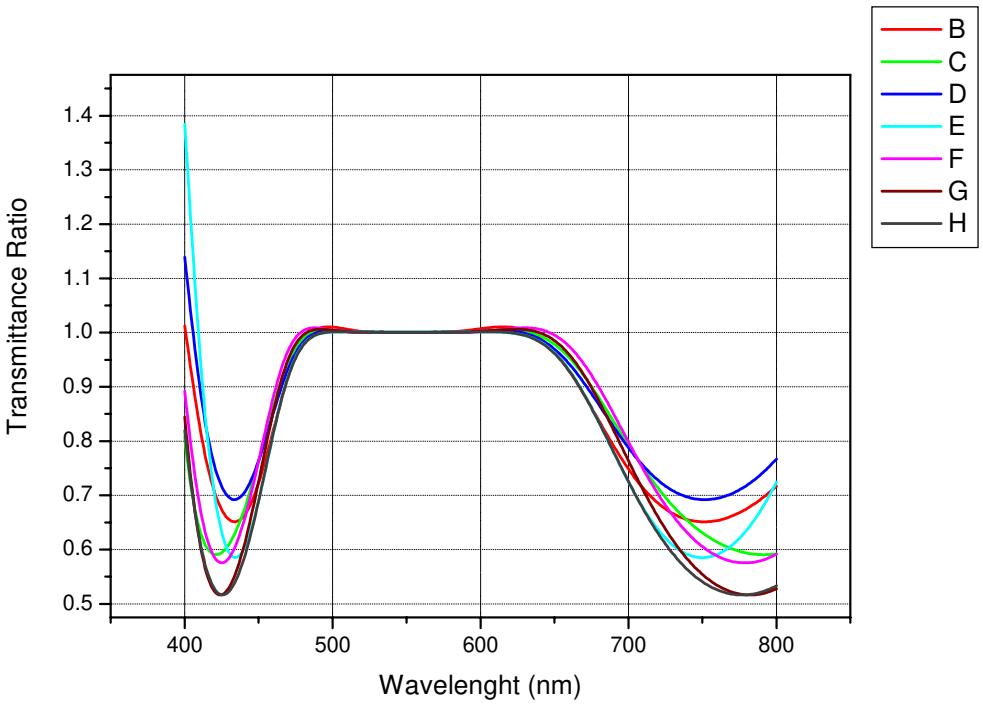

Figure 5.10. The transmittance ratios of eight different coded curves for 12 layers.

It is more clearly seen that transmittance ratios of selected curves from Figure 5.9 is nearly one in Figure 5.11. Curve B is the ratios of coded curve as a-LLHL LHLL LLHL-s to coded curve as a-HHHH HHLL LLHL-s and curve C is the ratios of coded curve as a-LLHL LHLL LLHL-s to coded curve as a-HHHH HHHH HHHL-s for 12 layers. The ratio value of curves is quite one in these curves.

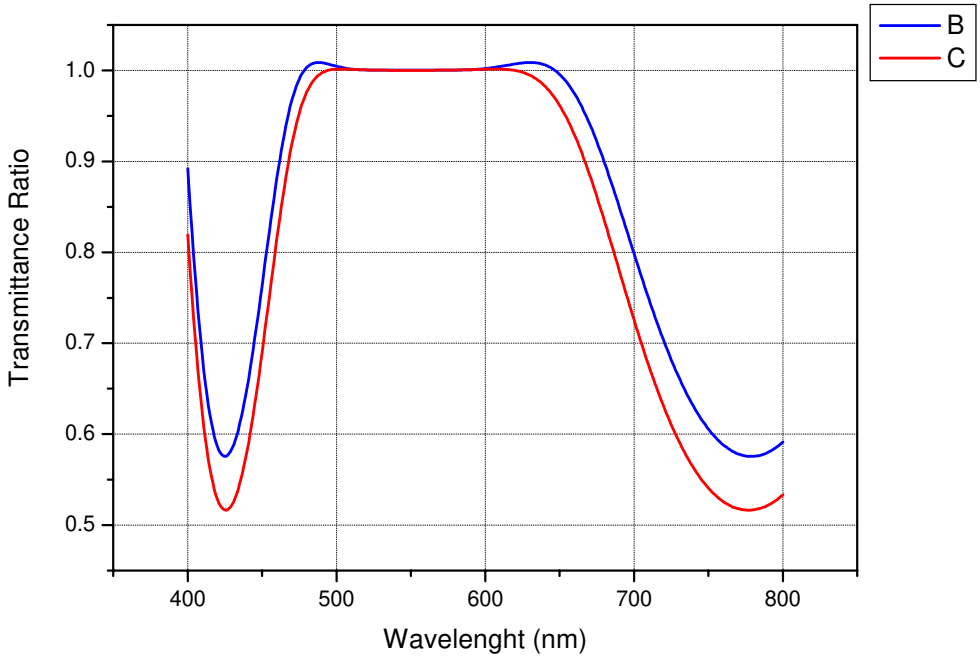

Figure 5.11. The transmittance ratios of three different coded curves for 12 layers.

As for Figure 5.12, it is transmittance ratio of coded curve as a-HHHH HHLL LLHL-s. The transmittance ratios of coded curve as a-HHHH HHLL LLHL-s to coded curve as a-LLLL HHLH HLHL-s, a-LLHH LLLL LLHL-s, a-HHHH LLHH HHHL-s, and a-HHHH HHHH HHHL-s is shown as curve B, C, D, and E respectively. The ratio value of curves is just about one in these curves.

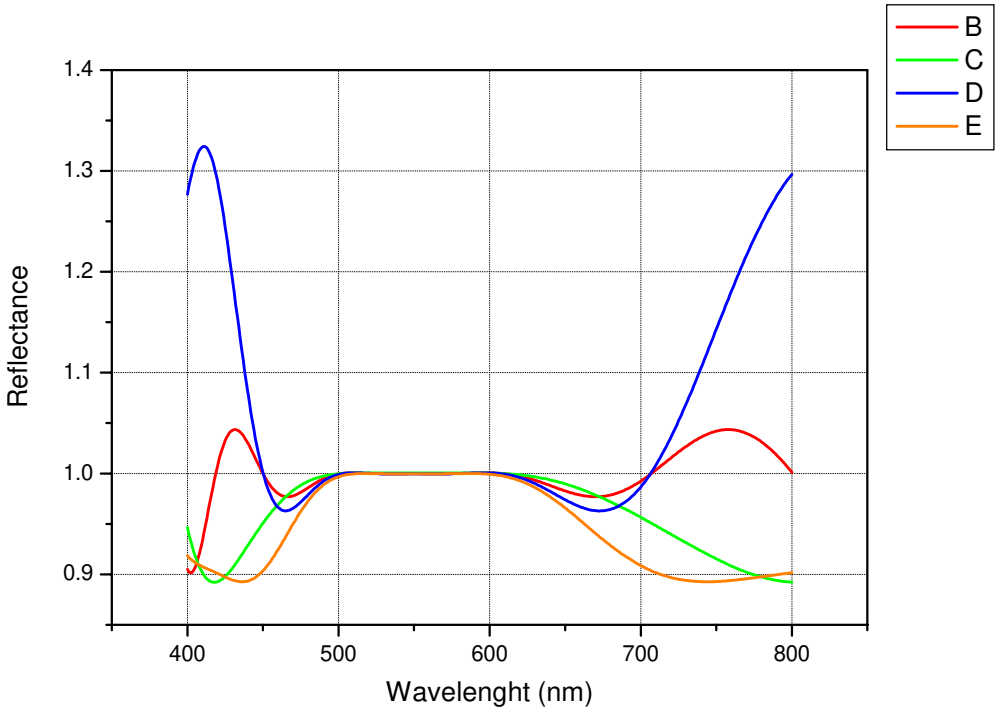

Figure 5.12. The transmittance ratios of five different coded curves for 12 layers.

Transmittance ratio of coded curve as a-HHHH HHHH HHHL-s is shown in Figure 5.13. The transmittance ratios of this coded curve to coded curve as a-HHHH HHLL LLHL-s, a-LLHH LLLL LLHL-s, and a-HHHH LLHH HHHL-s represents as curve B, C, and D correspondingly. The ratio value of curves is about one in these curves.

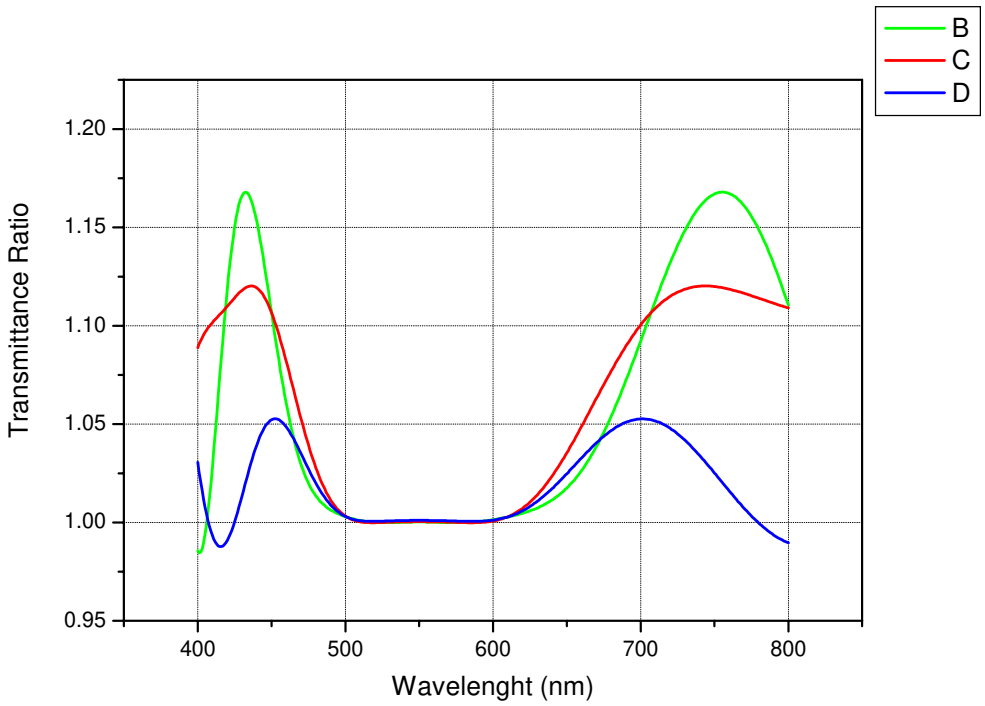

Figure 5.13. The transmittance ratios of four different coded curves for 12 layers.

Consequently, it is shown that in all transmittance ratio figures which we selected suitable materials to our aims since the transmittance ratio values of all curves is nearly one.

5.2.2. Odd Folded Multilayer Antireflection Coatings

In odd folded multilayer structure it is analyzed with three different materials. This materials are involved a convenient shorthand notation for quarter-wave optical thicknesses is H, M, and L which refer to the highest of the three indices, M the intermediate and L the lowest, and the layers having the refractive indices of n_H, n_M and n_L, respectively. Table 5.2 shows the general design data of each layer material and thickness. It has six possibilities to three-layer antireflection coating design. In order to give better result, we preferred two setting which are a-LHM-s and a-MHL-s coded. The optical thicknesses of the layers are equal to $\lambda_0/4$ at certain wavelength, λ_0=550 nm. An antireflection coating was designed for the visible spectral band on the basis of materials with the refractive indices of n_L=2.05 (ZrO_2), n_M=2.39 (ZnSe), n_H=2.97 (Ag_2AsS_3) with ferroelectric featuring n_s=2.28 ($LiNbO_3$) as the substrate and air n_0=1.00 as the outer space. The layer adjacent to the substrate had a low refractive index. Changing optical paths range from 0.113169 μm to 0.061659 μm as folds of $\lambda_0/4$, graphs is found in all analysis.

Table 5.2. Design data for layers used in all configuration.

Layer number	Material	Refractive Index (*n*)	Thickness (μm)
Layer #1	ZnSe	2.39	0.057531
Layer #2	ZrO_2	2.05	0.067073
Layer #3	Ag_2AsS_3	2.97	0.046296
Substrate	$LiNbO_3$	2.28	0.060307

Let's consider firstly the three-layer antireflection coating of a-LHM-s structure. It is investigated periodic configuration in other multilayer design which is a-LHM LHM-s settings for six-layer, a-$(LHM)^3$-s for nine-layer, and a-$(LHM)^4$-s for twelve-layer. The reflectance curve between 400 nm and 800 nm visible region of electromagnetic spectrum for these configurations is shown as curve E, D, C, and B respectively in Figure 5.14.

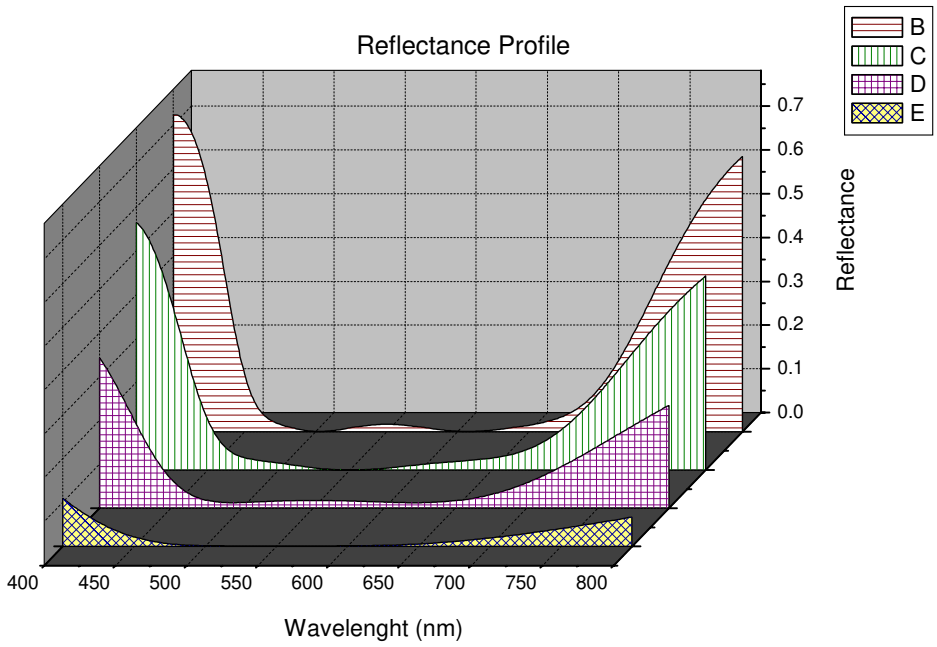

Figure 5.14. Reflectance Profile of 3, 6, 9, and 12 layers antireflection coating coded as a-LHM-s configuration.

In case of all layers configuration, the reflection curve of B stays almost 0.05% in the broadband between 485 nm and 640 nm with 72% at the maximum as to the wings of the curve. The reflection curve C is about 0.01% in the band between 520 nm and 590 nm. With the exception of this band, the C curve sees 56% at the highest between 400 nm and 800 nm range is seen to increase. The reflection curve of D is around 12% in the spectral range from 475 nm to 650 nm and maximum reflection is roughly 34% when it moves towards to the wings of the curve. The minimum reflection curve of E is just about 0.0085% in the range from 475 nm to 655 nm. The curve E is seen to rise up to 11% out of in the range. An increase in reflectance can be seen, but the important feature of this design is nearly zero reflectance at a spectral point.

As regards the other three-layer settings, it is coded a-MHL-s configuration. It is investigated periodically a-$(MHL)^2$-s settings for six-layer, a-$(MHL)^3$-s for nine-layer, and a-$(MHL)^4$-s for twelve-layer. In Figure 5.15, the reflectance curve in visible region for these configurations is shown as curve E, D, C, and B in that order.

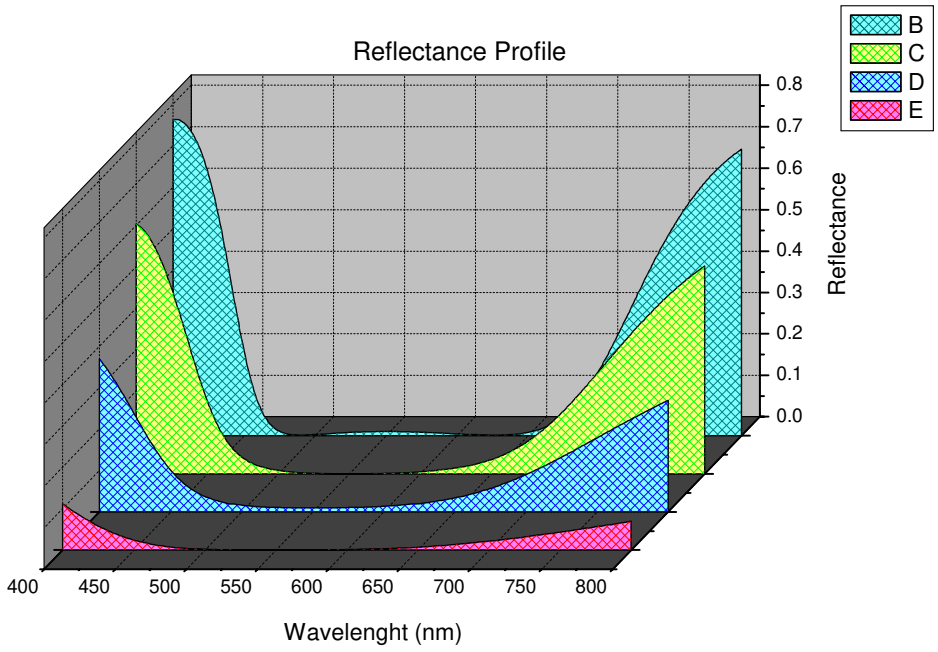

Figure 5.15. Reflectance Profile of 3, 6, 9, and 12 layers antireflection coating coded as a-MHL-s configuration.

It is clearly seen from the graphs that the reflection curve of B stays almost 0.1% in the broadband between 480 nm and 645 nm with 76% at the maximum as to the wings of the curve. The reflection curve C is about 0.001% in the band between 510 nm and 600 nm. With the exception of this band, the C curve sees 60% at the highest between 400 nm and 800 nm range is seen to increase. The reflection curve of D is around 0.94% in the spectral range from 500 nm to 610 nm and maximum reflection is roughly 36% when it moves towards to the wings of the curve. The minimum reflection curve of E is just about 0.00042% in the range from 475 nm to 650 nm. The curve E is seen to rise up to 11% out of in the range. The rising reflectance is seen, but the important feature of this design is virtually zero reflectance at a spectral point.

6. CONCLUSION AND DISCUSSION

The purpose of this thesis is to achieve a broader band visible antireflection coating design with multilayer structure which is consisted of insulator thin films. In order to design the normal incidence wideband visible multilayer AR coatings we used different types of layers which are two-different materials like ZnSe and ZrO_2 for even folded multilayer antireflection coatings, and three-different materials like ZnSe, ZrO_2, and Ag_2AsS_3 for odd folded. The ferroelectric material, $LiNbO_3$ is used as the substrate in this structure. The optical thickness of each layer is equal to a quarter-wave thick at certain wavelength λ_0=550 nm. The reflectance is investigated between 400 nm and 800 nm visible region of electromagnetic spectrum.

A short computer program for the design of two material antireflection coatings based on the theoretical considerations has been written in Fortran software program based on Fresnell formulas.

In order to obtain zero reflectance, we have designed a broad-band AR coating using high- and low-index layers on ferroelectric based substrate. The synthesis process started with a search for a two-layer antireflection coating with a-HL-s setting of the starting design. It is coded as a-HHHL-s, a-HH LLHL-s, a-LLHH LLHL-s, and a-HHH HHH HHHL-s settings for four-layer, six-layer, eight-layer, and ten-layer antireflection coating respectively. As for twelve-layer antireflection coating, eight configurations which are a-HHHH HHHH HHHL-s, a-HHLL HHHH LLHL-s, a-HHHH LLHH HHHL-s, a-HHHH HHLL LLHL-s, a-LLHH LLLL LLHL-s, a-LLLL HHLL LLHL-s, a-LLLL HHLH HLHL-s, and a-LLHL LHLL LLHL-s settings are researched to more lowly reflectance. The optical performance in all configurations is well and the average of minimum reflectivity across the entire visible region is approximately 0.05% or less. It is also investigated periodic settings for even folded multilayer antireflection coatings. But we are not got good results for these coded.

In the next design, three different materials are used which have the highest, the intermediate and the lowest refractive indices of the layers on the ferroelectric substrate. We analyzed two configurations which are a-LHM-s and a-MHL-s

settings. We investigated periodic configuration for all multilayer design in this configurations. This periodic configurations refers to a-$(LHM)^m$-s and a-$(MHL)^m$-s (m=1, 2, 3, and 4) for three-, six-, nine-, and twelve-layer. The maximum reflectance is approximately 74%, and the minimum is about 0.0053%. An increase in reflectance can be seen, but the important feature of this design is nearly zero reflectance at a spectral point. The values of reflectance are very high at the wings of the curves of odd folded multilayer antireflection coating. In order to make this value smaller than we have now, we will expand the spectral range considering a pyroelectric material of $LiNbO_3$ and using the refractive index formulas depending on polarization and temperature in future.

We also try to change the optical properties of substrate (ferroelectric material) using external electric and thermal fields. It seems to us, it is a first investigation, where the ferroelectric properties of substrate materials and their features are used in antireflection coating systems.

7. FUTURE PROSPECTS

It can be used different types of layers which are more than two-different materials for even folded and three materials for odd folded. It can be simulated other ferroelectric materials in our Fortran program to reduce reflection further. This Fortran software program is enhanced the optical thicknesses to a half-wave thick at a certain wavelength. The reflectance can be investigated not only the visible region but also infrared region of electromagnetic spectrum.

REFERENCES

ARNDT, D. P., AZZAM, R. M. A., BENNETT, J. M., BORGOGNO, J. P., CARNIGLIA, C. K., CASE, W. E., DOBROWOLSKI, J. A., GIBSON, U. J., TUTTLE HART, T., HO, F. C., HODGKIN, V. A., KLAPP, W. P., MACLEOD, H. A., PELLETIER, E., PURVIS, M. K., QUINN, D. M., STROME, D. H., SWENSON, R., TEMPLE, P. A., THONN, T. F., 1984. Multiple Determination of The Optical Constants of Thin-Film Coating Materials, Applied Optics, V:23, N:20, P:3571-3596.

AROUTIOUNIAN, VM., MARTIROSYAN, KH., SOUKIASSIAN, P., 2006. Almost Zero Reflectance of a Silicon Oxynitrid\Porous Silicon Double Layer Antireflection Coating for Silicon Photovoltaic Cells, J. Phys. D:Appl. Phys. 39, p:1623-1625.

ASGHAR, MH., KHAN, MB., NASEEM, S., 2003a. Modeling High Performance Multilayer Antireflection Coatings for Visible and Infrared (3-5μm) Substrates, Semiconductors Physics, Quantum Electronics & Optoelectronics, V:6, N:4, P:508-513.

ASGHAR, MH., KHAN, MB., NASEEM, S., KHAN, ZA., 2005. Design and Preparation of Antireflection Films on Glass Substrate, TÜBİTAK Turk Jr. Phys 29, P:43-53.

ASGHAR, MH., KHAN, MB., QURESHI, JA., NASEEM, S., 2003b. Computer Aided Design and Analysis of Multilayer Antireflection Coatings in Visible Spectrum. 2nd International Bhurban Conference on Applied Sciences and Technology, Bhurban, Pakistan, June-16-21, P:1-10.

AZZAM, R.M.A., HOWLADER, M.M.K., 2001. Fourth-and Sixth-Order Polarization Aberrations of Antireflection-Coated Optical Surfaces, Optics Letters, V:26, N:20, P:1607-1608.

BORGOGNO, J. P., FLORY, F., ROCHE, P., SCHMITT, B., ALBRAND, G., PELLETIER, E., MACLEOD, H. A., 1984. Refractive Index and Inhomogeneity of Thin Films, Applied Optics, V:23, N:20, P:3567-3570.

BRAUN, D. M., JUNGERMAN, R. L., 1995. Broadband Multilayer Antireflection Coating for Semiconductor Laser Facets, Optics Letters, V:20, N:10, P:1154-1156.

BURFOOT, J. C., 1967. Ferroelectrics, D. Van Nostrand Company Ltd., Canada, P:261

DOBROWOLSKI, JA., 1965. Completely Automatic Synthesis of Optical Thin Film Systems, Appl. Optics, V:4, N:8, P:937-946.

DOBROWOLSKI, JA., 1986. Comparison of The Fourier Transform and Flip-Flop Thin-Film Synthesis Methods, Appl. Optics, V:25, N:12, P:1966-1972.

DOBROWOLSKI, JA., BROWNING, S., JACOBSON, MR, NADAL, M., 2006b. 2004 Optical Society of America's Topical Meeting on Optical Interference Coatings: Manufacturing Problem, Appl. Optics, V:45, N:7, P:1303-1311.

DOBROWOLSKI, JA., GUO, Y., TIWALD, T., MA, P., POITRAS, D., 2006a. Toward Perfect Antireflection Coatings. 3. Experimental Results Obtained with The Use of Reststrahlen Materials, Appl. Optics, V:45, N:7, P:1555-1562.

DOBROWOLSKI, JA., HO, F. C., WALDORF, A., 1983. Determination of Optical Constants of Thin Film Coating Materials Based on Inverse Synthesis, Appl. Optics, V:22, N:20, P:3191-3200.

DOBROWOLSKI, JA., KEMP, R.A., 1990. Refinement of Optical Multilayer Systems with Different Optimization Procedures, Appl. Optics, V:29, N:19, P:2876-2893.

DOBROWOLSKI, JA., LOWE, D., 1978. Optical Thin Film Synthesis Program Based on The Use of Fourier Transforms, Appl. Optics, V:17, N:19, P:3039-3050.

DOBROWOLSKI, JA., PIOTROWSKI, S.H.C., 1982. Refractive Index as a Variable in The Numerical Design of Optical Thin Film Systems, Appl. Optics, V:21, N:8, P:1502-1511.

DOBROWOLSKI, JA., SULLIVAN, BT., 1996. Universal Antireflection Coatings for Substrates for the Visible Spectral Region, Appl. Optics, V:35, N:25, P:4993-4997.

DOBROWOLSKI, JA., TIKHONRAVOV, AV., TRUBETSKOV, MK., SULLIVAN, BT., VERLY, PG., 1996. Optimal single-Band Normal-Incidence Antireflection Coatings, Appl. Optics, V:35, N:4, P:644-658.

DUYAR, Ö., DURUSOY, HZ., 2004. Design and Preparation of Antireflection and Reflection Optical Coatings, TÜBİTAK Turk Jr. Phys 28, P:139-144.

GERKEN, M., MILLER, DAB., 2004. Multilayer Thin-Film Coatings for Optical Communication Systems, OSA Topical Meeting on Optical Interference Coatings, Tucson, Poster ThF2.

HELLMICH, W., DEIMEL, PP., 1992. Optimal AR-Coating for Optical Waveguide Devices, Journal of Lightwave Technology, V:10, N:4, p:469-476.

KITTEL, C., 2005. Introduction to Solid State Physics, John Wiley & Sons, Inc., USA, P:680.

KNITTL, Z.,1976. Optics of Thin Films, John Wiley & Sons Ltd., Czechoslovakia, P:547.

KURT, HY., KIYMAZ, HS., SALAMOV, B., ÇOLAKOĞLU, K., 2002. Filamentation of Light Emission in an Infrared-Visible Image Converter with a Semiconductor Photodetector, TÜBİTAK Turk Jr. Phys 26, P:67-72.

KURT, HY., KURT, E, SALAMOV, BG., 2001. An Analysis of the Image Homogeneity in an Ionization-Type Infrared Image Converter Using the Fractal Dimension, The Imaging Science Journal, V:49, P:205-212.

LAMMINPÄÄ, A., NEVAS, S., MANOOCHERI, F., IKONEN, E., 2006. Characterization of Thin Films Based on Reflectance and Transmittance Measurements at Oblique Angles of Incidence, Appl. Optics, V:45, N:7, P:1392-1396.

LEE, J., TANAKA, T., SASAKI, S., UCHİYAMA, S., TSUCHIYA, M., KAMIYA, T., 1997. Novel Design Procedure of Broad-Band Multilayer Antireflection Coatings for Optical and Optoelectronic Devices, CLEO'97, P:451.

LEE, J., TANAKA, T., SASAKI, S., UCHİYAMA, S., TSUCHIYA, M., KAMIYA, T., 1998. Novel Design Procedure of Broad-Band Multilayer Antireflection Coatings for Optical and Optoelectronic Devices, Journal of Lightwave Technology, V:16, N:5, P:884-891.

LI, L., DOBROWOLSKI, JA., 1996. Visible Broadband, Wide-Angle, Thin-Film Multilayer Polarizing Beam Splitter, Appl. Optics, V:35, N:13, P:2221-2225.

LI, L., DOBROWOLSKI, JA., 2000. High-Performance Thin-Film Polarizing Beam Splitter Operating at Angles Greater than the Critical Angle, Appl. Optics, V:39, N:16, P:2754-2771.

LI, L., DOBROWOLSKI, JA., SANKEY, JD., WIMPERIS, JR., 1992. Antireflection Coatings for both Visible and Far-Infrared Spectral Regions, Appl. Optics, V:31, N:28, P:6150-6156.

LIOU, YY., 2002a. Digital Design of Broadband Antireflection Coating, Jpn. J. Appl. Phys., V:41, P:5578-5580.

LIOU, YY., 2002b. Universal Broad-Band Antire.ection Coating Designs for Substrates in the Visible Spectral Region, Jpn. J. Appl. Phys., V:41, P:6409-6410.

LIOU, YY., 2003. Designing a Broadband Visible Antireflection Coating by Flip-Flop Tuning Search Technique, Jpn. J. Appl. Phys., V:42, P:6879-6882.

LIOU, YY., 2004a. Tuning Iteration Method for Antireflection Coating Designs in the Visible Spectral Region, Jpn. J. Appl. Phys., V:43, N:2, P:547-549.

LIOU, YY., 2004b. Universal Visible Antireflection Coating Design for Various Substrate, Jpn. J. Appl. Phys., V:43, N:4A, P:1339-1342.

LIOU, YY., 2004c. Universal Visible Antireflection Coating Designs by Tuning Iteration Technique, Jpn. J. Appl. Phys., V:43, N:3, P:985-988.

LIOU, YY., 2004d. Minimizing Search Method for Wideband Visible or Wideband Infrared Antireflection Coating Designs, Jpn. J. Appl. Phys., V:43, N:4A, P:1343-1347.

LIOU, YY., 2004e. Universal Wideband Antireflection Coating Designs for Substrates over the Visible Spectral Region by Minimizing Search Method, Jpn. J. Appl. Phys., V:43, N:7A, P:4185-4189.

LIOU, YY., 2004f. Iteration Exchanging Search Method for Designing a Wideband Antireflection Coating over the Visible Spectral Region, Jpn. J. Appl. Phys., V:43, N:9A, P:6065-6068.

LIOU, YY., 2005. Designing a Broadband Visible Antireflection Coating by Jumping Search Method, Jpn. J. Appl. Phys., V:44, N:12, P:8462-8466.

LIOU, YY., 2006. Design of Wide-Angular-Incidence Antireflection Coating over the Visible Spectral Region, Jpn. J. Appl. Phys., V:45, N:5A, P:4051-4057.

LIOU, YY., LIU, YT., 2005a. Digital Designs of Broadband Visible Antireflection Coating for Wide Angular Incidence, Jpn. J. Appl. Phys., V:44, N:1A, P:163-167.

LIOU, YY., LIU, YT., 2005b. Optimizing the Universal Visible Antireflection Coating Designs for Substrates by Exchanging Search Algorithms, Jpn. J. Appl. Phys., V:44, N:4A, P:1748-1751.

LORCH, S., 2003. Theory and Measuring of Antireflection Coatings, Annual Report 2003, Optoelectronics Department, Uni. Of Ulm, P:1-6.

MACLEOD, HA., 1986. Thin Film Optical Filters. Adam Hilger Ltd, Brisol, P:519.

MACLEOD, A., 1999. The Early Days of Optical Coatings, J. Opt. A:Pure Appl. Opt. 1, P:779-783.

MCLACHLAN, AD., 1978. Two-Layer Low-Absorption Antireflection Coating for KCI, Appl. Optics, V:17, N:3, P:447-450.

MOUCHART, J., 1977. Thin Film Optical Coatings. 2:Three-LayerAntireflection Coating Theory, Appl. Optics, V:16, N:10, P:2722-2728.

MUSSET A & THELEN A, 1966. Multilayer Antireflection Coatings, Progress in Optics vol.8 ed. E Wolf, Amsterdam: North Holland, P:201-37.

NILSSON, PO., 1968. Determination of Optical Constants from Intensity Measurements at Normal Incidence, Appl. Optics, V:7, N:3, P:435-442

NOTNI, G., KOWARSCHIK, R., REHN, H., 1992. Incoherent-to-Coherent Conversion via Photorefractive Fan-Out and Two-Wave Mixing, Journal of Modern Optics, V:39, N:4, P:871-879.

POITRAS, D., DOBROWOLSKI, JA., 2004. Toward Perfect Antireflection Coatings. 2. Theory, Appl. Optics, V:43, N:6, P:1286-1295.

QIU, Y., ZHENG, Z., LU, T., HUANG, W., ZHUANG, J., TANG, DY., 2001. Incoherent-To-Coherent Conversion By Use Of The Photorefractive Beam-

Fanning Effect And Amplification By Two-Wave Coupling in a Photorefractive $Ba_{1-x}Sr_xTiO_3$ Crystal, Appl. Optics, V:40, N:5, P:687-690.

RANCOURT, J., KAMERLING, M., MONACO, D., 1991. New Antireflection Coating for Solar Cell Covers, IEEE CH2953-8-91-0000, P:1518-1520.

REFERMAT, S., 2004. A Jewel in the Crown, Chapter IV_25, Optical Thin Films at the Instute of Optics: A Brief History, The Laser: The 1960s, Carlos R. Stround Jr., P:140-145.

SALAMOV, BG., 2003. Dependence of the Characteristics on the Structure of a Coherent Infrared Image Converter, Infrared Physics & Technology, V:44, P:243-251.

SALAMOV, BG., AGASIEV, AA., LEBEDEVA, NN., ORBUKH, VI., YUCEL, H., ÇOLAKOGLU, K., 2002. Incoherent-to-Coherent IR Image Converter on the Basis of GaAs and $Bi_{12}SiO_{20}$ Crystals, J. Phys. D:Appl. Phys. 35, p:716-720.

SALAMOV, BG., GÜNEN, A., 2001a. The Mechanism of Non-Silver Image Recording in an Infrared Image Converter with a Semiconductor Photodetector, The Imaging Science Journal, V:49, P:101-111.

SALAMOV, BG., GÜNEN, A., 2003a. A New Coherent Infrared Image Converter, Eur. Phys. J. AP, V:21, P:81-87.

SALAMOV, BG., KURT, HY. KURT, E., 2003b. An Analysis of the Spatial Homogeneity of a Photodetector Surface in an Infrared Image Converter Using the Fractal Dimension, The Imaging Science Journal, V:51, P:187-196.

SALAMOV, BG., KURT, HY., LEBEDEVA, NN., ALTINDAL, S., OZER, M., 2001b. Coherent Infrared Image Converter Based on GaAs and BSO Crystals, The Imaging Science Journal, V:49, P:197-203.

SCHALLENBERG, UB., 2006. Antireflection Design Concepts With Equivalent Layers, Appl. Optics, V:45, N:7, P:1507-1514.

SCHOW, FL., RIAZI, A., GANDHI, OP., GROW, RW., 1983. Threshold Technique for Measuring Parametric Upconversion Efficiency, IEEE J. OF Quantum Electronics, V:QE-19, N:4, P:491-492.

SCHULZ, U., SCHALLENBERG, UB., KAISER, N., 2002. Antireflection Coating Design for Plastic Optics, Appl. Optics, V:41, N:16, P:3107-3110.

SOILEAU, MJ., 1980. Mechanism of Laser-Induced Failure in Antireflection-Coated $LiNbO_3$ Crystals, Appl. Optics, V:20, N:6, P:1030-1033.

SUN, CC., WANG, B., CHANG, JY, 1998. Photorefractive Incoherent-to-Coherent Optical Converter Based on Anisotropic Self-diffraction in $BaTiO_3$, Appl. Optics, V:37, N:35, P:8247-8253.

TANAKA, LT., UCHIYAMA, S., TSUCHIYA, M., KAMIYA, T., 1997. Novel Design Procedure of Broadband Multilayer Antireflection Coatings for Semiconductor Optoelectronic Devices, CLEO97, CThX4, p:451.

THELEN, A., TILSCH, M., TIKHONRAVOV, AV., TRUBETSKOV, MK., BRAUNECK, U., 2002. Topical Meeting on Optical Interference Coatings (OIC'2001): Design Contest Results, Applied Optics, V:41, No:16, P:3022-3038.

TIKHONRAVOV, AV., 1993. Some Theoretical Aspects of Thin-Film Optics and Their Applications, Applied Optics, V:32, No:28, P:5417-5426.

TIKHONRAVOV, AV., DOBROWOLSKI, JA., 1993. Quasi-Optimal Synthesis for Antireflection Coatings: A New Method, Applied Optics, V:32, No:22, P:4265-4275.

TIKHONRAVOV, AV., FURMAN, ShA., 1992. Basic of Optics of Multilayer Sytystems, Chapter I, Edition Frontiers, Gif-sur-Yuette, P:1-103.

TIKHONRAVOV, AV., TRUBETSKOV, MK., AMOTCHKINA, TV., KOKAREV, MA., KAISER, N., STENZEL, O., WILBRANDT, S., GBLER, D., 2006a. New Optimization Algorithm for the Synthesis of Rugate Optical Coatings, Applied Optics, V:45, No:7, P:1515-1524.

TIKHONRAVOV, AV., TRUBETSKOV, MK., AMOTCHKINA, TV., THELEN, A., 2006b. Optical Coating Design Algorithm Based on the Equivalent Layers Theory, Applied Optics, V:45, No:7, P:1530-1538.

TIKHONRAVOV, AV., TRUBETSKOV, MK., DEBELL, GW., 1996. Application of the Needle Optimization Technique to the Design of Optical Coatings, Applied Optics, V:35, no:28, P:5493-5508.

TILSCH, M., HENDRIX, K., VERLY, P., 2006. Optical Interference Coatings Design Contest 2004, Applied Optics, V:45, No:7, P:1544-1554.

TODOROVIĆ, DM., NIKOLIĆ, PM., BOJIĆIĆ, AI., VASILJEVIĆ-RADOVIĆ DG., RADULOVIĆ, KT., 2001. Thermoelastic and Electronic Deformation Components of Photoacoustic Signal in Two-layer System, Analytical Sciences, V:17, Special Issue, P:137-140.

VASSALLO, C., 1990. Theory and Practical Calculation of Antireflection Coatings on Semiconductor Laser Diode Optical Amplifiers, Optical Amplifiers for Communication ,IEE Proceedings, V:137, N:4, P:193-202.

VERLY, PG., 1995. Fourier Transform Technique with Frequency Filtering for Optical Thin-Film Design, Applied Optics, V:34, No:4, P:688-694.

VERLY, PG., DOBROWOLSKI, JA., 1990. Iterative Correction Process for Optical Thin Film Synthesis with the Fourier Transform Method, Applied Optics, V:29, No:25, P:3672-3684.

VERLY, PG., DOBROWOLSKI, JA., WILLEY, RR., 1992. Fourier-Transform Method for the Design of Wideband Antireflection Coatings, Applied Optics, V:31, No:19, P:3836-3846.

VERLY, PG., TIKHONRAVOV, AV., TRUBETSKOV, MK., 1997. Efficient Refinement Algorithm for the Synthesis of Inhomogeneous Optical Coatings, Applied Optics, V:36, No:7, P:1487-1495.

WANG, C., FEI, H., WEI, Z., QIU, Y., YANG, Y., 1999. Incoherent-to-Coherent Optical Conversion by Means of Azobenzene Liquid-Crystalline Films, Applied Physics B Lasers and Optics, V:68, P:221-224.

WYDEVEN, T., KUBACKI, R., 1976. Antireflection Coating Prepared by Plasma Polymerization of Perfluorobutene-2, Applied Optics, V:15, No:1, P:132-136.

XU, Y., 1991. Ferroelectric Materials and Their Applications, Elsevier Science Publishers B.V., Amsterdam: North-Holland, p.377.

YAMADA, M., YAMANE, Y., 1996. A Design Method for Dielectric Multilayer Optical Filters, Optical Review, V:3, N:6B, P:512-517.

YOLDAS, BE., PARTLOW, DP., 1984. Wide Spectrum Antireflective Coating for Fused Silica and Other Glasses, Applied Optics, V:23, No:9, P:1418-1424.

ZHANG, J., WANG, H., YOSHIKADO, S., ARUGA, T., 1999. High-Resolution Incoherent-to-Coherent Conversion by Use of the Photorefractive Fanning Effect, Applied Optics, V:38, No:6, P:995-1000.

BIOGRAPHY

I was born in Adana. I received my B.Sc. degree from Physics Engineering Department of Hacettepe University and MSc degree from Electrical and Electronics Engineering Department of Cukurova University. I worked there as a research assistant. I participated "9th National Workshop on Optics, Electro-Optics, and Photonics (PHOTONIC 2007)" in ASELSAN in Ankara, Turkey, September 28, 2007; "8th European Conference on Applications of Polar Dielectrics (ECAPD8 2006)" in Metz, France, September 5-8, 2006; "The 7th European Conference on Applications of Polar Dielectrics (ECAPD7 2004)" in Liberec, Czech Republic, September 6-9, 2004; "International Conference on Electrical and Electronics Engineering (ELECO` 2003)" in Bursa, Turkey, December 3-7, 2003; and "First Scientific Conference of The Balkan Region IEEE Student Branches" in "Panayot Volov" Artillery and Air Defence Military Academy in Shoumen, Bulgaria, May 21-23, 2001. I have four posters and one oral presentation in these National and International Conferences. I have two articles in "Ferroelectrics", 2005 and "Journal of Electromagnetic Waves and Applications (JEMWA)", 2004. I attended Physics Department of Cukurova University as PhD student since 2002.

APPENDIX

Appendix I. Application to Optical Coefficients of Refractive Index Depending on Polarization for Ferroelectric Materials

The refractive indices of each layer depending on polarization for the ferroelectric based multilayer antireflection coating system is

$$n(p) = n(0) + \frac{\partial n}{\partial p}\Delta p + \frac{1}{2!}\frac{\partial^2 n}{\partial p^2}\Delta p^2 + ... \tag{1.1}$$

The reflectance of our assembly is

$$R_5 = \left(\frac{n_0 - \frac{n_1^2 n_3^2}{n_2^2 n_4^2} n_5}{n_0 + \frac{n_1^2 n_3^2}{n_2^2 n_4^2} n_5} \right)^2 = \frac{\Delta}{\nabla}. \tag{1.2}$$

Numerator of eq. (1.2) is

$$\Delta = \left(n_0 n_2^2 n_4^2 - n_1^2 n_3^2 n_5 \right)^2 \tag{1.3}$$

and denominator of eq. (1.2) is

$$\nabla = \left(n_0 n_2^2 n_4^2 + n_1^2 n_3^2 n_5 \right)^2. \tag{1.4}$$

After small calculations eq. (1.3) and (1.4) are written as follows,

$$\Delta = n_0^2 n_2^4(0) n_4^4(0) + n_1^4(0) n_3^4(0) n_5^2 - 2n_0 n_1^2(0) n_2^2(0) n_3^2(0) n_4^2(0) n_5 + 6n_0^2 n_2^4(0) n_4^2(0) \left(\frac{\partial n_4}{\partial p}\right)^2 (\Delta p)^2$$

$$+6n_0^2 n_2^2(0) n_4^4(0) \left(\frac{\partial n_2}{\partial p}\right)^2 (\Delta p)^2 - 2n_0 n_1^2(0) n_2^2(0) n_4^2(0) n_5 \left(\frac{\partial n_3}{\partial p}\right)^2 (\Delta p)^2$$

$$-2n_0 n_2^2(0) n_3^2(0) n_4^2(0) n_5 \left(\frac{\partial n_1}{\partial p}\right)^2 (\Delta p)^2 - 2n_0 n_1^2(0) n_2^2(0) n_3^2(0) n_5 \left(\frac{\partial n_4}{\partial p}\right)^2 (\Delta p)^2$$

$$-2n_0 n_1^2(0) n_3^2(0) n_4^2(0) n_5 \left(\frac{\partial n_2}{\partial p}\right)^2 (\Delta p)^2 + 6n_1^4(0) n_3^2(0) n_5^2 \left(\frac{\partial n_3}{\partial p}\right)^2 (\Delta p)^2$$

$$+6n_1^2(0) n_3^4(0) n_5^2 \left(\frac{\partial n_1}{\partial p}\right)^2 (\Delta p)^2 + 2n_0^2 n_2^4(0) n_4^3(0) \frac{\partial^2 n_4}{\partial p^2} (\Delta p)^2 + 2n_0^2 n_2^3(0) n_4^4(0) \frac{\partial^2 n_2}{\partial p^2} (\Delta p)^2$$

$$-2n_0 n_1^2(0) n_2^2(0) n_3(0) n_4^2(0) n_5 \frac{\partial^2 n_3}{\partial p^2} (\Delta p)^2 - 2n_0 n_1(0) n_2^2(0) n_3^2(0) n_4^2(0) n_5 \frac{\partial^2 n_1}{\partial p^2} (\Delta p)^2$$

$$-2n_0 n_1^2(0) n_2^2(0) n_3^2(0) n_4(0) n_5 \frac{\partial^2 n_4}{\partial p^2} (\Delta p)^2 - 2n_0 n_1^2(0) n_2(0) n_3^2(0) n_4^2(0) n_5 \frac{\partial^2 n_2}{\partial p^2} (\Delta p)^2$$

$$+2n_1^4(0) n_3^3(0) n_5^2 \frac{\partial^2 n_3}{\partial p^2} (\Delta p)^2 + 2n_1^3(0) n_3^4(0) n_5^2 \frac{\partial^2 n_1}{\partial p^2} (\Delta p)^2 + 16n_0^2 n_2^3(0) n_4^3(0) \frac{\partial n_2}{\partial p} \frac{\partial n_4}{\partial p} (\Delta p)^2$$

$$-8n_0 n_1(0) n_2^2(0) n_3(0) n_4^2(0) n_5 \frac{\partial n_1}{\partial p} \frac{\partial n_3}{\partial p} (\Delta p)^2 - 8n_0 n_1^2(0) n_2^2(0) n_3(0) n_4(0) n_5 \frac{\partial n_3}{\partial p} \frac{\partial n_4}{\partial p} (\Delta p)^2$$

$$-8n_0 n_1(0) n_2^2(0) n_3^2(0) n_4(0) n_5 \frac{\partial n_1}{\partial p} \frac{\partial n_4}{\partial p} (\Delta p)^2 - 8n_0 n_1^2(0) n_2(0) n_3(0) n_4^2(0) n_5 \frac{\partial n_2}{\partial p} \frac{\partial n_3}{\partial p} (\Delta p)^2 \qquad (1.5)$$

$$-8n_0 n_1(0) n_2(0) n_3^2(0) n_4^2(0) n_5 \frac{\partial n_1}{\partial p} \frac{\partial n_2}{\partial p} (\Delta p)^2 - 8n_0 n_1^2(0) n_2(0) n_3^2(0) n_4(0) n_5 \frac{\partial n_2}{\partial p} \frac{\partial n_4}{\partial p} (\Delta p)^2$$

$$+16n_1^3(0) n_3^3(0) n_5^2 \frac{\partial n_1}{\partial p} \frac{\partial n_3}{\partial p} (\Delta p)^2$$

and

$$\nabla = n_0^2 n_2^4(0) n_4^4(0) + n_1^4(0) n_3^4(0) n_5^2 + 2n_0 n_1^2(0) n_2^2(0) n_3^2(0) n_4^2(0) n_5 + 6n_0^2 n_2^4(0) n_4^2(0) \left(\frac{\partial n_4}{\partial p}\right)^2 (\Delta p)^2$$

$$+6n_0^2 n_2^2(0) n_4^4(0) \left(\frac{\partial n_2}{\partial p}\right)^2 (\Delta p)^2 + 2n_0 n_1^2(0) n_2^2(0) n_4^2(0) n_5 \left(\frac{\partial n_3}{\partial p}\right)^2 (\Delta p)^2$$

$$+2n_0 n_2^2(0) n_3^2(0) n_4^2(0) n_5 \left(\frac{\partial n_1}{\partial p}\right)^2 (\Delta p)^2 + 2n_0 n_1^2(0) n_2^2(0) n_3^2(0) n_5 \left(\frac{\partial n_4}{\partial p}\right)^2 (\Delta p)^2$$

$$+2n_0 n_1^2(0) n_3^2(0) n_4^2(0) n_5 \left(\frac{\partial n_2}{\partial p}\right)^2 (\Delta p)^2 + 6n_1^4(0) n_3^2(0) n_5^2 \left(\frac{\partial n_3}{\partial p}\right)^2 (\Delta p)^2$$

$$+6n_1^2(0) n_3^4(0) n_5^2 \left(\frac{\partial n_1}{\partial p}\right)^2 (\Delta p)^2 + 2n_0^2 n_2^4(0) n_4^3(0) \frac{\partial^2 n_4}{\partial p^2} (\Delta p)^2 + 2n_0^2 n_2^3(0) n_4^4(0) \frac{\partial^2 n_2}{\partial p^2} (\Delta p)^2$$

$$+2n_0 n_1^2(0) n_2^2(0) n_3(0) n_4^2(0) n_5 \frac{\partial^2 n_3}{\partial p^2} (\Delta p)^2 + 2n_0 n_1(0) n_2^2(0) n_3^2(0) n_4^2(0) n_5 \frac{\partial^2 n_1}{\partial p^2} (\Delta p)^2$$

$$+2n_0 n_1^2(0) n_2^2(0) n_3^2(0) n_4(0) n_5 \frac{\partial^2 n_4}{\partial p^2} (\Delta p)^2 + 2n_0 n_1^2(0) n_2(0) n_3^2(0) n_4^2(0) n_5 \frac{\partial^2 n_2}{\partial p^2} (\Delta p)^2$$

$$+2n_1^4(0) n_3^3(0) n_5^2 \frac{\partial^2 n_3}{\partial p^2} (\Delta p)^2 + 2n_1^3(0) n_3^4(0) n_5^2 \frac{\partial^2 n_1}{\partial p^2} (\Delta p)^2 + 16n_0^2 n_2^3(0) n_4^3(0) \frac{\partial n_2}{\partial p} \frac{\partial n_4}{\partial p} (\Delta p)^2$$

$$+8n_0 n_1(0) n_2^2(0) n_3(0) n_4^2(0) n_5 \frac{\partial n_1}{\partial p} \frac{\partial n_3}{\partial p} (\Delta p)^2 + 8n_0 n_1^2(0) n_2^2(0) n_3(0) n_4(0) n_5 \frac{\partial n_3}{\partial p} \frac{\partial n_4}{\partial p} (\Delta p)^2$$

$$+8n_0 n_1(0) n_2^2(0) n_3^2(0) n_4(0) n_5 \frac{\partial n_1}{\partial p} \frac{\partial n_4}{\partial p} (\Delta p)^2 + 8n_0 n_1^2(0) n_2(0) n_3(0) n_4^2(0) n_5 \frac{\partial n_2}{\partial p} \frac{\partial n_3}{\partial p} (\Delta p)^2 \qquad .(1.6)$$

$$+8n_0 n_1(0) n_2(0) n_3^2(0) n_4^2(0) n_5 \frac{\partial n_1}{\partial p} \frac{\partial n_2}{\partial p} (\Delta p)^2 + 8n_0 n_1^2(0) n_2(0) n_3^2(0) n_4(0) n_5 \frac{\partial n_2}{\partial p} \frac{\partial n_4}{\partial p} (\Delta p)^2$$

$$+16n_1^3(0) n_3^3(0) n_5^2 \frac{\partial n_1}{\partial p} \frac{\partial n_3}{\partial p} (\Delta p)^2$$

The transmittance of the assembly is

$$T_5 = \frac{4n_0 n_1^2 n_3^2 \,\mathrm{Re}(n_5)}{n_2^2 n_4^2 \left(n_0 + \frac{n_1^2 n_3^2}{n_2^2 n_4^2} n_5\right)^2} . \qquad (1.7)$$

So eq.(1.7) can be written as,

$$T_5 = \frac{4n_0 n_1^2 n_2^2 n_3^2 n_4^2}{\left(n_0 n_2^2 n_4^2 + n_1^2 n_3^2 n_5\right)^2} \mathrm{Re}\left(n_5\right) = \frac{\Omega}{\nabla} \mathrm{Re}\left(n_5\right) \tag{1.8}$$

Denominator of eq. (1.8) is equal to denominator of eq. (1.4), so the result of this equation $\nabla = \left(n_0 n_2^2 n_4^2 + n_1^2 n_3^2 n_5\right)^2$ is eq. (1.6). and numerator of eq. (1.8) is

$$\Omega = 4n_0 n_1^2 n_2^2 n_3^2 n_4^2 \tag{1.9}$$

with some simple calculation, (1.9) is written as,

$$\begin{aligned}
\Omega = {} & 4n_0 n_1^2(0) n_2^2(0) n_3^2(0) n_4^2(0) + 4n_0 n_2^2(0) n_3^2(0) n_4^2(0) \left(\frac{\partial n_1}{\partial p}\right)^2 (\Delta p)^2 \\
& + 4n_0 n_1^2(0) n_3^2(0) n_4^2(0) \left(\frac{\partial n_2}{\partial p}\right)^2 (\Delta p)^2 + 4n_0 n_1^2(0) n_2^2(0) n_4^2(0) \left(\frac{\partial n_3}{\partial p}\right)^2 (\Delta p)^2 \\
& + 4n_0 n_1^2(0) n_2^2(0) n_3^2(0) \left(\frac{\partial n_4}{\partial p}\right)^2 (\Delta p)^2 + 4n_0 n_1(0) n_2^2(0) n_3^2(0) n_4^2(0) \frac{\partial^2 n_1}{\partial p^2} (\Delta p)^2 \\
& + 4n_0 n_1^2(0) n_2(0) n_3^2(0) n_4^2(0) \frac{\partial^2 n_2}{\partial p^2} (\Delta p)^2 + 4n_0 n_1^2(0) n_2^2(0) n_3(0) n_4^2(0) \frac{\partial^2 n_3}{\partial p^2} (\Delta p)^2 \\
& + 4n_0 n_1^2(0) n_2^2(0) n_3^2(0) n_4(0) \frac{\partial^2 n_4}{\partial p^2} (\Delta p)^2 + 16n_0 n_1(0) n_2(0) n_3^2(0) n_4^2(0) \frac{\partial n_1}{\partial p} \frac{\partial n_2}{\partial p} (\Delta p)^2 \\
& + 16n_0 n_1(0) n_2^2(0) n_3(0) n_4^2(0) \frac{\partial n_1}{\partial p} \frac{\partial n_3}{\partial p} (\Delta p)^2 + 16n_0 n_1(0) n_2^2(0) n_3^2(0) n_4(0) \frac{\partial n_1}{\partial p} \frac{\partial n_4}{\partial p} (\Delta p)^2 \\
& + 16n_0 n_1^2(0) n_2(0) n_3(0) n_4^2(0) \frac{\partial n_2}{\partial p} \frac{\partial n_3}{\partial p} (\Delta p)^2 + 16n_0 n_1^2(0) n_2(0) n_3^2(0) n_4(0) \frac{\partial n_2}{\partial p} \frac{\partial n_4}{\partial p} (\Delta p)^2 \\
& + 16n_0 n_1^2(0) n_2^2(0) n_3(0) n_4(0) \frac{\partial n_3}{\partial p} \frac{\partial n_4}{\partial p} (\Delta p)^2
\end{aligned} \tag{1.10}$$

The absorptance of the assembly is

$$A_5 = \frac{4n_0 n_1^2 n_3^2 \,\mathrm{Re}\left(BC^* - n_5\right)}{n_2^2 n_4^2 \left(n_0 + \frac{n_1^2 n_3^2}{n_2^2 n_4^2} n_5\right)^2}. \tag{1.11}$$

Eq.(1.11) can be written as,

$$A_5 = \frac{4n_0 n_1^2 n_2^2 n_3^2 n_4^2}{\left(n_0 n_2^2 n_4^2 + n_1^2 n_3^2 n_5\right)^2} \mathrm{Re}\left(BC^* - n_5\right) = \frac{\Omega}{\nabla} \mathrm{Re}\left(BC^* - n_5\right) \tag{1.12}$$

The result of numerator of eq. (1.12) is equal to eq. (1.10) and the result of denominator of eq. (1.12) is equal to eq. (1.6).

Appendix II. Application to Optical Coefficients of Refractive Index Depending on Temperature for Ferroelectric Materials

The refractive indices of each layer depending on temperature for the ferroelectric based multilayer antireflection coating system is

$$n(T) = n(0) + \frac{\partial n}{\partial T}\Delta T + \frac{1}{2!}\frac{\partial^2 n}{\partial T^2}\Delta T^2 + ... \tag{2.1}$$

The reflectance of our assembly is

$$R_5 = \left(\frac{n_0 - \frac{n_1^2 n_3^2}{n_2^2 n_4^2} n_5}{n_0 + \frac{n_1^2 n_3^2}{n_2^2 n_4^2} n_5} \right)^2 = \frac{\left(n_0 n_2^2 n_4^2 - n_1^2 n_3^2 n_5 \right)^2}{\left(n_0 n_2^2 n_4^2 + n_1^2 n_3^2 n_5 \right)^2} = \frac{\Delta}{\nabla}. \tag{2.2}$$

After small calculations, numerator and denominator are written as,

$$\Delta = n_0^2 n_2^4(0) n_4^4(0) + n_1^4(0) n_3^4(0) n_5^2 - 2n_0 n_1^2(0) n_2^2(0) n_3^2(0) n_4^2(0) n_5 + 6n_0^2 n_2^4(0) n_4^2(0) \left(\frac{\partial n_4}{\partial T}\right)^2 (\Delta T)^2$$

$$+6n_0^2 n_2^2(0) n_4^4(0) \left(\frac{\partial n_2}{\partial T}\right)^2 (\Delta T)^2 - 2n_0 n_1^2(0) n_2^2(0) n_4^2(0) n_5 \left(\frac{\partial n_3}{\partial T}\right)^2 (\Delta T)^2$$

$$-2n_0 n_2^2(0) n_3^2(0) n_4^2(0) n_5 \left(\frac{\partial n_1}{\partial T}\right)^2 (\Delta T)^2 - 2n_0 n_1^2(0) n_2^2(0) n_3^2(0) n_5 \left(\frac{\partial n_4}{\partial T}\right)^2 (\Delta T)^2$$

$$-2n_0 n_1^2(0) n_3^2(0) n_4^2(0) n_5 \left(\frac{\partial n_2}{\partial T}\right)^2 (\Delta T)^2 + 6n_1^4(0) n_3^2(0) n_5^2 \left(\frac{\partial n_3}{\partial T}\right)^2 (\Delta T)^2$$

$$+6n_1^2(0) n_3^4(0) n_5^2 \left(\frac{\partial n_1}{\partial T}\right)^2 (\Delta T)^2 + 2n_0^2 n_2^4(0) n_4^3(0) \frac{\partial^2 n_4}{\partial T^2} (\Delta T)^2 + 2n_0^2 n_2^3(0) n_4^4(0) \frac{\partial^2 n_2}{\partial T^2} (\Delta T)^2$$

$$-2n_0 n_1^2(0) n_2^2(0) n_3(0) n_4^2(0) n_5 \frac{\partial^2 n_3}{\partial T^2} (\Delta T)^2 - 2n_0 n_1(0) n_2^2(0) n_3^2(0) n_4^2(0) n_5 \frac{\partial^2 n_1}{\partial T^2} (\Delta T)^2$$

$$-2n_0 n_1^2(0) n_2^2(0) n_3^2(0) n_4(0) n_5 \frac{\partial^2 n_4}{\partial T^2} (\Delta T)^2 - 2n_0 n_1^2(0) n_2(0) n_3^2(0) n_4^2(0) n_5 \frac{\partial^2 n_2}{\partial T^2} (\Delta T)^2$$

$$+2n_1^4(0) n_3^3(0) n_5^2 \frac{\partial^2 n_3}{\partial T^2} (\Delta T)^2 + 2n_1^3(0) n_3^4(0) n_5^2 \frac{\partial^2 n_1}{\partial T^2} (\Delta T)^2 + 16n_0^2 n_2^3(0) n_4^3(0) \frac{\partial n_2}{\partial T} \frac{\partial n_4}{\partial T} (\Delta T)^2$$

$$-8n_0 n_1(0) n_2^2(0) n_3(0) n_4^2(0) n_5 \frac{\partial n_1}{\partial T} \frac{\partial n_3}{\partial T} (\Delta T)^2 - 8n_0 n_1^2(0) n_2^2(0) n_3(0) n_4(0) n_5 \frac{\partial n_3}{\partial T} \frac{\partial n_4}{\partial T} (\Delta T)^2$$

$$-8n_0 n_1(0) n_2^2(0) n_3^2(0) n_4(0) n_5 \frac{\partial n_1}{\partial T} \frac{\partial n_4}{\partial T} (\Delta T)^2 - 8n_0 n_1^2(0) n_2(0) n_3(0) n_4^2(0) n_5 \frac{\partial n_2}{\partial T} \frac{\partial n_3}{\partial T} (\Delta T)^2 \qquad (2.3)$$

$$-8n_0 n_1(0) n_2(0) n_3^2(0) n_4^2(0) n_5 \frac{\partial n_1}{\partial T} \frac{\partial n_2}{\partial T} (\Delta T)^2 - 8n_0 n_1^2(0) n_2(0) n_3^2(0) n_4(0) n_5 \frac{\partial n_2}{\partial T} \frac{\partial n_4}{\partial T} (\Delta T)^2$$

$$+16n_1^3(0) n_3^3(0) n_5^2 \frac{\partial n_1}{\partial T} \frac{\partial n_3}{\partial T} (\Delta T)^2$$

and

$$\nabla = n_0^2 n_2^4(0) n_4^4(0) + n_1^4(0) n_3^4(0) n_5^2 + 2n_0 n_1^2(0) n_2^2(0) n_3^2(0) n_4^2(0) n_5 + 6n_0^2 n_2^4(0) n_4^2(0) \left(\frac{\partial n_4}{\partial T}\right)^2 (\Delta T)^2$$

$$+6n_0^2 n_2^2(0) n_4^4(0) \left(\frac{\partial n_2}{\partial T}\right)^2 (\Delta T)^2 + 2n_0 n_1^2(0) n_2^2(0) n_4^2(0) n_5 \left(\frac{\partial n_3}{\partial T}\right)^2 (\Delta T)^2$$

$$+2n_0 n_2^2(0) n_3^2(0) n_4^2(0) n_5 \left(\frac{\partial n_1}{\partial T}\right)^2 (\Delta T)^2 + 2n_0 n_1^2(0) n_2^2(0) n_3^2(0) n_5 \left(\frac{\partial n_4}{\partial T}\right)^2 (\Delta T)^2$$

$$+2n_0 n_1^2(0) n_3^2(0) n_4^2(0) n_5 \left(\frac{\partial n_2}{\partial T}\right)^2 (\Delta T)^2 + 6n_1^4(0) n_3^2(0) n_5^2 \left(\frac{\partial n_3}{\partial T}\right)^2 (\Delta T)^2$$

$$+6n_1^2(0) n_3^4(0) n_5^2 \left(\frac{\partial n_1}{\partial T}\right)^2 (\Delta T)^2 + 2n_0^2 n_2^4(0) n_4^3(0) \frac{\partial^2 n_4}{\partial T^2} (\Delta T)^2 + 2n_0^2 n_2^3(0) n_4^4(0) \frac{\partial^2 n_2}{\partial T^2} (\Delta T)^2$$

$$+2n_0 n_1^2(0) n_2^2(0) n_3(0) n_4^2(0) n_5 \frac{\partial^2 n_3}{\partial T^2} (\Delta T)^2 + 2n_0 n_1(0) n_2^2(0) n_3^2(0) n_4^2(0) n_5 \frac{\partial^2 n_1}{\partial T^2} (\Delta T)^2$$

$$+2n_0 n_1^2(0) n_2^2(0) n_3^2(0) n_4(0) n_5 \frac{\partial^2 n_4}{\partial T^2} (\Delta T)^2 + 2n_0 n_1^2(0) n_2(0) n_3^2(0) n_4^2(0) n_5 \frac{\partial^2 n_2}{\partial T^2} (\Delta T)^2$$

$$+2n_1^4(0) n_3^3(0) n_5^2 \frac{\partial^2 n_3}{\partial T^2} (\Delta T)^2 + 2n_1^3(0) n_3^4(0) n_5^2 \frac{\partial^2 n_1}{\partial T^2} (\Delta T)^2 + 16n_0^2 n_2^3(0) n_4^3(0) \frac{\partial n_2}{\partial T} \frac{\partial n_4}{\partial T} (\Delta T)^2$$

$$+8n_0 n_1(0) n_2^2(0) n_3(0) n_4^2(0) n_5 \frac{\partial n_1}{\partial T} \frac{\partial n_3}{\partial T} (\Delta T)^2 + 8n_0 n_1^2(0) n_2^2(0) n_3(0) n_4(0) n_5 \frac{\partial n_3}{\partial T} \frac{\partial n_4}{\partial T} (\Delta T)^2$$

$$+8n_0 n_1(0) n_2^2(0) n_3^2(0) n_4(0) n_5 \frac{\partial n_1}{\partial T} \frac{\partial n_4}{\partial T} (\Delta T)^2 + 8n_0 n_1^2(0) n_2(0) n_3(0) n_4^2(0) n_5 \frac{\partial n_2}{\partial T} \frac{\partial n_3}{\partial T} (\Delta T)^2 \qquad .(2.4)$$

$$+8n_0 n_1(0) n_2(0) n_3^2(0) n_4^2(0) n_5 \frac{\partial n_1}{\partial T} \frac{\partial n_2}{\partial T} (\Delta T)^2 + 8n_0 n_1^2(0) n_2(0) n_3^2(0) n_4(0) n_5 \frac{\partial n_2}{\partial T} \frac{\partial n_4}{\partial T} (\Delta T)^2$$

$$+16n_1^3(0) n_3^3(0) n_5^2 \frac{\partial n_1}{\partial T} \frac{\partial n_3}{\partial T} (\Delta T)^2$$

The transmittance of the assembly is

$$T_5 = \frac{4n_0 n_1^2 n_3^2 \,\mathrm{Re}(n_5)}{n_2^2 n_4^2 \left(n_0 + \frac{n_1^2 n_3^2}{n_2^2 n_4^2} n_5\right)^2} = \frac{4n_0 n_1^2 n_2^2 n_3^2 n_4^2}{\left(n_0 n_2^2 n_4^2 + n_1^2 n_3^2 n_5\right)^2} \mathrm{Re}(n_5) = \frac{\Omega}{\nabla} \mathrm{Re}(n_5). \qquad (2.5)$$

Denominator of eq. (2.5) is equal to denominator of eq. (2.2). After some simple calculation, numerator of eq. (2.5) is written as,

$$\Omega = 4n_0 n_1^2(0) n_2^2(0) n_3^2(0) n_4^2(0) + 4n_0 n_2^2(0) n_3^2(0) n_4^2(0) \left(\frac{\partial n_1}{\partial T}\right)^2 (\Delta T)^2$$
$$+4n_0 n_1^2(0) n_3^2(0) n_4^2(0) \left(\frac{\partial n_2}{\partial T}\right)^2 (\Delta T)^2 + 4n_0 n_1^2(0) n_2^2(0) n_4^2(0) \left(\frac{\partial n_3}{\partial T}\right)^2 (\Delta T)^2$$
$$+4n_0 n_1^2(0) n_2^2(0) n_3^2(0) \left(\frac{\partial n_4}{\partial T}\right)^2 (\Delta T)^2 + 4n_0 n_1(0) n_2^2(0) n_3^2(0) n_4^2(0) \frac{\partial^2 n_1}{\partial T^2} (\Delta T)^2$$
$$+4n_0 n_1^2(0) n_2(0) n_3^2(0) n_4^2(0) \frac{\partial^2 n_2}{\partial T^2} (\Delta T)^2 + 4n_0 n_1^2(0) n_2^2(0) n_3(0) n_4^2(0) \frac{\partial^2 n_3}{\partial T^2} (\Delta T)^2$$
$$+4n_0 n_1^2(0) n_2^2(0) n_3^2(0) n_4(0) \frac{\partial^2 n_4}{\partial T^2} (\Delta T)^2 + 16n_0 n_1(0) n_2(0) n_3^2(0) n_4^2(0) \frac{\partial n_1}{\partial T} \frac{\partial n_2}{\partial T} (\Delta T)^2$$
$$+16n_0 n_1(0) n_2^2(0) n_3(0) n_4^2(0) \frac{\partial n_1}{\partial T} \frac{\partial n_3}{\partial T} (\Delta T)^2 + 16n_0 n_1(0) n_2^2(0) n_3^2(0) n_4(0) \frac{\partial n_1}{\partial T} \frac{\partial n_4}{\partial T} (\Delta T)^2$$
$$+16n_0 n_1^2(0) n_2(0) n_3(0) n_4^2(0) \frac{\partial n_2}{\partial T} \frac{\partial n_3}{\partial T} (\Delta T)^2 + 16n_0 n_1^2(0) n_2(0) n_3^2(0) n_4(0) \frac{\partial n_2}{\partial T} \frac{\partial n_4}{\partial T} (\Delta T)^2$$
$$+16n_0 n_1^2(0) n_2^2(0) n_3(0) n_4(0) \frac{\partial n_3}{\partial T} \frac{\partial n_4}{\partial T} (\Delta T)^2 \qquad (2.6)$$

The absorptance of the assembly is

$$A_5 = \frac{4n_0 n_1^2 n_3^2 \,\mathrm{Re}\left(BC^* - n_5\right)}{n_2^2 n_4^2 \left(n_0 + \frac{n_1^2 n_3^2}{n_2^2 n_4^2} n_5\right)^2} = \frac{4n_0 n_1^2 n_2^2 n_3^2 n_4^2}{\left(n_0 n_2^2 n_4^2 + n_1^2 n_3^2 n_5\right)^2} \mathrm{Re}\left(BC^* - n_5\right) = \frac{\Omega}{\nabla} \mathrm{Re}\left(BC^* - n_5\right). \qquad (2.7)$$

The result of numerator of eq. (2.7) is equal to eq. (2.6) and the result of denominator of eq. (2.7) is equal to eq. (2.4).